Optimisation of Feedwater Heaters and Geothermal Preheater in Fossil-Geothermal Hybrid Power Plant

By

CHRISTA NSANZUBUHORO

in full fulfilment of the requirements for the degree

MASTER OF SCIENCE (Mechanical Engineering)

in the

Faculty of Engineering and the Built Environment

Supervisor: PROF. TUNDE BELLO-OCHENDE

Co-Supervisor: PROF. ARNAUD MALAN

University of Cape Town

Cape Town

November 2018

ACKNOWLEDGEMENTS

I am very grateful to God for granting me the grace, mercy and blessings to see this project to completion.

I would like to express my sincere gratitude to my supervisor Prof. Tunde Bello-Ochende for the continuous support of my research, for his patience, encouragement and immense knowledge. I extend my gratitude to my co-supervisor, Prof. Arnaud Malan for his motivation and financial support.

I owe a deep sense of gratitude to my family, whom I consider my greatest blessing. I am grateful for their unending support, love, and encouragement.

On the whole, to all those who knowingly and unknowingly, directly and indirectly helped me, I thank you.

DECLARATION

I know the meaning of plagiarism and declare that all the work in the document, save for that which is properly acknowledged, is my own. This thesis/dissertation has been submitted to the Turnitin module and I confirm that my supervisor has seen my report and any concerns revealed by such have been resolved with my supervisor.

Signed by candidate

Christa Nsanzinteko Nsanzubuhoro

November 2018

ABSTRACT

Sufficient energy supply is a fundamental necessity for the stimulation of socio-economic advancement. However, the current rapid rise in urbanisation has resulted in the significant increase in energy demands. Consequently, the current conventional energy supply systems are facing numerous challenges in meeting the world's growing demand for energy sustainably. Thus, there is an urgent and compelling need to develop innovative, more effective ways to integrate sustainable renewable energy solutions into the already existing systems or better yet, create new systems that all together make use of renewable energy.

This research aims to investigate and establish the optimum working conditions of a feedwater heater and geothermal preheater in a power plant that makes use of both renewable and non-renewable energy resources, where renewable energy (geothermal energy) is used to boost the power output in an environmentally sustainable way. Henceforth, a simplified model of a Rankine cycle with single reheat and regeneration and another model with a geothermal preheater substituting the low-pressure feedwater heater were designed.

The Engineering Equations Solver (EES) software was used to perform an analysis of the thermodynamic performance of the two models designed. The models were used to analyse the energetic and exergetic effects of replacing a low-pressure feedwater heater with a geothermal preheater sourcing heat from a low temperature geothermal resource (temperature generally < 150°C). The results of this research work reveal that the replacement of the low-pressure feedwater heater with a geothermal preheater increases the power generated since less heat is bled from the low-pressure turbine (allowing more heat energy from the steam to be converted into mechanical energy in the turbine). Applying the principle of the Second Law of thermodynamics analysis, the Number of Entropy Generation Units (EGU) and Entropy Generation Minimisation (EGM) analysis were employed to optimise the designed hybrid system. The feedwater heaters and geothermal preheater were modelled as counter-flow heat exchangers and a downhole co-axial heat exchanger, respectively. The feedwater heaters were optimised by means of the method of Number of Entropy Generation Units whereas the geothermal preheater was optimised by means of the Entropy Generation Minimisation analysis method. Owing to the optimisation of these components, the operating conditions of the boiler and turbines were secondarily improved.

Overall, this research emphasises the impact renewable energy has on major power plant systems that are in operation and run on non-renewables.

Table of Contents

ACKNOWLEDGEMENTS ii

DECLARATION iii

ABSTRACT iv

Table of Contents v

List of Tables ix

List of Figures x

Nomenclature xiii

Alphabetic symbols xiii

Abbreviations xiv

Greek Symbols xv

Subscripts xvi

1 INTRODUCTION 1

1.1 Subject and Motivation for Report 1

1.2 Background to Investigation 1

1.3 Objectives of the Report 2

1.4 Scope and Limitations 3

1.5 Plan of Development 3

2 LITERATURE REVIEW 5

2.1 Characteristics of Geothermal Energy 5

2.1.1 Advantages and Disadvantages of Geothermal Energy 5

2.1.2 Impacts of geothermal development 5

2.1.3 Geothermal Power Plant as a Base Load Plant 6

2.2 Geothermal Energy Statistics 7

2.3 Geothermal Energy Resources 8

2.3.1 Hydrothermal Sources 8

2.3.2 Geopressured Sources 9

2.3.3 Petrothermal Sources 9
2.4 Geothermal Power Plants 9
2.4.1 Dry steam 10
2.4.2 Flash steam 11
2.4.3 Binary system 11
2.4.4 Hybrid power plants 12
2.4.5 Back pressure power plants 16
2.5 Geothermal Trends 16
2.5.1 Trends in geothermal investment 17
2.5.2 Development Costs 19
2.5.3 Trends in the Cost of Energy 19
2.6 Geothermal Energy Exploration in Africa 20
2.6.1 Potential for Electricity Production from Geothermal Energy in South Africa 21
2.7 Advanced Geothermal Systems 22
2.7.1 Enhanced Geothermal Systems (EGS) 22
2.7.2 Using End-of-Life Oil Fields 23
2.7.3 CPG (CO_2 Plume Geothermal Power) 24
2.8 Heat Exchangers 24
2.8.1 Selection Criteria 26
2.8.2 Shell and Tube Heat Exchangers 26
2.8.3 Downhole Coaxial Heat Exchanger (DCHE) 27
2.8.4 Deaerator 28
3 METHODOLOGY 30
3.1 Modelling 30
3.1.1 Hybrid Concepts 30
3.2 Heat Exchanger Design 31
3.2.1 LMTD method: 32

3.2.2 E-NTU METHOD: 33
3.3 Assumptions 35
3.3.1 Downhole Coaxial Heat Exchanger: 35
3.3.2 Counter-Flow Shell and Tube Heat Exchanger: 35
3.4 Operating Parameters 36
3.4.1 Thermodynamic cycle 36
3.4.2 Geothermal Resource 37
3.5 Exergy/Irreversibility Analysis 38
3.5.1 Condensate Pump/Boiler Feed Pump 39
3.5.2 Heat Exchanger (Case 1) 40
3.5.3 Heat Exchanger (Case 2) 41
3.5.4 Turbine 42
3.5.5 Energy and Exergy analysis of Geothermal Preheater system 42
3.5.6 Summary 44
3.6 Pressure drop analysis 45
3.6.1 Counter-flow shell and tube heat exchanger 45
3.6.2 Downhole Co-Axial Heat Exchanger 46
3.7 Optimisation 46
3.7.1 Counter-flow Shell and Tube Heat Exchanger 47
3.7.2 Downhole Coaxial Heat Exchanger (DCHE) 55
3.8 Design and Sizing of Components 59
3.8.1 Condenser and Feedwater Heaters Design 59
3.8.2 Turbine Design 61
4 RESULTS AND DISCUSSION 62
4.1 Thermodynamic Analysis 62
4.1.1 Low Pressure Feedwater Heater System 62
4.1.2 Geothermal Preheater System 66

4.1.3 Model Validation of Fossil-Geothermal Hybrid Power Plant 70
4.2 Results of Energy and Exergy Analysis 72
4.2.1 Results of First Law Efficiency 72
4.2.2 Results of Second Law Efficiency 75
4.2.3 Results of Organic Rankine Cycle 78
4.3 Optimisation 80
4.3.1 Feedwater Heater 80
4.3.2 Model Validation of Feedwater Heater Optimisation 89
4.3.3 Sensitivity Analysis of Feedwater Heater Optimisation 90
4.3.4 Geothermal Preheater 91
4.3.5 Sensitivity Analysis of Geothermal Preheater Optimisation 95
5 Conclusion and Recommendations 96
6 REFERENCES 99
7 APPENDICES 107
7.1 Appendix A-Matlab Code for Shell and Tube Counter-Flow Heat Exchanger with Area Constraint 107
7.2 Appendix B- Matlab Code for Shell and Tube Counter-Flow Heat Exchanger with Lrh Constraint 109
7.3 Appendix C- Matlab Code for Downhole Coaxial Heat Exchanger with variation in Temperature Gradient 110
7.4 Appendix D- Matlab Code for Downhole Coaxial Heat Exchanger with variation in Resource Temperature 113
7.5 Appendix E-First and Second Law Efficiency of Organic Rankine Cycle 115
7.6 Appendix F-EES Code for Thermodynamic Cycles 117
7.7 Appendix G-Thermodynamic Cycle with two LPFWH 119
7.8 Appendix H-Assessment of Ethics in Research Projects form 121

List of Tables

Table 3.1: Operating Parameters for the Rankine cycle 36
Table 3.2: Parameters for the geothermal source [67] 37
Table 3.3: Summary of Exergy balance and Exergy efficiency [74] 44
Table 4.1: Process parameters of Rankine Cycle with reheat, regeneration and LP feedwater Heater 64
Table 4.2: Power Balance of the main power plant components 66
Table 4.3: Process parameters of Rankine cycle with geothermal preheater in place of low-pressure feedwater heater 68
Table 4.4: Power Balance of the main power plant components in hybrid system 70
Table 4.5: Exergy destruction rate of the power plant components 76
Table 4.6: Exergy destruction rate of the power plant components in hybrid system 76

List of Figures

Figure 1.1: Temperatures in the earth [Geothermal Education Office] 2
Figure 2.1: World Geothermal Potential [source: Islandsbanki]-provide date of the source ... 7
Figure 2.2: Top 10 Geothermal Countries based on Installed Power Generation Capacity [source: Think GeoEnergy]-provide date of the source 8
Figure 2.3: Diagram of dry steam geothermal system [8] 10
Figure 2.4: Diagram of a single flash geothermal system [8] 11
Figure 2.5: Diagram of a binary geothermal system using iso-butane as the secondary working fluid [8] 12
Figure 2.6: Geothermal preheat hybrid system with multiple feedwater heaters [21] 13
Figure 2.7: Two-stage fossil superheat hybrid system [21] 14
Figure 2.8: One-stage Compound Hybrid System [21] 14
Figure 2.9: Diagram of hybrid solar-geothermal system [25] 15
Figure 2.10: Annual New Investment in Geothermal Energy, 2004-2015 (USD BILLION) [1] **Provide labels 17
Figure 2.11: Global Investment by region from 2010-2015 by region, in percentage [1] 18
Figure 2.12: Regions with low-enthalpy geothermal potential 22
Figure 2.13: Basic layout of an EGS type geothermal power plant [41] 23
Figure 2.14: Schematic of a Counterflow Shell and Tube Heat Exchanger [54] 27
Figure 2.15: Sketch of single-well, coaxial downhole heat exchanger with fractures [59] 28
Figure 2.16: Schematic of spray-type deaerator [28] 29
Figure 2.17: Schematic of tray-type deaerator [Industrial Steam] 29
Figure 3.1: Two operational models of a geothermal preheat hybrid system: (a) Fuel saver; (b) Power booster 31
Figure 3.2: Schematic Diagram of Pump 39
Figure 3.3: Heat Exchanger with two inlets and two outlets [74] 40
Figure 3.4: Heat exchanger with three inlets and two outlets [74] 41
Figure 3.5: Turbine Schematic [74] 42
Figure 3.6: Counter-flow Heat Exchanger with specified capacity rates and inlet conditions 48
Figure 3.7: A concept of the Downhole Coaxial Heat Exchanger [26] 55
Figure 3.8: Tube arrangements [94] 59

Figure 4.1: Schematic of Rankine Cycle with reheat, regeneration (including low pressure feedwater heater).....63
Figure 4.2: T-s diagram of Rankine cycle with single reheat, regeneration (including low pressure feedwater heater) 64
Figure 4.3: Rankine Cycle with reheat, regeneration and geothermal preheater.....67
Figure 4.4: Schematic of Rankine Cycle with reheat, regeneration (with geothermal preheater) 68
Figure 4.5: Extra power generated for different proportions of replaced bled steam [61].....71
Figure 4.6: Extra power generated for different proportions of replaced bled steam in hybrid system 72
Figure 4.7: Effect of High Pressure Turbine Inlet Pressure on First Law Efficiency.....74
Figure 4.8: Effect of High Pressure Turbine Inlet Pressure on Second Law Efficiency 78
Figure 4.9: Maximum first law efficiency of geothermal power plant (Organic Rankine Cycle) as a function of rejection temperature and with variation in resource temperature.....79
Figure 4.10: Maximum second law efficiency of geothermal power plant (Organic Rankine Cycle) as a function of rejection temperature and with variation in resource temperature 80
Figure 4.11: Optimal dimensionless mass velocity with variation in cross sectional area.....82
Figure 4.12: Minimum entropy generation number with variation in cross sectional area 83
Figure 4.13: Minimum entropy generation number versus optimal dimensionless mass velocity with variation in cross sectional area 84
Figure 4.14: Heat transfer and fluid friction contributions to minimum entropy generation number versus optimal dimensionless mass velocity with variation in cross sectional area...85
Figure 4.15: Optimum tube length to tube radius ratio versus Reynolds number at varying mass velocity.....86
Figure 4.16: Minimum entropy generation number with variation in cross sectional area 87
Figure 4.17: Minimum entropy generation number versus optimal length to radius ratio at varying mass flow rates 88
Figure 4.18: Heat transfer and fluid friction contributions to minimum entropy generation number versus optimal Lrh ratio with variation in mass velocity number.....89
Figure 4.19: Number of entropy generation units per side as a function of Reynolds number, dimensionless mass velocity, and tube length to tube radius ratio [83].....90
Figure 4.20: Optimal mass flow rate of geothermal fluid with variation in temperature gradient 91

Figure 4.21: Optimal mass flow rate of geothermal fluid with variation in resource temperature 92
Figure 4.22: Optimal DCHE outer diameter with variation in temperature gradient 93
Figure 4.23: Optimal DCHE outer diameter with variation in resource temperature.....93
Figure 4.24: Optimal DCHE outer diameter at varying mass flow rates with variation in temperature gradient 94
Figure 4.25: Optimal DCHE outer diameter at varying mass flow rates with variation in resource temperature.....94
Figure 4.26: Minimum entropy generated with variation in temperature gradient 95

Nomenclature

Alphabetic symbols

$\boldsymbol{A}$	Heat transfer area, m^2
$\mathbf{a}$	Dimensionless heat transfer area
$\boldsymbol{C}$	Mass flow parameter, J/s.K
$\boldsymbol{Cp}$	Isobaric specific heat capacity, J/kg.K
$\boldsymbol{D}$	Diameter, m
$\boldsymbol{D_e}$	Equivalent diameter, m
$\boldsymbol{D_h}$	Hydraulic diameter, m
$\boldsymbol{\dot{E}x}$	Exergy rate, W
$\boldsymbol{f}$	Fanning friction factor
$\boldsymbol{G}$	Mass flux, $kg/m^2.s$
$\boldsymbol{g}$	Dimensionless mass flux
$\boldsymbol{h}$	Convective heat transfer coefficient, $W/m^2.K$ or specific enthalpy, J/kg
$\dot{\boldsymbol{I}}$	Exergy destruction (Irreversibility), W
$\boldsymbol{k}$	Thermal conductivity, W/m.K
$\boldsymbol{K}$	Local loss coefficient
$\boldsymbol{L}$	Length, m
$\dot{\boldsymbol{m}}$	Mass flow rate, kg/s
$\boldsymbol{N_B}$	Number of baffles
$\boldsymbol{N_s}$	Non-dimensional entropy generation number
$\boldsymbol{Nu}$	Nusselt number

$\boldsymbol{P}$	Pressure, Pa
$\boldsymbol{\Delta P}$	Pressure drop, Pa
$\boldsymbol{Pr}$	Prandtl number
$\boldsymbol{Sv}$	Svelteness
$\boldsymbol{q}$	Heat flux, W/m^2, or specific heat transfer, J/kg
$\boldsymbol{\dot{Q}}$	Heat transfer rate, W
$\boldsymbol{r}$	Diameter ratio
$\boldsymbol{R}$	Radius, m or thermal resistance, W/m^2.K
$\boldsymbol{Re}$	Reynolds number
$\boldsymbol{s}$	Specific entropy, J/kg.K
$\boldsymbol{\dot{S}_{gen}}$	Entropy generation rate, W/K
$\boldsymbol{\dot{S}'_{gen}}$	Entropy generation rate per unit length, W/K.m
$\boldsymbol{St}$	Stanton number
$\boldsymbol{T}$	Temperature, °C
$\boldsymbol{\Delta T_{lm}}$	Log mean temperature difference for counter-flow heat exchanger, °C
$\boldsymbol{U}$	Overall heat transfer coefficient
$\boldsymbol{V}$	Volume, m^3
$\boldsymbol{\dot{V}}$	Volume flow rate, m^3/s
$\boldsymbol{\dot{W}}$	Power, W

Abbreviations

$\boldsymbol{CA}$	Cooling air
$\boldsymbol{CS}$	Carbon Capture and Storage

CS	Cooling system
$DCHE$	Downhole Coaxial Heat Exchanger
EGM	Entropy Generation Minimisation
EES	Engineering Equations Solver
HE	Heat exchanger
HDR	Hot-Dry-Rock
GP	Geothermal Preheater
GWP	Global Warming Potential
$HPFWH$	High Pressure Feedwater Heater
K	Kelvin
kg	Kilogram
kJ	kiloJoule
kPa	kiloPascal
kW	kilowatt
$LPFWH$	Low Pressure Feedwater Heater
MW	Megawatt
$O\&M$	Operation and Maintenance
ORC	Organic Rankine Cycle

Greek Symbols

ϵ	Heat exchanger effectiveness, %
η_I	First law efficiency, %
η_{II}	Second law efficiency, %
η_{th}	Thermal efficiency, %

$\boldsymbol{\mu}$	Dynamic Viscosity, kg/m.s
$\boldsymbol{\nu}$	Specific volume, m^3/kg or dimensionless volume
$\boldsymbol{\rho}$	Density, kg/m^3
$\boldsymbol{\tau}$	Dimensionless temperature difference
$\boldsymbol{\psi}$	Specific exergy, J/kg

Subscripts

$\mathbf{0}$	Reference state
$\mathbf{1-18}$	Thermodynamic states
$\boldsymbol{a}$	Annulus
$\boldsymbol{ac}$	Actual
$\boldsymbol{B}$	Baffles
$\boldsymbol{C\ or\ c}$	Condenser or cold stream
$\boldsymbol{D}$	Diameter
$\boldsymbol{dest}$	Destruction
$\boldsymbol{E}$	Evaporator
$\boldsymbol{frict}$	Friction
$\boldsymbol{geo}$	Geothermal fluid
$\boldsymbol{gen}$	Generation
$\boldsymbol{H\ or\ h}$	Hot stream
$\boldsymbol{i}$	Inner
$\boldsymbol{in}$	Inlet
$\boldsymbol{is}$	Isentropic
$\boldsymbol{lam}$	Laminar

$\boldsymbol{m}$	Mean
$\boldsymbol{max}$	Maximum
$\boldsymbol{min}$	Minimum
$\boldsymbol{net}$	Net
$\boldsymbol{o}$	Outlet or overall
$\boldsymbol{opt}$	Optimal
$\boldsymbol{p}$	Pump
$\boldsymbol{pp}$	Pinch point
$\boldsymbol{PH}$	Preheater
$\boldsymbol{rej}$	Rejection
$\boldsymbol{rev}$	Reversible
$\boldsymbol{s}$	Shell side
$\boldsymbol{sat}$	Saturated
$\boldsymbol{t}$	Turbine or Tube side
$\boldsymbol{th}$	Thermal
$\boldsymbol{turb}$	Turbulent flow
vap	Vaporisation

1 INTRODUCTION

1.1 Subject and Motivation for Report

Energy-related projects have had significant negative impacts on the environment for many years. Therefore, it is crucial to initiate and develop energy projects that sustain the economy while preserving the environment [1].

Over the years, we have seen increasing international concerns regarding air quality, water quality and greenhouse gas emissions. In light of these concerns, policy analysts and planners are realising the potential that geothermal energy has to help meet clean air obligations and decarbonise the energy sector both of which essentially involve the displacement of fossil fuels [1].

Energy security, energy equity and environmental sustainability are three goals that constitute the Energy Trilemma as coined by the World Energy Council [2;3]. These three goals are the main drivers of structural changes within the energy sector. They provide a clear framework to ensure that sustainable energy systems become a reality.

More than 80% of our current energy needs are met by coal, gas and oil. As of 2016, geothermal energy accounts for less than 1% of electricity generated [1]. Unfortunately, this situation shows very little sign of changing over the medium term without drastic policy changes.

1.2 Background to Investigation

The global warming crisis has led to a worldwide call for the exploration of renewable sources of energy. The use of renewable energy is a solution that is currently being explored extensively. There are different kinds of renewable energy resources: solar, wind, ocean, hydro, geothermal, etc. This project focuses on the use of geothermal resources by integrating them with non-renewable resources in a bid to improve efficiency primarily through harnessing electrical energy and reducing the carbon footprint.

Geothermal energy is derived from the Greek word ‘geo’ meaning from Earth and thermal from ‘thermos’ meaning heat. Therefore, geothermal means heat from the Earth (heat energy extracted from underground).

Geothermal energy is considered renewable because its source is unlimited [1]. However, according to Axelsson [4], the classification of geothermal energy as renewable is an

oversimplification of the potential of geothermal energy. This claim is backed by highlighting the double nature of geothermal resources where it can either be a combination of an energy current through heat convection and conduction or just stored energy. Geothermal power plants use heat from deep within the earth to generate steam to make electricity. Wells are drilled up to 3 km into the earth to pump steam or hot water to the surface. Figure 1.1 shows a cross-section of the Earth and gives an idea of the unlimited heat contained within the Earth's core.

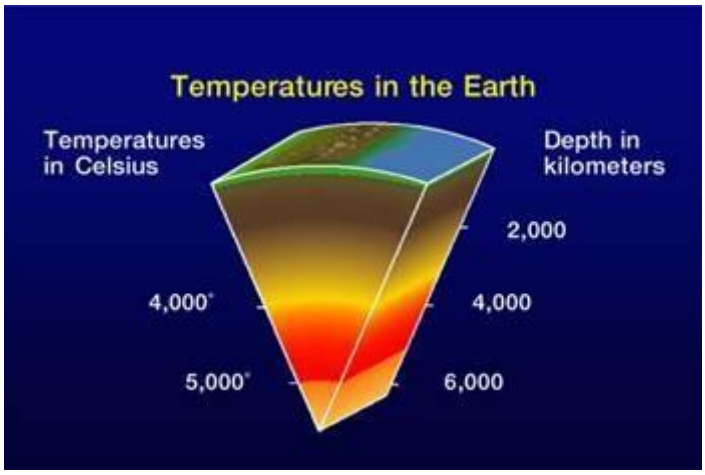

Figure 1.1: Temperatures in the earth [Geothermal Education Office]

1.3 Objectives of the Report

Technological advancements around the world are making it easier to harness energy from low temperature resources. For this reason, low-enthalpy geothermal energy is becoming increasingly popular. One of the main objectives of this report is to show how low temperature geothermal resource can be retro-fitted into a traditional fossil-fuelled power plant to increase efficiency and thus produce more power. Another main objective is to optimise a hybrid fossil geothermal system by minimising entropy generation in the feedwater heaters as well as the geothermal heat exchanger which is used as a replacement for a low-pressure feedwater heater. The lost work (inefficiency/irreversibilities) in the system is due to entropy generated (also known as exergy destroyed). Therefore, optimisation will involve the energy and exergy analysis of the designed power plant followed by minimisation of the entropy generated. (List objectives with numbers or bullets

The results of this study will show that reducing the system inefficiencies will allow more work to be done and thereby increase the power generated from the system.

1.4 Scope and Limitations

The analysis and results reported in this study are based on different forms of a simplified model of a Rankine cycle that were modelled to achieve the research objectives. The models represent simplified versions of existing power plants, where each model excludes the intermediate turbine and consists of a limited number of feedwater heaters. The geothermal resource was selected to be a moderately low-temperature, liquid dominated source in the range of 110°C to 160°C. The results inferred from the analysis were validated and therefore, can be applied to already existing power plants. Two main hybridization approaches were discussed: Fuel Saving approach and the Power Boosting approach.

Literature reports several investigations where entropy is used as an evaluation parameter. The measure of entropy has thus been used in different forms including: Entropy generation rate; Entropy generation number; Augmentation entropy generation number; Heat exchange reversibility norm (HERN); Witte–Shamsundar efficiency and Local entropy generation number. The research work presented here is limited to: entropy generation rate and entropy generation number as well as second law efficiency and exergy analysis, used for the optimisation of the Downhole Coaxial Heat Exchanger and the Counterflow Heat Exchanger respectively.

There are also various constraints regarding the optimisation of the feedwater heater that are discussed in the methodology. However, of these constraints, only two are analysed in detail.

1.5 Plan of Development

This report sets out to describe the process that was undertaken to achieve the objectives of the research. It begins with a literature review. In the literature review, background information is given on renewable energy which is then narrowed down to geothermal energy. The review gives details on the various applications of geothermal energy as well, paying specific attention to the potential market for geothermal energy in South Africa.

The literature review is then followed by methodology. The methodology gives a detailed theoretical analysis of the methods used to generate the results needed to achieve the objectives which include thermodynamic analysis as well as thermodynamic optimisation.

The results are then reported and discussed. Since research is an ongoing process, the research undertaken here is part of the broader research of renewable energy and therefore, there is

always room for further development, recommendations and/or insights which are discussed along with the conclusion. The conclusion gives a summary of the important results and reflects on the objectives and whether they were all obtained.

2 LITERATURE REVIEW

2.1 Characteristics of Geothermal Energy

Like any other energy resources, geothermal energy has both advantages and disadvantages. However, in light of the energy crisis (discussed before), the environmental advantages are quickly outweighing economic advantages of fossil-fuelled power plants.

The advantages, disadvantages and other critical characteristics of geothermal energy are subsequently discussed.

2.1.1 Advantages and Disadvantages of Geothermal Energy

Some of the merits of geothermal energy are that it is non-polluting and environmentally friendly; it does not generate any by-products or wastage. It can be used directly (e.g. heating buildings, heating water) or indirectly (e.g. for electricity generation). Also, it does not occupy a lot of space, it is not dependent on the weather condition and it is not affected by the fluctuations in fuel costs. Geothermal energy also has cultural, social and economic benefits in terms of tourism and recreational values. Additionally, it greatly reduces the dependence on imported oil and therefore, countries like Kenya, that have a good portion of their electricity produced from geothermal energy, save a great deal in terms of imported oils [5]. And since its source is unlimited, the growth of geothermal energy potential and use is not resource constrained.

Unfortunately, there are a few areas with high geothermal energy potential and where these areas do exist, they are far from towns and cities which makes the direct and indirect use of them costlier due to increased transportation costs. Further, they are prone to triggering seismic activity like earthquakes and dormant volcanoes. Installation costs of geothermal power plants are very high and unfortunately, there is no guarantee that the energy produced from the geothermal source will justify the capital expenditure.

2.1.2 Impacts of geothermal development

Geothermal development can affect the land use in different ways including:

- Triggering seismic effects such as earthquakes
- Land subsidence

Land subsidence occurs when large amounts of groundwater have been taken from underground natural water sources. Since water is partly responsible for holding the ground up, when too much water has been taken from underground, the ground appears to sink because the rocks compact [6;7] .

There are documented cases of land subsidence (Steamboat Springs, USA and Waira-Tauhara, NZL). Subsidence can damage infrastructure like roads and buildings as well as irrigation systems. In the early years of electricity production from geothermal energy, land subsidence was a common problem but now, because of improved methods of re-injection, and improved surface monitoring techniques by regulatory authorities, the chances of its (subsidence) occurrence have been reduced [1;8].

Relative to other energy technologies, geothermal power plants use less land. They (power plants utilising geothermal energy) also require minimal transportation because they are usually built around the energy source. On the downside, geothermal extraction involves the discharge of harmful gases into the air and chemicals into the water and onto the land. The geothermal fluids that are used contain several dissolved gases, mostly carbon dioxide and nitrogen and a few traces of ammonia and hydrogen sulphide. Low and moderate temperature fluids have lower concentrations of these harmful gases than do high temperature fluids [1].

Power plants that make use of geothermal energy also have the potential to impact the local community, if operated close to one. Noise, odour and the rights to fresh ground water would quickly become the main concerns of the local community [1].

Greenhouse gas emissions from geothermal power plants mentioned beforehand are much lower compared to those from fossil-fuel power plants.

2.1.3 Geothermal Power Plant as a Base Load Plant

A base load power plant is a power plant that produces power at a constant rate. There is a long-standing myth that renewable energy sources cannot provide baseload power. As mentioned above, geothermal energy is a reliable source of energy because it is always available as solar and wind energy. For this reason, geothermal can produce power all day hence it is a renewable energy source capable of providing baseload power. Geothermal energy has a higher capacity factor than wind and solar energy. This means that compared to solar and wind energy, geothermal can produce more electricity with a smaller capacity.

Other renewables that can provide baseload power are concentrated solar-thermal power and bio-electricity which is generated from burning the residues of crops and plantation forests [9].

2.2 Geothermal Energy Statistics

Geothermal is a reliable source because it is always available. Unlike wind and solar, it is independent of the weather conditions. The best locations for geothermal power plants are in the Ring of Fire which is a geologically and volcanically active region that stretches from one side of the Pacific to another. Almost 90% of all earthquakes and volcanoes occur in this region because hot magma is very close to the surface [10;11].

In Africa, the Great East African Rift System is also a great location for geothermal power plants. The Great East African Rift is a major tectonic structure of the Earth. Figure 2.1 shows the regions around the world with high geothermal potential. It also gives a rough estimate of the amount of power that has been harnessed in the few regions where this renewable source has been explored.

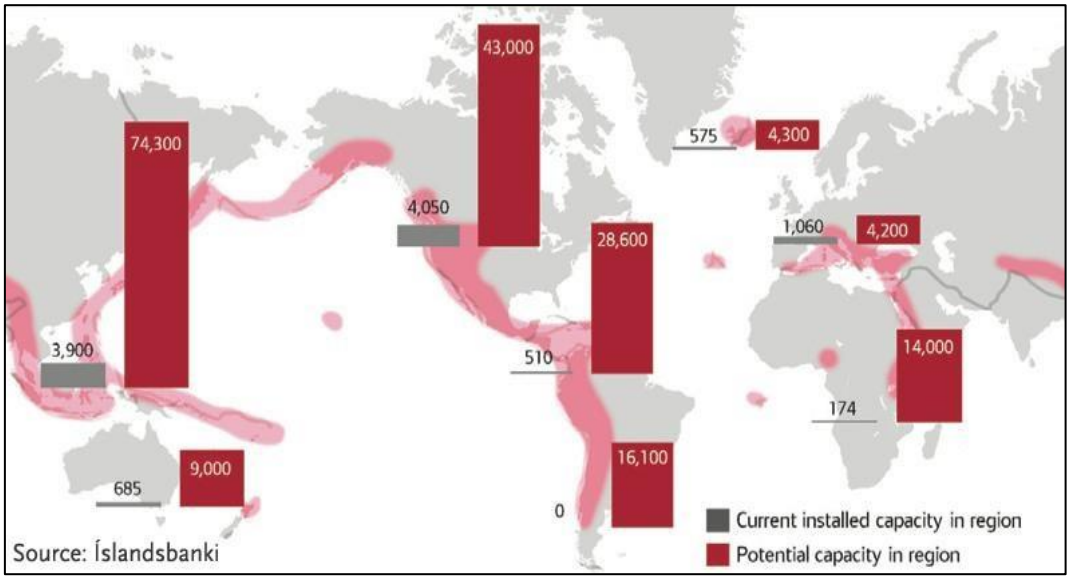

Figure 2.1: World Geothermal Potential [source: Islandsbanki]-provide date of the source

Figure 2.2 shows the top 10 leaders in geothermal power capacity at the end of 2017, with the USA leading with a capacity of 3.6 GW. The top 10 is dominated by Asian countries (Phillipines, Indonesia and Japan) as well as European (Italy, Turkey and Iceland). Kenya is the only African country that makes this top 10. Countries like Ethiopia share the riches of the Great Rift Valley with Africa. However, development of geothermal projects has been very

limited. This shows that there is not enough investment being pumped into the development of geothermal energy projects [12].

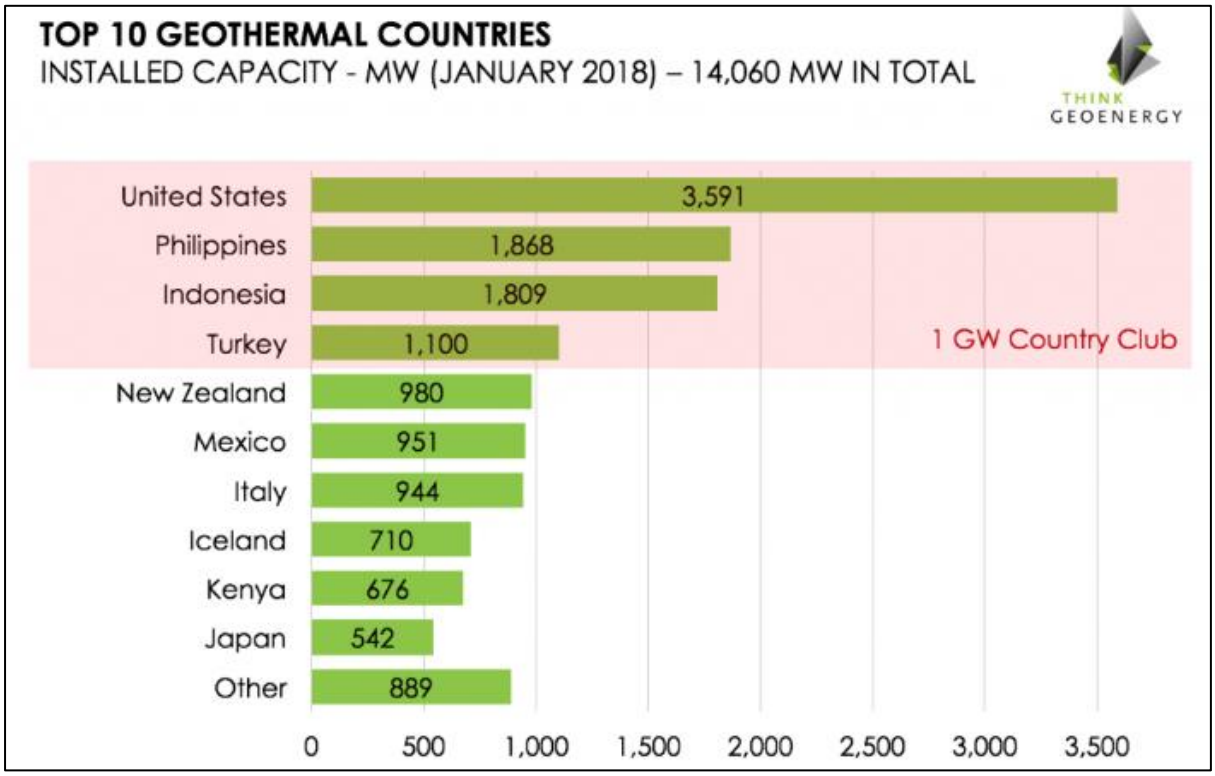

Figure 2.2: Top 10 Geothermal Countries based on Installed Power Generation Capacity [source: Think GeoEnergy]-provide date of the source

2.3 Geothermal Energy Resources

Geothermal resources can be categorised into three different types: hydrothermal sources, geopressured sources and petrothermal sources.

2.3.1 Hydrothermal Sources

With hydrothermal sources, there are two sub-types: vapour-dominated and liquid dominated. These are high temperature sources (>160 $^{\circ}$C) and they are used mainly for power generation. The water is brought to the surface by either pumping it or drilling wells. The pressure drop experienced during this process results to the fluid flashing into two-phase mixture of low quality. One of the major problems associated with this source is that the fluid often contains high concentration of dissolved solids. This poses a problem with power generation because these dissolved solids are notorious for causing scaling in pipes and heat exchangers [13].

2.3.2 Geopressured Sources

Geopressured systems are essentially water-based resources (like the hydrothermal liquid-dominated resource). The difference is that with geopressured sources, the water is trapped and pressurised in deeper underground aquifers, saturated with natural gas or methane. Although this source has great thermal and mechanical potential for power generation, it poses economic challenges because of the high cost of drilling at such depths [13].

2.3.3 Petrothermal Sources

Petrothermal sources, as the name suggests, involve rock: hot dry rock heated by the Earth's magma. To extract thermal energy from petrothermal sources, water is pumped into the resource and back out to the surface. The hot water can then be used for power generation, as with the hydrothermal sources. Petrothermal systems provide more flexibility in design and operation: although the ability to drill to various depths is economically constrained, it allows the operators to control the water flow rate and temperatures [13].

2.4 Geothermal Power Plants

Geothermal power plants differ from the conventional fossil or nuclear power plants in the way they produce steam and the quality of steam that is produced. In geothermal power plants, steam is produced from the Earth's heat. It is produced naturally. The steam could either be in the form of dry, superheated steam or pressurised hot water depending on the nature of the reservoir.

Geothermal fluids are classified using temperatures or enthalpy. The most common being enthalpy. Geothermal fluids have a temperature range of 30-350 $^{\circ}$C and therefore exist as either dry steam, two-phase (steam and liquid mixture) or as liquid. High enthalpy geothermal resources are typically most effective for electricity generation and low enthalpy geothermal sources for direct use e.g. heating. Medium and high enthalpy resources can be used to wash and dry wool, manufacture pulp or treat biomass.

High enthalpy geothermal resources were explored as early as 1913 when the first geothermal power plant in history was built in Larderello, Italy [14;15]. Geothermal energy plays a major role in some countries. For instance, 17% of the electricity produced in the Phillipines comes from geothermal energy and geothermal sources account for a staggering 66% of Iceland's primary energy use [1].

There are various technologies being used to convert geothermal energy into electricity. These include [16]:

- Condensing power plants which include dry steam, single flash and double flash systems for high temperature sources.
- Back pressure power plants which make use of back-pressure turbines.
- Binary power plants for lower temperature sources.
- Hybrid power plants.

Some of the geothermal power plants listed above are discussed in detail:

2.4.1 Dry steam

Dry steam power plants are found mostly in areas with a high geothermal resource temperature. Figure 2.3 shows a schematic of a dry steam. It is a one-cycle system that makes use of naturally occurring dry, saturated or slightly superheated steam that is filtered by a rock catcher (to prevent damage to turbine blades) prior to driving the turbine. This steam is sourced from geothermal reservoirs with temperatures exceeding 170 °C. The condensed water is re-injected into the reservoir through the injection well.

Some operating dry steam geothermal power plants include: PG&E, unit 18, 120 MW (The Geysers, California) and Valle Secolo, unit 2, 57 MW (Larderello, Tuscany, Italy) [17].

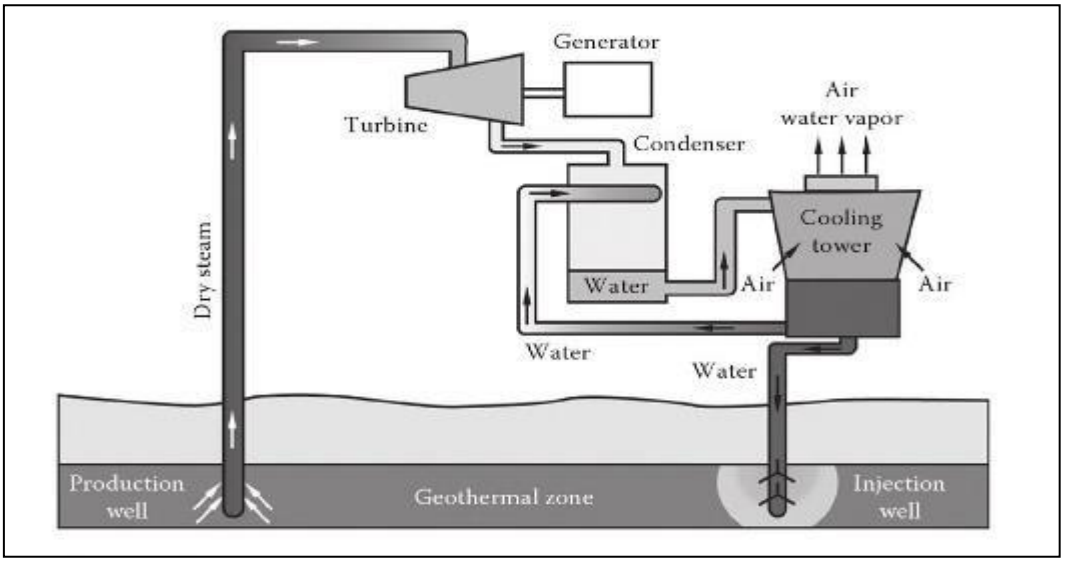

Figure 2.3: Diagram of dry steam geothermal system [8]

2.4.2 Flash steam

These are the most common type of geothermal power plants (shown in Figure 2.4). Fluid at very high temperatures is pumped to the surface under very high pressure. It is pumped into a tank on the surface which is held at low pressure. This causes the fluid to flash to steam. The steam is then used to drive the turbine which drives the generator thereby producing electricity. There are two basic types of flash steam power plants:

- Single flash
- Double flash

Some existing single-flash steam geothermal power plants are: Miravalles, unit 1, 55MW (Guanacaste, Costa Rica); and Blundell, 24 MW (Milford, Utah) [17].

Some existing double-flash steam geothermal power plants include: Hatchobaru unit 2, 55MW (Kyushu, Japan); and Beowawe, 16.7 MW (Beowawe, Nevada) [17].

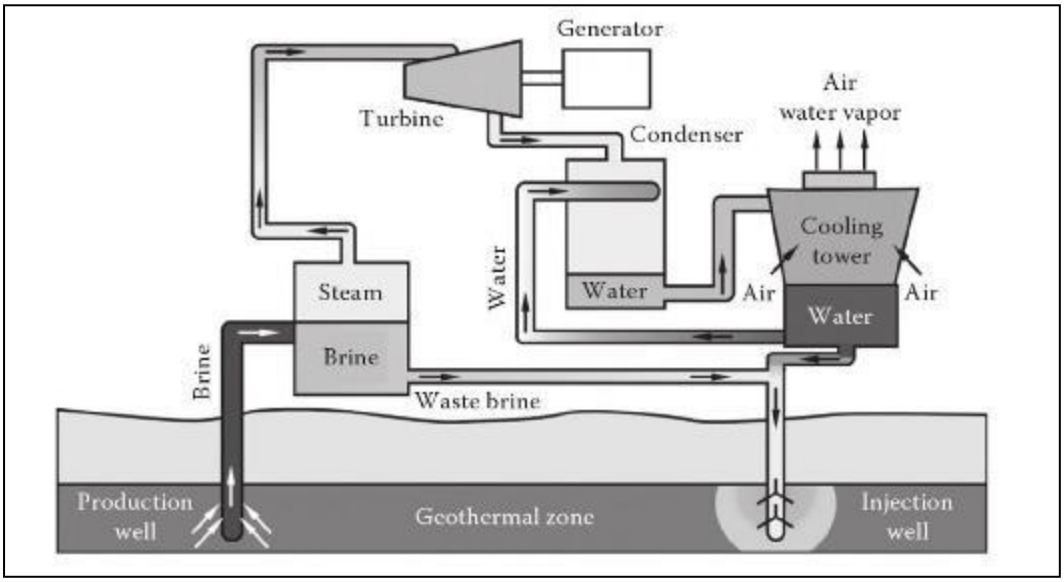

Figure 2.4: Diagram of a single flash geothermal system [8]

2.4.3 Binary system

In binary cycle power plants, two fluids (a primary fluid and a secondary fluid) are utilised. This system is typically found in areas with low-to-medium geothermal resource temperatures. Most geothermal power plants around the world utilise a variation of this power plant. The primary fluid is the geothermal fluid and, in an ORC, (Organic Rankine Cycle), the secondary

fluid is a hydrocarbon such as isobutane or isopentane, that has a lower boiling point than water. In a Kalina cycle, the secondary fluid comprises of a water solution of ammonia [18]. The two fluids do not mix and the secondary fluid functions as the working fluid.

Figure 2.5 illustrates this type of geothermal power plant. Because of its low boiling point, a low-to-medium geothermal resource temperature is adequate to boil the working fluid. Some existing operating binary plants include: Heber binary demonstration, 65 MW (Heber, California); Second Imperial Geothermal Co., 12x 40 MW (Heber, California); and Amedee, 2x 2 MW (Wendel, California) [17].

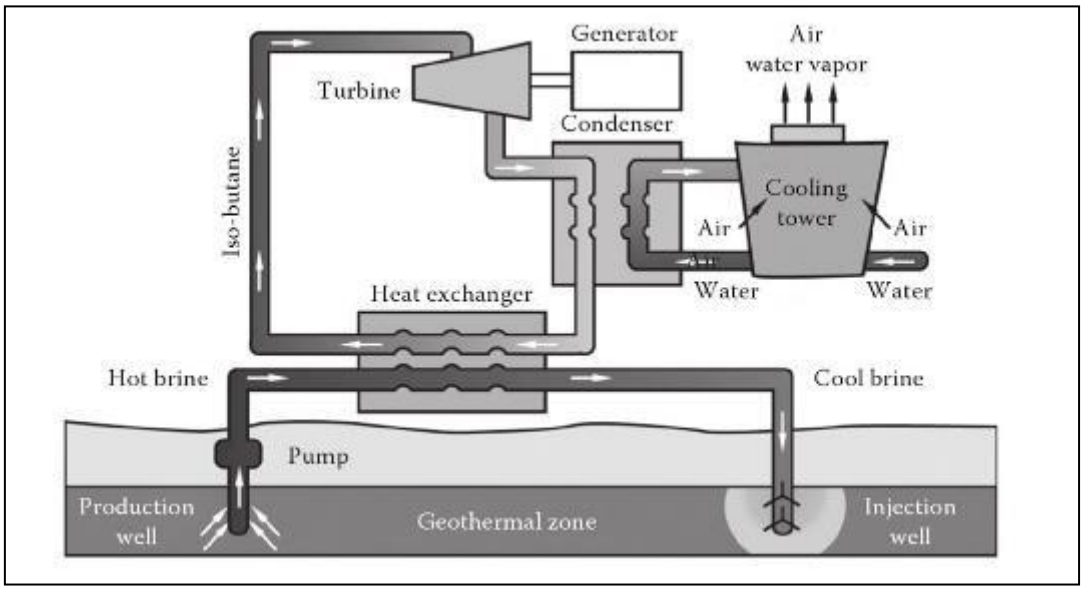

Figure 2.5: Diagram of a binary geothermal system using iso-butane as the secondary working fluid [8]

2.4.4 Hybrid power plants

The concept of hybrid power plants was first presented in the late 70s by DiPippo et al. [19; 20]. The hybrid power plants include both: hybrids of two different energy sources (e.g.: fossil-geothermal or solar-geothermal); or hybrids of two different geothermal technologies (e.g. binary and flash). Fossil fuel technologies are very carbon-intensive technologies. Therefore, the power plants that combine a fossil-fuel technology with geothermal energy aim to reduce natural resource consumption as well as the negative environmental impacts associated with the use of fossil fuels. Some hybrid power plants are elaborated below:

2.4.4.1 Fossil-geothermal hybrid system

As the global warming crisis continues, the ideal solution to environmental conservation is to replace all non-renewables with renewables. However, this is not a realistic solution. Power plants that run on fossil fuels will continue to function for many years to come. Therefore, it is important to implement solutions that will help to reduce the emissions from existing fossil-fuelled power plants.

Hybrid fossil-geothermal systems have been studied in detailed for many years. They were first presented in the late 1970s by DiPippo et al. [21-23]. As the name suggests, these kinds of power plants use both fossil fuels and geothermal energy. There are different hybrid configurations. The two main ones being the geothermal preheat system and the fossil superheat system. In the geothermal preheat system, shown in Figure 2.6, geothermal energy is used in a fossil-fuelled power plant to preheat the working fluid or the feedwater prior to entering the boiler. This increases the overall. The feasibility of implementing such a power plant requires that the existing traditional steam power plant be located close to a geothermal resource. [16; 22; 23]. A real-life example of a power plant that makes use of geothermal energy to preheat the feedwater is the Neustadt-Glewe power plant in Germany [24].

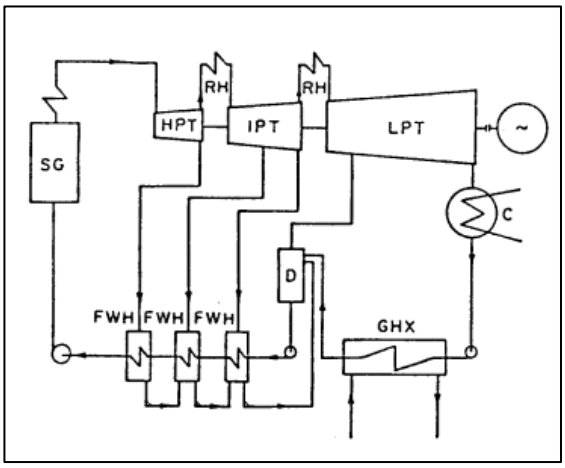

Figure 2.6: Geothermal preheat hybrid system with multiple feedwater heaters [21]

In the fossil superheat system configuration, as shown in Figure 2.7, fossil fuel is used to superheat the working fluid in a geothermal power plant. The fluid is superheated prior to entering the turbine. This increases the overall efficiency of the system because more work can be generated by the turbines. It also protects the turbine from premature wear as the moisture in the working fluid is removed in the superheater. The superheater is important because it improves the cycle efficiency by increasing the average temperature at which heat is added.

Metallurgical concerns are the most common and major concerns regarding the superheating of steam.

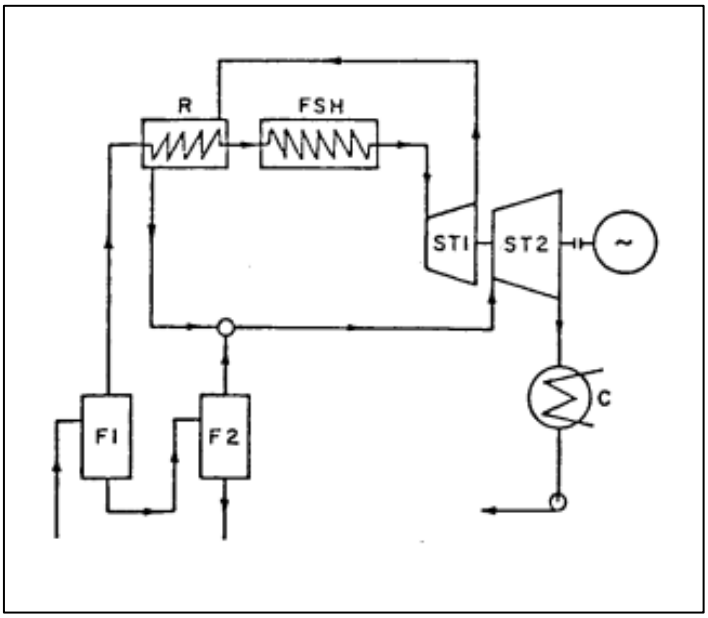

Figure 2.7: Two-stage fossil superheat hybrid system [21]

Finally, the two hybrid systems described above can be combined to form what is known as a compound hybrid system as illustrated in Figure 2.8.

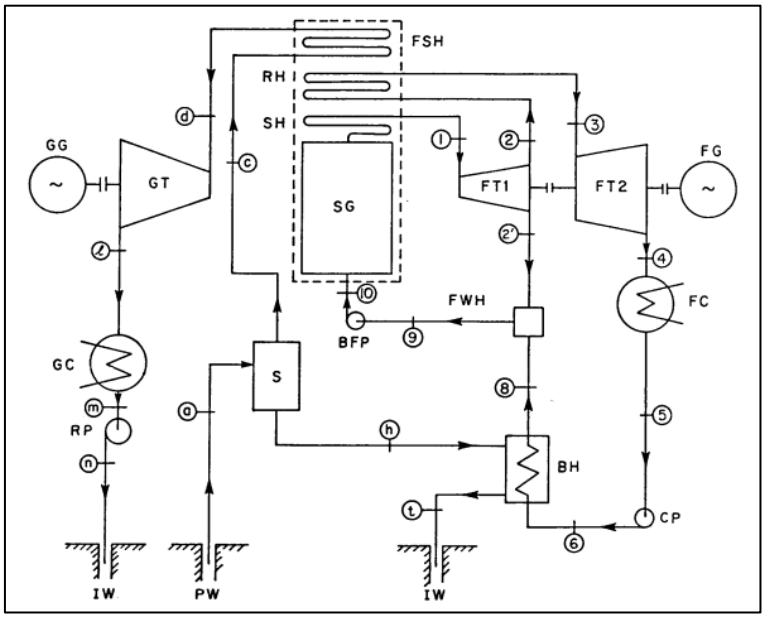

Figure 2.8: One-stage Compound Hybrid System [21]

Hybrid wood-waste/geothermal plant, 30 MW (Honey Lake, California) is an example of a hybrid fossil-geothermal power plant currently in operation.

2.4.4.2 Solar-geothermal hybrid

As the name suggests, both solar and geothermal energy are used to produce electricity. There are different configurations of the solar-geothermal hybrid power plant as well. The three main types are solar preheat system, solar superheating system and a geothermal preheat system. In the former configuration, solar energy is used to preheat the temperature of the brine from underground or to increase the steam temperature. In the solar superheat system (Figure 2.9), solar energy superheats the working fluid in a geothermal power plant, like the function of the fossil fuel in the fossil superheat system. Finally, the geothermal preheat system uses the geothermal energy to preheat the feedwater in a solar thermal power plant.

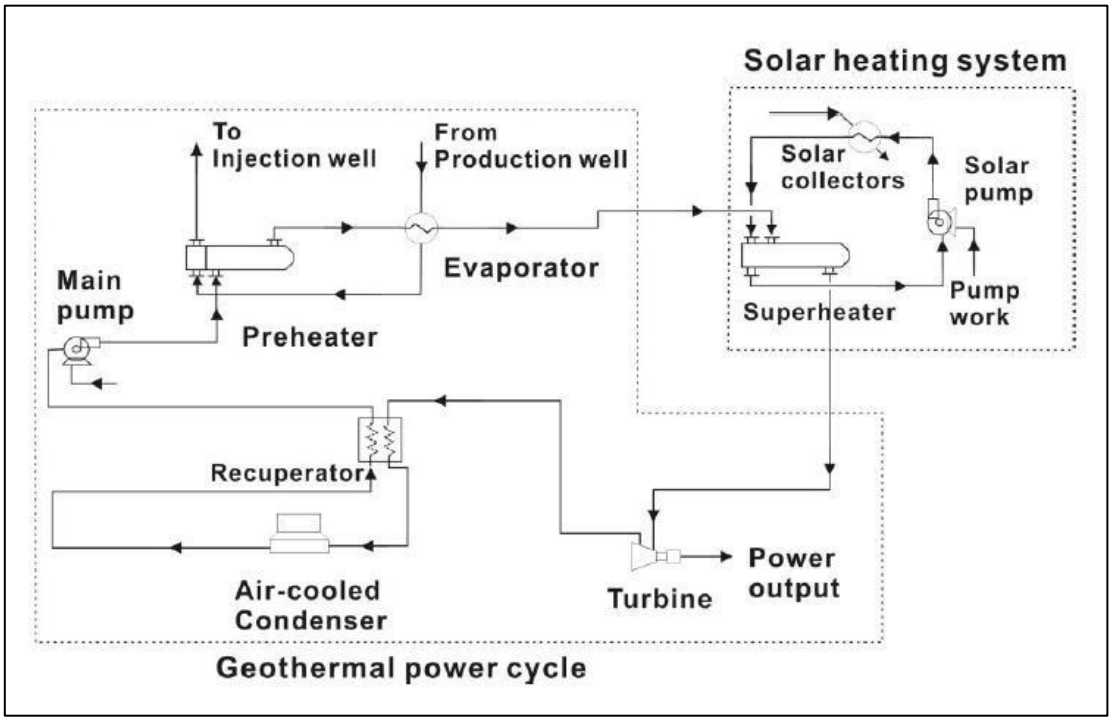

Figure 2.9: Diagram of hybrid solar-geothermal system [25]

The first operating hybrid solar-geothermal power plant was developed in Fallon, Nevada in early 2012. It is known as the Stillwater geothermal project. This power plant has advanced the local economic growth and it has contributed to the local reduction of pollution. The National Renewable Energy Laboratory conducted a study that revealed the creation of 75,000 jobs through the development of the hybrid power plant.

2.4.4.3 Hybrid binary-flash

These power plants are a hybrid of the flash system and the binary system. They allow for the optimisation of both flash and binary technologies. The geothermal fluid is separated into steam

and liquid in the separator. The steam is used to power a flash steam generator and the liquid serves as the primary fluid in the binary system.

Other hybrid systems include [26]:

- Hybrid single-flash and double-flash
- Hybrid geothermal-biomass

2.4.4.4 *Ellipse Law for Multistage Turbine*

When renewable energy such as solar or geothermal is used to replace the bled steam from one or more of the turbines (hybrid system), the mass flow rates change resulting in the turbines being operated under off design conditions. The Ellipse law, developed by Aruel Stodola [27], establishes a method to calculate the changes and thus determine the new mass flow rates through the various stages in the turbine. Applying the Ellipse law to the geothermal preheat power plant analysed in this research would generate more accurate results of the performance of the turbine and therefore, the cycle. The analytical equation for the flow ratio is [27]:

$$\frac{D_1}{D_{10}} = \sqrt{\frac{P_1^2 - P_2^2}{P_{10}^2 - P_{20}^2}} \sqrt{\frac{T_{10}}{T_1}} \tag{2.1}$$

Where D_1 is the design flow rate, D_{10}: the off-design flow rate; P_1 and P_2: the designed inlet and outlet pressures respectively; P_{10} and P_{20}: the off-design inlet and outlet pressures respectively; and lastly, T_1 and T_{10}: are the design and off-design inlet temperatures respectively.

2.4.5 Back pressure power plants

These make use of back-pressure turbines which are also known as 'non-condensing' turbines. These types of turbines are used when the need for low to medium pressure steam arises. Back pressure type systems are the least expensive and have the lowest overall thermal efficiency [18].

2.5 Geothermal Trends

The worldwide installed geothermal capacity, as of 2010 was 10.7 GW. Out of which, 29% is from dry steam power plants, 37% from single flash, 25% from double flash, 8% from binary/combined cycle/hybrid power plants and the remaining 1% from back-pressure power plants [9]. Kenya, Indonesia and the Philippines are all countries that are rich in geothermal

resources. Kenya and Indonesia are two countries that have put frameworks in place that will ensure significant geothermal development in the coming years. GEA (Geothermal Energy Association 2016 Geothermal Power: International Market Update) states that 1 562.5 MW of developing geothermal energy capacity was added between March and September of 2016. This developing capacity is a product of 44 new geothermal projects across 23 countries that began development in 2016. The increase in electricity production using geothermal energy can be attributed to the advancements in drilling and excavation technologies [28].

In 2015, Olkario geothermal power plant in Kenya, which is the largest geothermal power plant in Africa, produced 280 MWe. The Geysers in California USA boasts the biggest geothermal installation in the world, with an installed capacity of 1,517 MW. The Geysers is a complex geothermal system consisting of 18 geothermal power plants [29].

2.5.1 Trends in geothermal investment

According to the World Energy Council, the global investment in geothermal energy in 2015 was US$2billion. This investment was estimated to be about 23% less than that made in 2014. Figure 2.10 traces the new investment in geothermal energy spanning the period: 2004-2015. And Figure 2.11 shows the global investing by region spanning the same period.

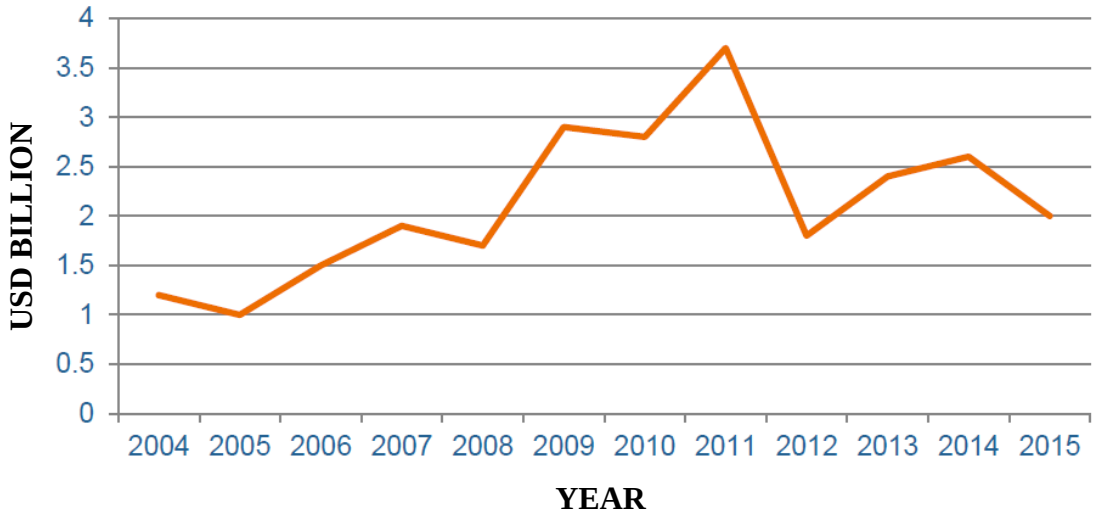

Figure 2.10: Annual New Investment in Geothermal Energy, 2004-2015 (USD BILLION) [1] **Provide labels

Figure 2.11 shows Africa to be the region with the least investment in geothermal energy and Asia with the highest. Investment banks like JICA (Japan International Corporation Agency)

and IADB (InterAmerican Development Bank) are two key major players in driving an increase in electricity production from geothermal energy.

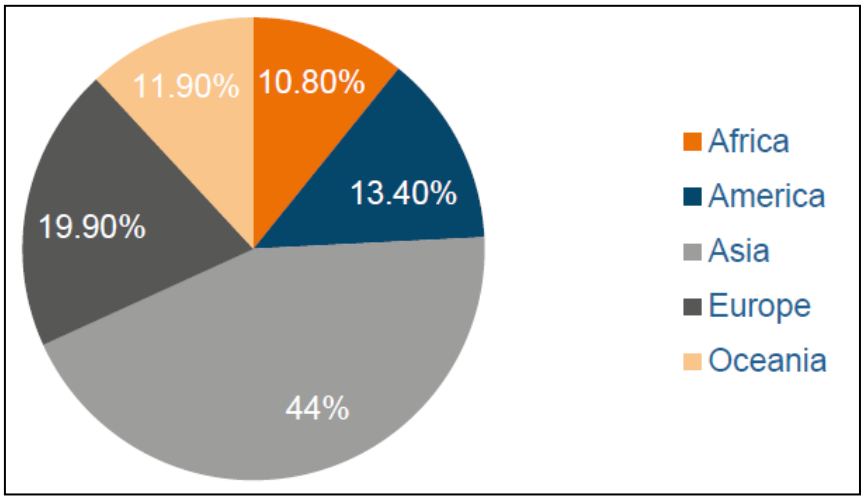

Figure 2.11: Global Investment by region from 2010-2015 by region, in percentage [1]

In Africa, the African Development Bank (AfDB) is committed to invest in projects that will contribute to alleviating Africa's energy deficit. The AfDB was extensively involved in financing the development of Menengai power projects in Kenya [30]. These projects have proved to be a major success and because of this success, AfDB has vowed to increase the share of its clean energy financing portfolio to 100%. The AfDB is clearly paving the path to ensure that industrialisation in Africa takes place in a green way [31].

There are several factors that limit investment in geothermal energy projects. Allie Nelson, a Geothermal News and Communications Specialist at the GEA states: "if geothermal is freed of bureaucratic red tape and can achieve parity with wind and solar for incentives, a new and brighter future is on the horizon" [28].

The above statement indicates that there are excessive regulations on the exploration of geothermal sources of energy which essentially gets in the way of decision making, particularly when comparisons are made with other renewable energy sources. This slows down potential progress and advancements in the exploration of geothermal energy. The community along with the state and governments have a major role to play in ensuring the success of geothermal technologies. Success in geothermal energy use is dependent on the integrated efforts of all concerned parties

2.5.2 Development Costs

Drilling costs associated with the geological and reservoir conditions or the drilling equipment itself account for most high costs and cost overruns. Well costs are also a significant economic component of the development of a geothermal power plant. These costs can account for approximately 60% of the total capital investment [32].

Advances in drilling practices are necessary because they are projected to be more economic in the long run. Less civil construction and improved productivity compensates for the high costs of advanced drilling practices. Essentially, a new geothermal power plant can cost more than a natural gas or fossil fuel facility at the initial stages but they are economically comparable in the long run. The initial investment of a geothermal power plant is high but the operation and maintenance (O&M) costs are low compared to lower initial investment costs and high O&M costs of fossil fuelled power plants [32].

2.5.3 Trends in the Cost of Energy

Although the cost of fossil fuels continues to rise, it is still significantly cheaper than geothermal energy and other renewable energy sources. However, fossil fuels are being depleted at an exponential rate and energy demand is increasing. At some facilities, the cost of electricity production from geothermal energy has decreased to nearly half the original price (back in the 1980s when the first geothermal power plant was commissioned). Geothermal costs have steadily decreased over the years but the same cannot be said for fossil-fuelled power plants. This is partly due to the environmental costs imposed on these power plants, which include: land degradation, emission of toxic chemicals, forced extinction of animals and health impact to humans. The fluctuations in the costs of fossil fuels negatively impact the economy and therefore the stable cost of geothermal energy is what makes it an attractive solution to the current energy crisis. Essentially, geothermal energy is competitive with other non-renewable energy technologies when environmental costs are taken into consideration.

Research-driven improvements are needed in the following areas:

- Drilling technology
- Power conversion technology
- Reservoir technology

Improvements in the above-mentioned areas can lead to further reductions in the cost of geothermal energy [33].

2.6 Geothermal Energy Exploration in Africa

Regarding geothermal energy, Africa is predicted to be a high-growth region given that the upcoming years will see other East African countries such as Uganda, Ethiopia, Rwanda and Tanzania developing their geothermal power production sector. These countries lie within the region known as the East African Rift System (EARS). The EARS consists of three main arms namely: the Red Sea Rift, the Gulf of Aiden Rift and the East African Rift. As mentioned previously, in this system, tectonic forces try to create new tectonic plates by splitting old ones apart. The East African Rift is one of the geological wonders of the world. This region is estimated to have a geothermal potential of approximately 10 000 MWe [34].

Exploration of this potential could help to significantly reduce the impacts of global warming and provide a solution to the global energy crisis. The increasing demand for electricity, the silting of hydropower resources, natural disasters like drought as well as the high import costs and the unpredictable nature of petroleum prices has led to East African countries exploring the geothermal energy contained within the EARS [35-36].

There is a great need to tap into geothermal energy for electricity production. Currently, Kenya is the only country in East Arica with active geothermal operations. This is due to its limited hydro resources which have been affected by severe droughts and it is also due to its success in geothermal development. The greatest drawback faced by most East African countries is the lack of investment as well as a lack of expertise in electricity production from geothermal energy. Governments in East Africa plan to promote geothermal resource exploration by attracting private investors through the establishment of incentives and long-term conducive policies; apply for loans and grants from International Organisations to finance geothermal exploration and development [35].

In Africa, a continent with a developing economy and increasing energy demand, most of the growth in electricity production from geothermal is likely to take place in Kenya due to easier accessibility to the abundant geothermal resource [37]. And since it has a developing economy, the development bank can be employed to facilitate the construction of geothermal structures, as cited previously.

2.6.1 Potential for Electricity Production from Geothermal Energy in South Africa

South Africa is not geographically favoured to economically exploit geothermal resources: it does not have any active volcanoes and unlike East African countries like Kenya with an upper crust that is ever expanding, South Africa has a thick upper crust. Because of this, heat from the mantle cannot penetrate close enough to the surface and that is why drilling for geothermal sources >5km becomes a very expensive development (about R1.45 billion for only 50MW geothermal power). An additional factor that holds back the use of geothermal sources in South Africa is the lack of renewable energy feed in tariff in South Africa: for example, where Germany offers 1-5 ZAR/kWh, South Africa offers R0. There are no incentives to encourage the exploration of this renewable energy source [38].

The low price and high availability of fossil-fuels along with a lack of knowledge of the technology necessary to explore geothermal resources are also factors that limit South Africa's prospects for geothermal energy production.

Although South Africa is not geographically advantaged to make optimum use of geothermal sources, it is not devoid of geothermal potential. Low to medium temperature sources can be used to preheat feedwater in fossil-fuelled power plants; the ORC technology could be implemented and used to generate high pressure steam from very low-quality heat (using low temperature geothermal sources) [38-39].

Taufeeq Dhansay et al. [38] investigated South Africa's geothermal energy hotspots inferred from subsurface temperature and geology. From their study, they identified five promising regions in South Africa (Figure 2.12) where low enthalpy geothermal energy can be explored and developed.

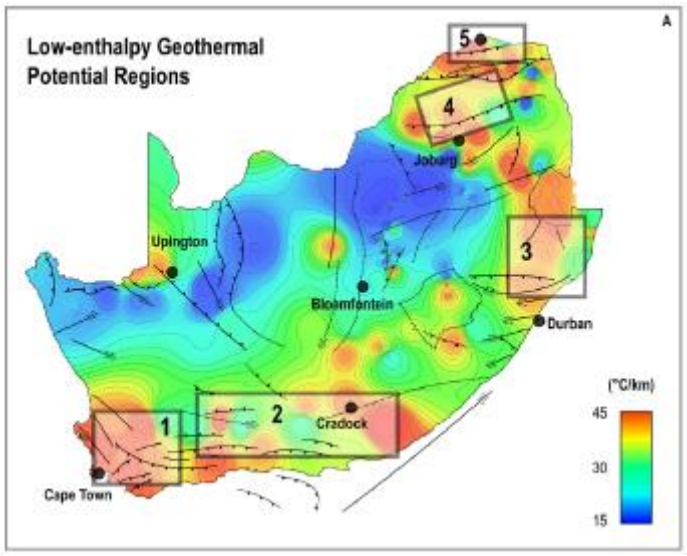

Figure 2.12: Regions with low-enthalpy geothermal potential

One of the major factors inhibit South Africa's growth in the harnessing geothermal energy is the need for significant research and data acquisition which will allow for a more precise evaluation of South Africa's geothermal energy potential [38]. It will also highlight the negative impacts to be expected from exploring geothermal energy. To enable this research, and encourage development, it is imperative to create sustainable economic models as is commonly the case when investing in new developments.

2.7 Advanced Geothermal Systems

2.7.1 Enhanced Geothermal Systems (EGS)

Enhanced Geothermal Systems (EGS), sometimes called Engineered Geothermal Systems (EGS): Over the past few years, new technologies have been developed to create energy by injecting water into dry (low permeability) rocks such as fractured granite. Therefore, hot underground water is not the only source of geothermal energy.

Essentially this system consists of drilling two wells, not too far from each other, as illustrated in Figure 2.13. In one well, cold water is injected at very high pressure (represented by Well 1 in Figure 2.13). This water then creates a network of fractures in the rock. Once the water has been heated, well 2 is used to extract the heated water (represented by Well 2 in Figure 2.13). Thereafter cold water is constantly injected into the ground via well 1 and extracted after being heated via well 2 and pumped to the surface to be used for power generation [40 - 42].

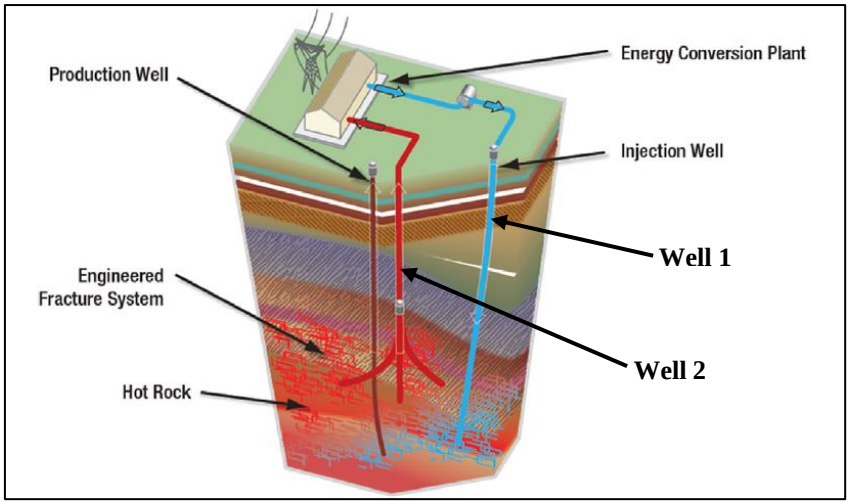

Figure 2.13: Basic layout of an EGS type geothermal power plant [41]

EGS provides the opportunity to expand the use of geothermal energy considerably. Additional production wells are drilled to extract enough heat to produce electricity that will meet demand. EGS allows for power to be generated from geothermal resources that are otherwise not economical because they lack water and permeability. This is a very clean and renewable way of geothermal energy because It completes a circulation.

One of the major problems associated with EGS is the danger of inducing seismic activity. Although researchers say that seismic activity induction can be used as a diagnostic tool, public concern cannot be overlooked. The World Energy Council has reported that EGS purposely induces micro-earthquakes to increase permeability. This characteristic of EGS cannot be overlooked in future developments. Making EGS more cost-effective would mean making technological advances that will make EGS competitive with other energy sources [42].

2.7.2 Using End-of-Life Oil Fields

There is an increasing need to elongate the life of ageing oil fields and reduce operating costs. Depleted oil fields could be converted into geothermal reservoirs. The co-production of geothermal energy from oil or gas fields is a possibility. Some oil and gas developments have high temperature as well as large volumes of water. Geothermal energy could be harnessed from the hot water associated with oil reservoirs in sedimentary basins [43-44].

Another perspective to this technology involves the sequestering of CO_2. This is an option to reduce the amount of CO_2 emitted into the atmosphere. End-Of-Life oil fields are one of the

geological targets considered for sequestration. The sequestration process and how it can be used to harness geothermal energy is explained in the section below.

2.7.3 CPG (CO_2 Plume Geothermal Power)

As mentioned previously, a promising strategy to combat global warming involves the capture and storage of carbon dioxide, also known as Carbon Capture and Storage (CCS). Essentially, the CO_2 produced from fossil fuelled power plants is captured or removed before it is emitted into the atmosphere. The CO_2 that is captured is then compressed into a liquid. From there, it can be pumped into a large geological reservoir. Since CO_2 has a relatively light density, when it reaches the underground reservoir, it lies above the other fluids [45].

CO_2 flows more easily than water and therefore it can extract the same amount of energy as water but with less effort. The amount of power that can be generated is dependent on the difference between the pressures of the two wells (low pressure at injection well and high pressure at extraction well). CO_2 expands to the extent that it buoyantly rises to the surface, a phenomenon known as the thermo-siphon effect. This eliminates the need to use well pumps to draw the CO_2 to the surface. A new type of geothermal power plant known as the CO_2 plume geothermal power plant makes use of the improved flow rate of CO_2, the increased pressure difference as well as the thermo-siphon effect to produce electricity. Also, this is possible at shallower, cooler depths than is possible with water. This technology can also be used to store wind and solar energy when it is not in high demand. This will help to reduce wastage [46-47].

2.8 Heat Exchangers

Heat Exchangers are thermal systems that allow the transfer of heat from one fluid to another. The heat transfer may be needed for varying reasons such as: using a hotter fluid to heat up a cooler fluid; using a cooler fluid to reduce the temperature of a hotter fluid; using a hot fluid to boil a liquid; using a cooler fluid to condense a gaseous fluid; and boiling a liquid while condensing a hotter gaseous fluid.

Heat exchangers play a major role in energy conservation and are used extensively in power plant engineering, chemical industries, refrigeration, air conditioning, etc. [48].

Typical applications of heat exchangers in the different industries mentioned above include: heating or cooling of the fluid stream and evaporation or condensation of the fluid stream. In other applications, they recover or reject heat, sterilise, pasteurise, concentrate, crystallise or

control a process fluid. The primary objective of the heat exchanges optimised in this research are to preheat (feedwater) and reject heat (condenser) [49].

There are different flow arrangements that can be found in heat exchangers. The difference between them lies in the amount of heat transfer surface area required to allow a certain amount of heat transfer to take place. There are three main types of flow arrangements namely:

- Parallel flow or concurrent where two fluids enter the heat exchanger at the same end, travel in parallel and exit at the same end.
- Counterflow or counter current where two fluids enter the heat exchanger on opposite ends and exit at opposite ends as well. This flow arrangement is the most efficient.
- Cross flow:
  - Single pass cross flow where the two fluids flow roughly perpendicular to one another through the heat matrix.
  - Multi pass cross flow where one fluid moves back and forth across the flow path of the other flow path of the other fluid stream, giving a crossflow approximation to counter-flow.

Of the three types of flow arrangements, counterflow is the most efficient. It is thermodynamically superior to any other flow arrangement. This can be attributed to the fact that the average temperature between the two fluids over the length of the heat exchanger is maximised in a counterflow arrangement. The log mean temperature for a counterflow heat exchanger is larger than that of a parallel or cross flow heat exchanger [50].

However, in reality, the flow arrangement of most heat exchangers is a combination of at least two or even all three flow arrangements mentioned above. This enables the heat exchanger effectiveness to be maximised within the restrictions that have been placed on the heat exchanger design. Some of these restrictions include: size, cost, weight, required efficiency, operating pressures and operating temperature [50-51].

Heat exchangers can also be classified as regenerative or non-regenerative. This research project focuses on the regenerative type. A regenerative type is one where the same fluid is both the cooling fluid and the heating fluid. Essentially, the hot fluid gives up its heat to regenerate or heat up the fluid returning to the system. They are usually found in high temperature systems like power plants, where a portion of the system's fluid is removed from the main process and then returned. These are therefore used to improve efficiency because the

fluid removed from the main process contains energy which is used to reheat or regenerate the returning fluid instead of being rejected to an external cooling medium such as air or water (as in the condenser). Regenerative refers to the workings of the heat exchangers and not necessarily the type [49;52].

2.8.1 Selection Criteria

The following criteria can be used to select the most suitable heat exchanger from the available ones:

- The heat exchanger must satisfy the process requirements and function properly until the next scheduled maintenance.
- Related to the former point, the heat exchanger must be maintainable which essentially means that it must be built in a way that allows for the cleaning and replacement of any component.
- The heat exchanger must resist corrosion and fouling from the process streams and the environment as well.
- The heat exchanger must be cost-effective.
- The heat exchanger must comply with size limitations imposed.

2.8.2 Shell and Tube Heat Exchangers

The regenerators in the system that was designed for this project were modelled as shell and tube heat exchangers. Shell and tube heat exchangers are the most versatile type of heat exchangers. They provide relatively large ratios of heat transfer area to volume and weight. They can be cleaned easily, and they offer great flexibility to meet almost any service requirement. Shell and tube heat exchangers can be designed for very high pressures relative to the environment. They are built of round tubes mounted in large cylindrical shells with the tube axis parallel to that of the shell. One fluid flows inside the tubes while the other flows across and along the tubes [53-54].

Figure 2.14 shows the working mechanisms of a counterflow shell and tube heat exchanger. The baffles are commonly placed in the shell to force the shell side fluid to flow across the shell to enhance heat transfer and to maintain equal spacing between the tubes.

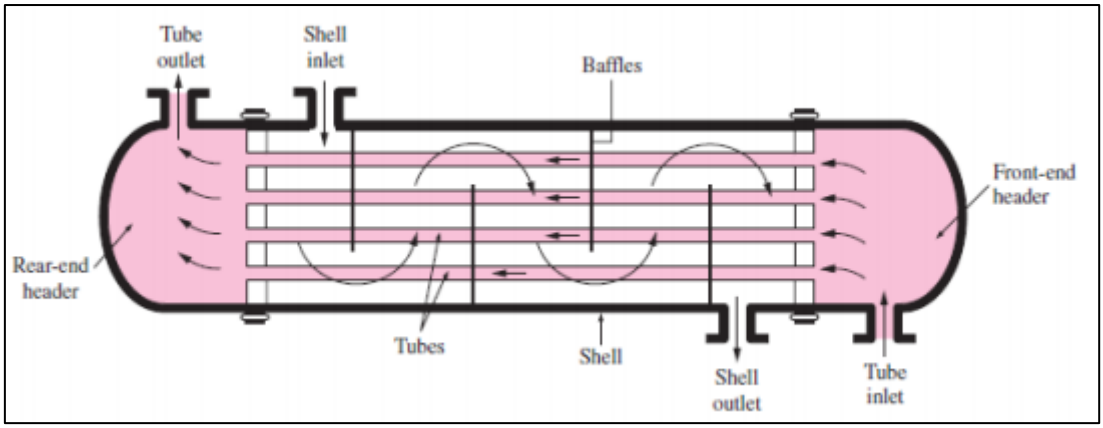

Figure 2.14: Schematic of a Counterflow Shell and Tube Heat Exchanger [54]

Shell and tube heat exchangers are classified and constructed according to TEMA (Tubular Exchangers Manufacturers Association) standards.

An ideal heat exchanger is completely reversible. Unfortunately, the heat transfer process is inherently irreversible and therefore, the closest to reversible we can get is minimising the irreversibility [55]. Heat exchangers are characterised by two main types of thermodynamic losses: one is associated with the heat transfer across a finite temperature difference and the second is associated with pressure drop due to friction. The losses associated with heat transfer can be mitigated by increasing the heat transfer area and decreasing the local temperature difference. However, an increase in the heat transfer area can lead to increased frictional losses and therefore increased pressure drop. This illustrates the conflicting nature of these two losses. These losses are elaborated numerically in the methodology section to follow [56].

2.8.3 Downhole Coaxial Heat Exchanger (DCHE)

This heat exchanger consists of a gravel-filled well, closed loop system where the heat transfer fluid is continuously circulated through the Earth in a closed pipe system without ever directly contacting the soil or water in which the loop is buried. The cold water is pumped downwards into the annular space, and heated across the annular wall by the increasingly warmer rock material as it flows [57]. The heated stream then returns to the surface through the inner pipe which is insulated to minimise heat loss to the surrounding. This is illustrated in Figure 2.15. Although the use of downhole coaxial heat exchangers is limited, they eliminate the problem of geothermal fluid disposal because only heat is extracted from the well [57-58].

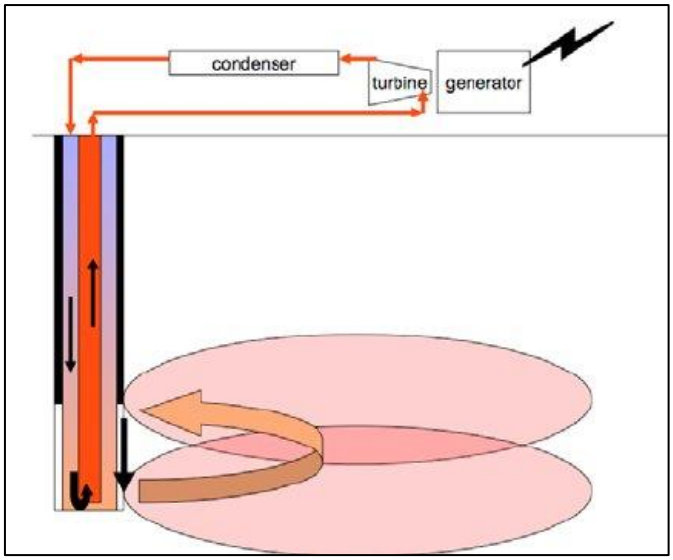

Figure 2.15: Sketch of single-well, coaxial downhole heat exchanger with fractures [59]

2.8.4 Deaerator

Oxygen and other non-condensable gases in the feedwater are the major causes of corrosion in the piping and boiler. It is important to remove these gases because they have the potential to damage the boiler which is a very expensive power plant component to replace. The deaerator is part of the feedwater heating system. It can be modelled as a mixing chamber that mixes extraction steam from the turbine with the condensate (feedwater) that has just been preheated in the geothermal heat exchanger [27]. The condensate and the extraction steam then mix in the deaerator with the condensate being heated to saturation conditions and the steam being condensed. In a conventional Rankine Cycle power plant, with regeneration, the feedwater exits the deaerator as a saturated liquid at the same pressure as the extracted steam from the low-pressure turbine. Heating the deaerator to saturation conditions allows for the solubility of the gases to be lowered to zero. Dissolved gases are then released into the atmosphere. The ideal exit state of the mixture in the deaerator is a saturated liquid at the deaerator pressure [60].

There are two main types of deaerators: the spray type (which is the most commonly used, shown in Figure 2.16) and the tray type (shown in Figure 2.17).

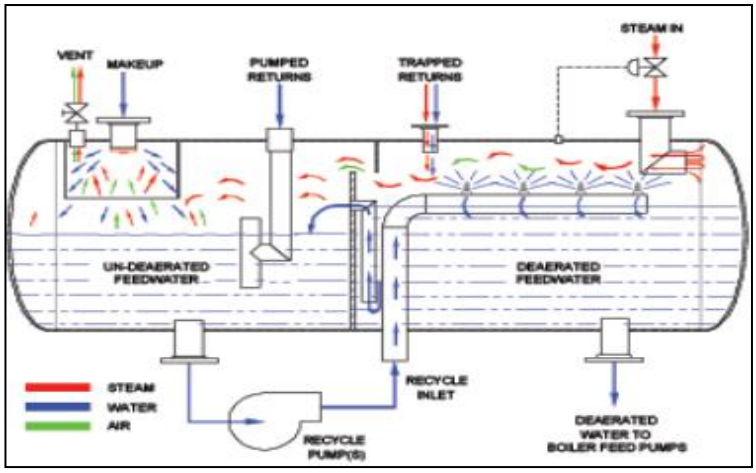

Figure 2.16: Schematic of spray-type deaerator [28]

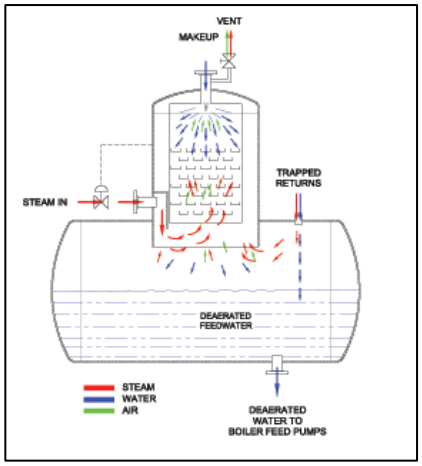

Figure 2.17: Schematic of tray-type deaerator [Industrial Steam]

3 METHODOLOGY

The exergy method and the entropy generation minimisation method can both be used for thermodynamic optimisation of system components. The exergy method makes use of the first law, the second law and environmental properties. The EGM method on the other hand, is characterised by system modelling, development of entropy generation rate as a function of the parameters of the model and the ability to minimise the entropy generation rate.

Geothermal energy is integrated into a fossil-fuelled power plant. Software was used to predict the effect of this integration on the overall efficiency as well as optimise system components, in particular, the preheaters, feedwater heaters and the geothermal preheaters.

3.1 Modelling

Two cycles were modelled in this study: A simplified reheat regenerative cycle (with two high pressure feedwater heaters) and a single low-pressure feedwater heater. In the second cycle, the low-pressure feedwater heater was replaced with a geothermal preheater. Both designs were modelled using Engineering Equations Solver (EES). And the components of interest (preheaters: feedwater heaters and geothermal preheater) were optimised using Matlab.

3.1.1 Hybrid Concepts

Kolb [61], discussed two functional basic approaches to hybridizing a renewable energy source to a fossil fuelled power plant: Fuel Saver approach and Power Booster approach. Figure 3.1 illustrates the two operational modes. In the fuel saving mode, the power output of the steam turbine remains constant (in the fossil-fuelled power plant and the hybridized fossil-fuelled power plant). Therefore, geothermal energy is used to decrease the boiler heat load by reducing the mass flow rate of feedwater into the boiler.

In the power boosting mode, the boiler consumes the same amount of fuel (in the fossil-fuelled power plant and the hybridized fossil-fuelled power plant). Therefore, unlike in fuel saving mode, the mass flow rate of feedwater heater entering the boiler does not change. The geothermal energy is therefore primarily used as preheater and eliminates the need for steam to be extracted for preheating thereby allowing for further expansion in the low-pressure turbine. This results to an increase in generated power [61-63].

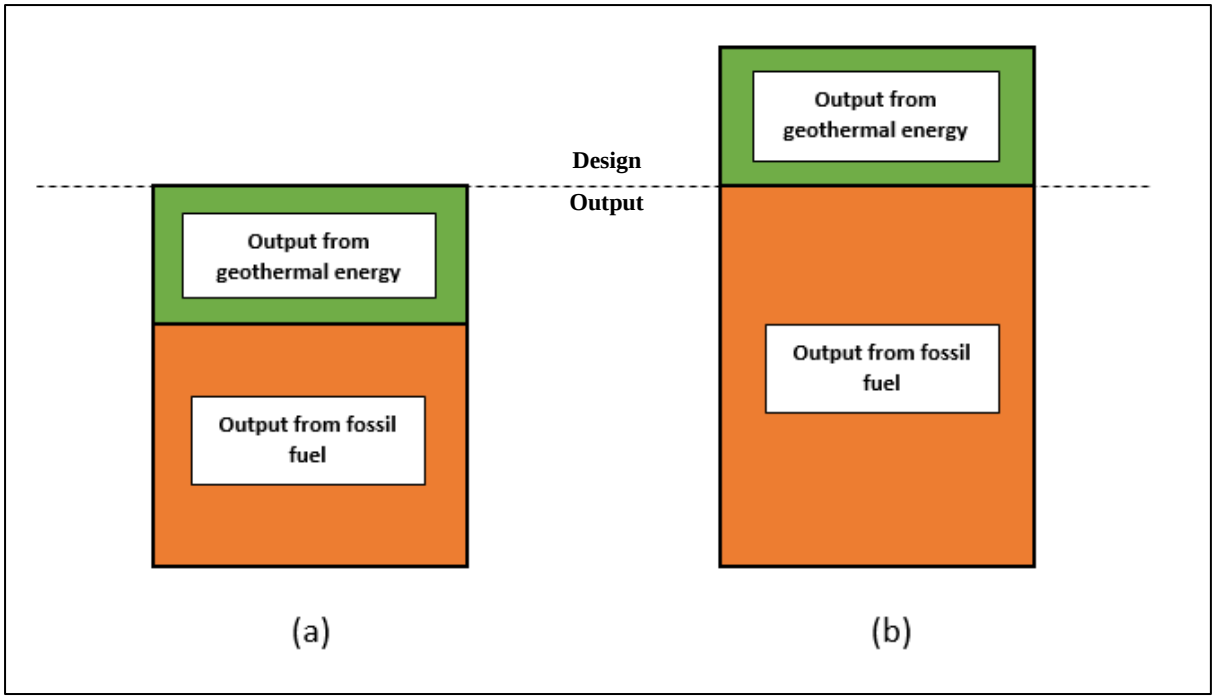

Figure 3.1: Two operational models of a geothermal preheat hybrid system: (a) Fuel saver; (b) Power booster

3.2 Heat Exchanger Design

Equation 3.1 represents a summary of four core heat exchanger design methods. The equation is based on energy balances which are a result of the first law of thermodynamics as well as the mass conservation principle [50].

$$\begin{pmatrix} \boldsymbol{heat\ transfer} \\ \boldsymbol{rate\ q} \end{pmatrix} = \begin{pmatrix} \boldsymbol{effectiveness/} \\ \boldsymbol{correction\ factor} \end{pmatrix} * \begin{pmatrix} \boldsymbol{heat\ capacity\ rate\ or} \\ \boldsymbol{thermal\ conductance} \end{pmatrix} * \begin{pmatrix} \boldsymbol{temperature} \\ \boldsymbol{difference} \end{pmatrix}$$

$$= \begin{Bmatrix} \varepsilon C_{min} \Delta T_{max} & in\ \varepsilon - NTU\ method \\ P_1 C_1 \Delta T_{max} & in\ P - NTU\ method \\ FUA\Delta T_{lm} & in\ LMTD\ method \\ \psi UA\Delta T_{max} & in\ \psi - NTU\ method \end{Bmatrix} \quad (3.1)$$

The most common design methods used are the $\varepsilon - NTU$ method as well as the $LMTD$ method. The two methods will be analysed for a tubular, counter-flow, heat exchanger case. Firstly, the overall heat transfer coefficient "U" for a clean (no fouling) tubular heat exchanger can be calculated using the following equation:

$$U_o A_o = U_i A_i = \frac{1}{R_t} = \frac{1}{\frac{1}{h_i A_i} + \frac{ln(r_o/r_i)}{2\pi kL} + \frac{1}{h_o A_o}} \quad (3.2)$$

Where: R_t is the total thermal resistance to the heat flow across the surface between the inside and the outside flow.

3.2.1 LMTD method:

A trial and error method would be used if the LMTD method is being applied and the inlet and outlet temperatures of the fluid streams are unknown. The LMTD method is discussed below.

$$\ln \frac{T_{h2} - T_{c1}}{T_{h1} - T_{c2}} = UA \left(\frac{1}{C_c} - \frac{1}{C_h} \right) \quad (3.3)$$

Substituting C_c and C_h yields the following expression for the heat transfer:

$$Q = UA \frac{(T_{h1} - T_{c2}) - (T_{h2} - T_{c1})}{\ln\left(\frac{T_{h1} - T_{c2}}{T_{h2} - T_{c1}}\right)} \quad (3.4\text{ a})$$

OR:

$$Q = UA \frac{\Delta T_1 - \Delta T_2}{\ln\left(\frac{\Delta T_1}{\Delta T_2}\right)} \quad (3.4\text{ b})$$

Where: ΔT_1 is the temperature difference between the two fluids at the one end and ΔT_2 is the temperature difference on the other end of the heat exchanger.

From the above equation, the average temperature difference between the hot and cold fluids over the entire length of the heat exchanger can be expressed as:

$$\Delta T_{lm} = \frac{\Delta T_1 - \Delta T_2}{\ln\left(\frac{\Delta T_1}{\Delta T_2}\right)} \quad (3.5)$$

The above equation is known as the Log Mean Temperature Difference. The total heat transfer rate in a counterflow heat exchanger can be expressed as:

$$Q = UA\Delta T_{lm} \quad (3.6)$$

3.2.2 E-NTU METHOD:

To avoid using the trial and error procedure, the method of Number of Transfer Units (NTU) based on the concept of heat exchanger effectiveness can be used. This method is based on the fact that the inlet or exit temperatures are a function of:

$$\frac{UA}{C_c} \quad \text{and} \quad \frac{C_c}{C_h} \tag{3.7a,b}$$

Where "c" and "h" denote the cold stream and hot stream respectively.

The heat capacity rate ratio is defined as:

$$C^* = \frac{C_{min}}{C_{max}} \tag{3.8}$$

The heat transfer effectiveness is expressed as:

$$\varepsilon = \frac{Q}{Q_{max}} \tag{3.9}$$

Where Q represents the **actual** heat transfer.

The actual and maximum heat transfers can be calculated as follows:

$$Q = \left(\dot{m}c_p\right)_h (T_{h1} - T_{h2}) = \left(\dot{m}c_p\right)_c (T_{c2} - T_{c1}) \tag{3.10}$$

If $C_h > C_c$ then $(T_{h1} - T_{h2}) < (T_{c2} - T_{c1})$ (3.11a)

If $C_h < C_c$ then $(T_{h1} - T_{h2}) > (T_{c2} - T_{c1})$ (3.11b)

$$Q_{max} = \begin{cases} \left(\dot{m}c_p\right)_c (T_{h1} - T_{c1}) \ \textbf{if} \ C_h > C_c \\ \left(\dot{m}c_p\right)_h (T_{h1} - T_{c1}) \ \textbf{if} \ C_h < C_c \end{cases} \tag{3.12 a,b}$$

From equations (3.9) and (3.12), the heat transfer rate can be expressed in terms of ε as:

$$Q = \varepsilon\left(\dot{m}c_p\right)_{min} (T_{h1} - T_{c1}) \tag{3.13}$$

From equations (3.10) and (3.12), heat exchanger effectiveness can be expressed as:

$$\varepsilon = \frac{C_h(T_{h1} - T_{h2})}{C_{min}(T_{h1} - T_{c2})} = \frac{C_c(T_{c2} - T_{c1})}{C_{min}(T_{h1} - T_{c1})} \tag{3.14}$$

The number of transfer units, NTU, defined as the ratio of the overall thermal conductance to the smaller heat capacity rate is expressed as:

$$NTU = \frac{UA}{C_{min}} = \frac{1}{C_{min}} \int UdA \tag{3.15}$$

NTU designates the non-dimensional heat transfer size of the heat exchanger. There are a number of expressions that have been developed for different flow types, to relate the effectiveness to the NTU. Considering a single-pass counterflow heat exchanger and assuming $C_h < C_c$ so that $C_h = C_{min}$ and $C_c = C_{max}$ we obtain [50]:

$$\varepsilon = \frac{1-exp\left[-NTU\left(1-\frac{c_{min}}{C_{max}}\right)\right]}{1-\left(\frac{c_{min}}{C_{max}}\right)exp\left[-NTU\left(1-\frac{c_{min}}{C_{max}}\right)\right]} \tag{3.16}$$

Two limiting cases are of interest:

Case 1: $\frac{c_{min}}{C_{max}} = 1$ (3.17 a)

Case 2: $\frac{c_{min}}{C_{max}} = 0$ (3.17 b)

For **Case 1**, the effectiveness equation becomes indeterminate. Applying L'Hopital's rule yields:

$$\varepsilon = \frac{NTU}{1+NTU} \tag{3.18}$$

For **Case 2** (as is the case in boilers and condensers), the effectiveness equation becomes:

$$\varepsilon = 1 - e^{-NTU} \tag{3.19}$$

The magnitude of NTU influences the performance of the heat exchanger, with high NTU values representing high heat transfer rate.

3.3 Assumptions

Several assumptions were made to simplify the model. The environment was assumed to be at ambient conditions of 25°C and 101.3 kPa, reference temperature and atmospheric pressure respectively. The other assumption made for the system components to be optimised are listed below:

3.3.1 Downhole Coaxial Heat Exchanger:

A fundamental design question concerns the selection of the diameter of the inner pipe D_i. The flow is at risk of being impeded if the inner diameter D_i is much smaller than the outer diameter D_o, or if D_i is nearly the same as D_o. In both cases, the pump would be required to overcome an excessive pressure drop. However, fixing D_o, allows for the existence of an optimal D_i or optimal ratio D_i/D_o that would ensure that the pressure drop is minimised. The following assumptions for a DCHE were used in this study:

- The underground temperature increases linearly with depth from the surface of the Earth
- The outer pipe of the DCHE has a very thin wall and is highly conductive
- Negligible heat transfer from the hot stream flowing up and the cold stream flowing down the annular space is ensured by applying an effective layer of insulation to the inner pipe.
- All control volumes operate under steady-state conditions

3.3.2 Counter-Flow Shell and Tube Heat Exchanger:

The following assumptions for a counter flow shell and tube heat exchanger were made in this study:

- There is no significant heat transfer that occurs from the outer surface of the shell.
- Heat losses to the surrounding air are neglected.
- The tubes are straight with smooth inner and outer surfaces.
- Fully developed flow.
- The pressure drops due to contraction and enlargement are negligible.
- Thermal resistance of the tube walls is negligible.
- The two fluids are in counter-flow and under steady-state conditions.

- The viscosity, thermal conductivity and specific fluid of each fluid are constant within the corresponding temperature range.
- The temperature is uniform at any cross section of the stream.
- The overall heat transfer co-efficient U is constant throughout the heat exchanger.
- No change of phase takes place in either fluid.
- Both fluids are stable under operating conditions.
- Both ends of the heat exchanger are adiabatic [64].

3.4 Operating Parameters

3.4.1 Thermodynamic cycle

Table 3.1 shows the operating parameters that were used to model the systems. Note that the T_{in} and T_{out} values refer to the cold and hot water temperatures respectively, used for cooling in the condensing system.

Table 3.1: Operating Parameters for the Rankine cycle

P_0 (kPa) [65]	101.3
T_0 (ºC) [65]	25
Condenser pressure (kPa) [66]	10-60
Deaerator pressure (kPa) [66]	8000-2700
Boiler exit steam temperature (ºC)	600
HP turbine pressure (kPa)	10000
η_{LPT}	0.85
η_{HPT}	0.85
η_P	0.8
T_{in} (ºC)	25
T_{out} (ºC)	37
Pinch point (˚C)	2
Drain Cooler Approach (˚C)	8
$\dot{m}_8$ **(kg/s)**	1

The Terminal Temperature Difference (TTD) and the Drain Cooler Approach temperature (DCA) are two parameters typically used to measure the efficiency of feedwater heaters.

The TTD is a measure of how close the outlet feedwater temperature is to the feedwater saturation temperature. It provides feedback on the feedwater heater's performance relative to heat transfer. An increase in TTD is indicative of a decrease in heat transfer whereas a decrease in TTD is indicative of an improvement in heat transfer.

The DCA is the temperature difference between the drain cooler outlet and the feedwater inlet. It provides feedback on the feedwater heater levels. The DCA temperature is inversely proportional to the feedwater heater level where an increase in DCA temperature represents a decrease in the feedwater heater level and a decrease in DCA temperature represents an increase in the feedwater heater level.

There is a third parameter that is used to monitor the performance of a feedwater heater known as the feedwater temperature rise (TR) which is merely the temperature difference between the feedwater outlet and the feedwater inlet.

3.4.2 Geothermal Resource

Table 3.2 shows the geothermal resource specifications. Low temperature resources have a temperature range of 100 to 160 and a geothermal gradient of 2.4-4.8 °C/100 m [67]. The higher the geothermal temperature gradient, the better because a high temperature gradient leads to lower drilling costs. The gradient is a result of the dissipation of subsurface heat which varies from region to region. The variance can be attributed to the difference in the rock as well as the heat source in that particular region [68]. The environmental temperature is selected to be the same as the $\mathbf{T_0}$ value listed in the Rankine cycle operating parameters table because the geothermal resource will not be located very far from the power plant, hence the environmental conditions are similar.

Table 3.2: Parameters for the geothermal source [67]

Geothermal Source Temperature (°C)	100 - 160
Geothermal Rejection Temperature (°C)	50 - 110
Environmental temperature (°C)	25
Temperature Gradient (°C/100 m)	2.4 - 4.8

3.5 Exergy/Irreversibility Analysis

Energy exists in different forms and it is a quantitative measure. Exergy, is the qualitative measure of energy, it is the work potential of energy in a given environment. An exergy analysis is different from an energy analysis. While energy analysis is based on the law of conservation of energy, exergy analysis is based on the law of degradation of energy. Energy degradation is essentially the loss of exergy through consumption or destruction due to the irreversible nature of real processes. The irreversibility of a system provides a quantitative measure of process inefficiencies [38;39;69-72]

Equations (3.21) and (3.22) demonstrate the difference between energy and exergy:

$$\dot{E}_{in} - \dot{E}_{out} = \dot{E}_{total} \tag{3.21}$$

$$\dot{X}_{in} - \dot{X}_{out} - \dot{X}_{destroyed} = \dot{X}_{total} \tag{3.22}$$

Where E denotes energy and X denotes exergy.

The exergy destruction rate (which is also known as the irreversibility rate) of a process can be expressed in various forms. However, the Guoy-Stodola relation [71,73] provides the most general form (which shows that it is directly proportional to the entropy generated in the system due to the irreversibilities). It is written as:

$$\dot{I} = T_0 \dot{S}_{gen} \tag{3.23}$$

Which states the irreversibility rate is a product of the system's rate of entropy generation and the temperature of the environment.

It is vital to understand energy and exergy efficiencies so that careful consideration can be taken regarding the quality and quantity of energy used to obtain a given objective. This will also enable the attainment of effective and efficient use of energy resources (geothermal and fossil fuels) [71].

Two different exergy efficiencies are defined below:

- A brute force exergy efficiency which is defined as the ratio of the sum of all the output exergy terms to the sum of all the input exergy terms.

- A functional exergy efficiency which is defined as the ratio of the exergy associated with the desired energy output to the exergy associated with the energy expended to achieve the desired output.

The subsequent sub-sections below present the exergy analysis for each power plant component.

3.5.1 Condensate Pump/Boiler Feed Pump

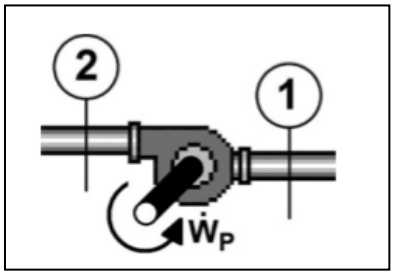

Figure 3.2: Schematic Diagram of Pump

The pump work is a very vital component of the power plant. Its efficient operation can ensure an improvement in power plant performance. For the thermodynamic analysis, the details at the inlet and outlet of the pump will be needed. The primary function of the pump is to provide sufficient pressure to the fluid to move it through the system at the required mass flow rate. In terms of the second law, the pump raises the exergy of the fluid using the least amount of work.

The system consists of two pumps: the condensate pump as well as the feedwater pump. The condensate pump increases the pressure of the condensate from 10 kPa to 1500 kPa. The feedwater pump increases the pressure of the feedwater from 1500 kPa to 10000 kPa. The turbines reverse this process by expanding the pressurised steam and in so doing generate power.

An ideal pump undergoes an isentropic process. However, in reality the irreversibilities within the pump do not allow it to operate isentropically. Hence the isentropic efficiency is a measure of the pump's degree of degradation. It is calculated as:

$$\eta_p = \frac{h_{2s} - h_1}{h_2 - h_1} \tag{3.24 a}$$

The exergy loss is given as:

$$\Delta\varepsilon = \varepsilon_1 + w_p - \varepsilon_2 \tag{3.24 b}$$

(Note: Exergy associated with work is the work itself)

The second law efficiencies are as follows:

Brute force efficiency:

$$\eta_{p,BF}^{II} = \frac{\varepsilon_2}{\varepsilon_1 + \varepsilon_{w_p}} \quad (3.24\ c)$$

Functional efficiency:

$$\eta_{p,FUN}^{II} = \frac{\varepsilon_2 - \varepsilon_1}{\varepsilon_{w_p}} \quad (3.24\ d)$$

3.5.2 Heat Exchanger (Case 1)

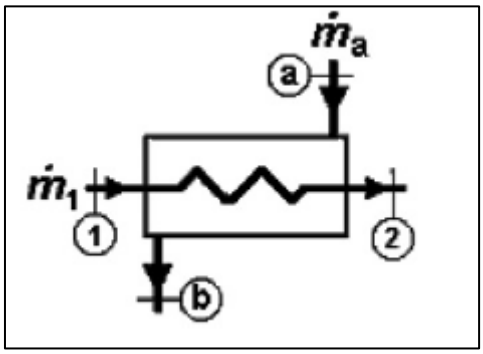

Figure 3.3: Heat Exchanger with two inlets and two outlets [74]

$$\dot{E}x_{IN} = \dot{m}_a(\varepsilon_a - \varepsilon_b) \quad (3.25\ a)$$

$$\dot{E}x_{OUT} = \dot{m}_1(\varepsilon_2 - \varepsilon_1) \quad (3.25\ b)$$

$$\Delta\dot{E}x = \dot{E}x_{IN} - \dot{E}x_{OUT} \quad (3.25\ c)$$

$$\Delta\dot{E}x = \dot{m}_a(\varepsilon_a - \varepsilon_b) - \dot{m}_1(\varepsilon_2 - \varepsilon_1) \quad (3.25\ d)$$

The second law efficiencies are calculated as follows:

Brute Force Efficiency:

$$\eta_{HXer,BF}^{II} = \frac{\dot{m}_1\varepsilon_2 + \dot{m}_a\varepsilon_b}{\dot{m}_a\varepsilon_a + \dot{m}_1\varepsilon_1} \quad (3.25\ e)$$

Functional efficiency:

$$\eta^{II}_{HXer,FUN} = \frac{\dot{m}_1(\varepsilon_2-\varepsilon_1)}{\dot{m}_a(\varepsilon_a-\varepsilon_b)} \quad (3.25\ f)$$

3.5.3 Heat Exchanger (Case 2)

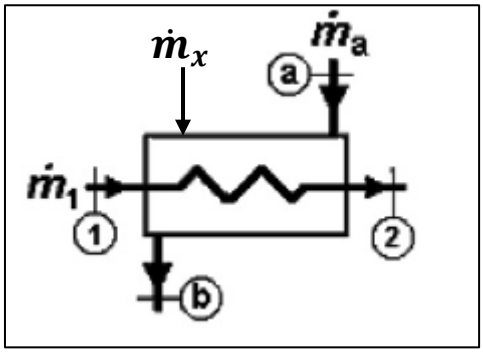

Figure 3.4: Heat exchanger with three inlets and two outlets [74]

$$\dot{E}x_{IN} = \dot{m}_a\varepsilon_a + \dot{m}_x\varepsilon_x - (\dot{m}_a + \dot{m}_x)\varepsilon_b \quad (3.26\ a)$$

$$\dot{E}x_{OUT} = \dot{m}_1(\varepsilon_2 - \varepsilon_1) \quad (3.26\ b)$$

$$\Delta\dot{E}x = \dot{E}x_{IN} - \dot{E}x_{OUT} \quad (3.26\ c)$$

$$\Delta\dot{E}x = \dot{m}_a\varepsilon_a + \dot{m}_x\varepsilon_x - (\dot{m}_a + \dot{m}_x)\varepsilon_b - \dot{m}_1(\varepsilon_2 - \varepsilon_1) \quad (3.26\ d)$$

The second law efficiencies are represented as:

Brute Force Efficiency:

$$\eta^{II}_{HXer,BF} = \frac{\dot{m}_1\varepsilon_2+(\dot{m}_a+\dot{m}_x)\varepsilon_b}{\dot{m}_a\varepsilon_a+\dot{m}_x\varepsilon_x+\dot{m}_1\varepsilon_1} \quad (3.26\ e)$$

Functional efficiency:

$$\eta^{II}_{HXer,FUN} = \frac{\dot{m}_1(\varepsilon_2-\varepsilon_1)}{\dot{m}_a\varepsilon_a+\dot{m}_x\varepsilon_x-(\dot{m}_a+\dot{m}_x)\varepsilon_b} \quad (3.26\ f)$$

3.5.4 Turbine

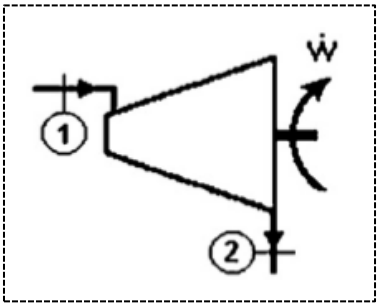

Figure 3.5: Turbine Schematic [74]

The incoming fluid rotates the turbine blades and in so doing, the turbine produces work. There is exergy associated with the work as well as the two streams (inlet and outlet). Heat transfer between the turbine and the surroundings is neglected. The exergy can therefore be represented as follows:

$$\Delta \dot{E}x = \dot{m}\varepsilon_1 - \dot{m}\varepsilon_2 - \dot{W}_t \quad (3.27\text{ a})$$

The second law efficiencies are represented as:

Brute Force Efficiency:

$$\eta^{II}_{t,BF} = \frac{\varepsilon_{w_t} + \varepsilon_2}{\varepsilon_1} = \frac{\mathrm{w} + \varepsilon_2}{\varepsilon_1} \quad (3.27\text{ b})$$

Functional efficiency:

$$\eta^{II}_{p,FUN} = \frac{\varepsilon_{w_p}}{\varepsilon_1 - \varepsilon_2} = \frac{\mathrm{w}}{\varepsilon_1 - \varepsilon_2} \quad (3.27\text{ c})$$

An ideal turbine produces work isentropically. However, as with pumps, irreversibilities do not allow for the ideal case. Hence, turbine isentropic efficiency is used to determine the real work produced by a turbine. It is represented as follows:

$$\eta_t = \frac{h_1 - h_2}{h_1 - h_{2s}} \quad (3.27\text{ d})$$

3.5.5 Energy and Exergy analysis of Geothermal Preheater system

The energy and exergy destroyed equations for the system with a geothermal preheater are shown below. The equations are applicable to the hybrid system that was designed for this study (Figure 4.3). Exergy analysis is important because it helps to identify the increased

sources of irreversibility in different components of a power plant cycle [98]. The exergy analysis reflects the actual performance degradation. The analysis is performed as follows:

The First Adiabatic High-Pressure Feed Water Heater:

$$\dot{\sigma}_2 h_{10} + \dot{\sigma}_1 h_{15} + \dot{m}_5 h_5 - \dot{m}_6 h_6 - (\dot{\sigma}_1 + \dot{\sigma}_2) h_{16} = 0 \quad (3.28a)$$

$$\dot{I}_{First\ FWH} = -T_0 \left[\dot{\sigma}_2 s_{10} + \dot{\sigma}_1 s_{15} + \dot{m}_5 s_5 - \dot{m}_6 s_6 - (\dot{\sigma}_1 + \dot{\sigma}_2) s_{16}\right] \quad (3.28\ b)$$

The Second Adiabatic High-Pressure Feed Water Heater:

$$\dot{\sigma}_1 h_9 - \dot{\sigma}_1 h_{15} - \dot{m}_7 h_7 + \dot{m}_6 h_6 = 0 \quad (3.29\ a)$$

$$\dot{I}_{Second\ FWH} = -T_0 \left[\dot{\sigma}_1 s_9 - \dot{\sigma}_1 s_{15} - \dot{m}_7 s_7 + \dot{m}_6 s_6\right] \quad (3.29\ b)$$

The Geothermal Preheater:

$$\dot{m}_2 h_2 - \dot{m}_3 h_3 = 0 \quad (3.30\ a)$$

$$\dot{I}_{GPH} = \dot{m}_2 h_2 - \dot{m}_3 h_3 - T_0 \left[\dot{m}_3 s_3 - \dot{m}_4 s_4\right] + \dot{q}_{geo} \left(1 - \frac{T_0}{T_{geo}}\right) \quad (3.30\ b)$$

The Adiabatic Deaerator:

$$\dot{\sigma}_3 h_{13} - \dot{m}_4 h_4 + \dot{m}_3 h_3 + (\dot{\sigma}_1 + \dot{\sigma}_2) h_{16} = 0 \quad (3.31\ a)$$

$$\dot{I}_{Deaerator} = T_0 \left[\dot{\sigma}_3 s_{13} - \dot{m}_4 s_4 + \dot{m}_3 s_3 + (\dot{\sigma}_1 + \dot{\sigma}_2) s_{16}\right] \quad (3.31\ b)$$

The Condenser:

$$\dot{Q}_c = \dot{m}_{14}(h_{14} - h_1) \quad (3.32\ a)$$

$$\dot{I}_{Condensor} = \dot{m}_{14}(h_{14} - h_1) - T_0 \left[\dot{m}_{14}(s_{14} - s_1)\right] + \dot{m}_{w,in}(h_{w,in} - h_{out}) - T_0 \left[\dot{m}_{14}\left(s_{w,in} - s_{out}\right)\right] \quad (3.32\ b)$$

The Adiabatic Feed Water Pump:

$$\dot{W}_{FWP} = \dot{m}_6(h_5 - h_6) \quad (3.33\ a)$$

$$\dot{I}_{FWP} = \dot{m}_6(h_5 - h_6) - T_0 \left[\dot{m}_6(s_5 - s_6)\right] + \left|\dot{W}_{FWP}\right| \quad (3.33\ b)$$

The Adiabatic Condensate Extraction Pump:

$$\dot{W}_{CEP} = \dot{m}_1(h_2 - h_1) \quad (3.34\ a)$$

$$\dot{I}_{CEP} = \dot{m}_1(h_1 - h_2) - T_0\,[\dot{m}_1(s_1 - s_2)] + \left|\dot{W}_{CEP}\right| \quad (3.34\ b)$$

The Adiabatic Turbine:

$$\dot{W}_T = \dot{m}_8 h_8 + \dot{m}_{12} h_{12} - \dot{m}_9 h_9 - \dot{m}_{10} h_{10} - \dot{m}_{13} h_{13} - \dot{m}_{14} h_{14} \quad (3.35\ a)$$

$$\dot{I}_T = T_0\,[\dot{m}_8 s_8 + \dot{m}_{12} s_{12} - \dot{m}_9 s_9 - \dot{m}_{10} s_{10} - \dot{m}_{13} s_{13} - \dot{m}_{14} s_{14}] \quad (3.35\ b)$$

The Boiler:

$$\dot{Q}_B = \dot{m}_8 h_8 - \dot{m}_7 h_7 + \dot{m}_{12} h_{12} - \dot{m}_{11} h_{11} \quad (3.36\ a)$$

$$\dot{I}_B = \{\dot{m}_7 h_7 - \dot{m}_8 h_8 + \dot{m}_{11} h_{11} - \dot{m}_{12} h_{12} - T_0\,[\dot{m}_7 s_7 - \dot{m}_8 s_8 + \dot{m}_{11} s_{11} - \dot{m}_{12} s_{12}]\} + \dot{q}_B\left(1 - \frac{T_0}{T_B}\right) \quad (3.36\ b)$$

3.5.6 Summary

Table 3.3 presents a summary of the exergy destruction and second law efficiency formulas used in this study, for the different system components.

Table 3.3: Summary of Exergy balance and Exergy efficiency [74]

	EXERGY DESTRUCTION	**2ND LAW EFFICIENCY**
Pumps	$\dot{I}_p = \dot{X}_{in} - \dot{X}_{out} + \dot{W}_p$	$\eta_{II,pump} = 1 - \frac{\dot{I}_p}{\dot{W}_p}$
Heaters	$\dot{I}_h = \dot{X}_{in} - \dot{X}_{out}$	$\eta_{II,heater} = 1 - \frac{\dot{I}_h}{\dot{X}_p}$
Turbines	$\dot{I}_t = \dot{X}_{in} - \dot{X}_{out} + \dot{W}_t$	$\eta_{II,turbine} = 1 - \frac{\dot{I}_t}{\dot{X}_{in} - \dot{X}_{out}}$

Condensers	$\dot{I}_c = \dot{X}_{in} - \dot{X}_{out} + \dot{Q}_c$	$\eta_{II,condenser} = 1 - \frac{\dot{X}_{out}}{\dot{X}_{in} + \dot{W}_c}$
Cycle components	$\dot{I}_{total} = \sum_{All\ components} \dot{I}$	$\eta_{II,total} = \frac{\dot{W}_{net,out}}{\dot{X}_{fuel}}$

3.6 Pressure drop analysis

In many applications, fluids need to be pumped through the heat exchanger. Therefore, as part of the system design, it is essential to determine the pumping power required. The pumping power is proportional to the fluid pressure drop which is associated with fluid flow. The pressure drop affects the heat transfer process and therefore affects the size of the heat exchanger. The pressure drop is a result of two main contributions: pressure drop associated with fluid distribution devices (e.g. inlet and outlet manifolds in a shell and tube heat exchanger); pressure drop associated with the core. A pressure drop analysis is discussed in the next sections for the counter-flow shell and tube heat exchanger as well as the downhole co-axial heat exchanger.

There are various assumptions that were made prior to performing a pressure drop analysis [75]:

- The flow is steady and isothermal and Fluid properties are independent of time
- There are no energy sinks or sources along the fluid stream line
- The friction factor is considered constant with flow length
- Fluid density is treated as a constant
- The pressure at any point in the fluid is independent of direction

3.6.1 Counter-flow shell and tube heat exchanger

3.6.1.1 Tube Side

Assuming the core frictional pressure drop to be the major contributor to the total pressure drop, and assuming the density remains constant, the following equation is established [75;76]:

$$\Delta P = \frac{G^2}{g_c \rho}\left(f\frac{L}{r_h}\right) \tag{3.37}$$

Where g_c represents proportionality constant in Newton's second law of motion, $g_c = 1$. The pressure drop equation shows above omit contributions from entrance and exit pressure drops because they are small in comparison to the core pressure drop.

3.6.1.2 Shell Side

The shell side pressure drop is more complicated due to various factors including: presence of bypass and leakage streams. However, a relatively simple approach given by Peters et al. [77] to determine the shell side pressure drop is:

$$\Delta P = \frac{2fG^2D(N_B+1)}{\rho D_e\left(\frac{\mu}{\mu_S}\right)^{0.14}} \qquad \text{for } 400 < Re = \frac{GD}{\mu} \leq 1x10^6 \tag{3.38}$$

Where: $f = e^{(0.576-\ln Re)}$; $N_B$represents the number of baffles; and D_e represents the equivalent diameter.

3.6.2 Downhole Co-Axial Heat Exchanger

The ratio of local pressure drop to distributed pressure drop was developed by Yekoladio [57] in the following form:

$$\frac{\Delta P_{local}}{\Delta P_{distributed}} = \frac{0.45\left[1-\left(\frac{D_i}{D_o}\right)^2\right]}{4f_i\left(\frac{4}{\pi}\right)^{\frac{1}{2}}Sv^{\frac{3}{2}}} \tag{3.39}$$

Where Sv represents the Svelteness of the flow geometry defined by Bejan [78] as:

$$Sv = \frac{external\ flow\ length\ scale}{internal\ flow\ length\ scale} = \left(\frac{4}{\pi}\right)^{\frac{1}{3}}\left(\frac{L_i}{D_i}\right)^{\frac{2}{3}} \tag{3.40}$$

Analysis of the pressure drop ratio proved that, for a downhole coaxial pipe with length that is twenty times greater than it diameter, the local pressure drop at the lower extremity of the well can be neglected for both laminar and turbulent flow [57].

3.7 Optimisation

Several opportunities for advancements in thermodynamics stem from the development of strategies for optimal allocation of resources. This optimal allocation is commonly referred to as: exergy destruction minimisation, irreversibility (entropy generation) minimisation or thermodynamic optimisation. Review of literature shows that thermodynamic optimisation is

making fast progress in the fields of cryogenics, heat transfer, energy storage, fossil-fuel power plants, etc. [79].

The methods of number of entropy generation units and entropy generation minimisation (EGM) were used to optimise the shell and tube heat exchanger and the downhole coaxial heat exchanger respectively. The two methods used to optimise the components were both developed by Bejan [64;80].

Optimisation using Non-dimensionalising techniques

The non-dimensionalising technique (also known as scaling or normalizing) was used to optimise two components within the system: feedwater heaters and the geothermal preheater. Non-dimensionalising assists in the modelling and analysis of complex geometries, complex flows and complex machinery.

3.7.1 Counter-flow Shell and Tube Heat Exchanger

The feedwater heater was modelled as a counter-flow shell and tube heat exchanger, where the shell side contains the steam inlet and condensate outlet and the tube side contains the feedwater inlet and outlet. As discussed earlier, the high-pressure turbine supplies heat to the heat exchanger shell. Heat is transferred from the steam to the feedwater by convection and conduction through the tube walls [81].

The method of number of entropy generation units is discussed as follows.

It is the heat exchanger design method that has been selected to optimise one of the high-pressure feedwater heaters. This method was used to obtain a system that produces minimum irreversibility in the feedwater heaters (optimisation by EGM). The optimum geometry can then be inferred. The entropy generation number is derived from the second law. This number is comparable to the older concept of the number of heat transfer units (NTU), traditionally used in first law analyses of heat exchangers [82].

Applying an entropy balance, the entropy generation rate of the overall heat exchanger is [83]:

$$\dot{S} = \dot{m}_1(s_{out} - s_{in})_1 + \dot{m}_2(s_{out} - s_{in})_2 \tag{3.41}$$

$$\dot{S} = C_{min}\left[\ln\left(\frac{T_{1,out}}{T_1}\right) - \left(\frac{R}{c_p}\right)_1 \ln\left(\frac{P_{1,out}}{P_1}\right)\right] +$$

$$C_{max}\left[\ln\left(\frac{T_{2,out}}{T_2}\right)-\left(\frac{R}{c_p}\right)_2\ln\left(\frac{P_{2,out}}{P_2}\right)\right] \tag{3.42}$$

Where:

$$C_{min}=\left(\dot{m}c_p\right)_1 \text{ and } C_{max}=\left(\dot{m}c_p\right)_2 \tag{3.43}$$

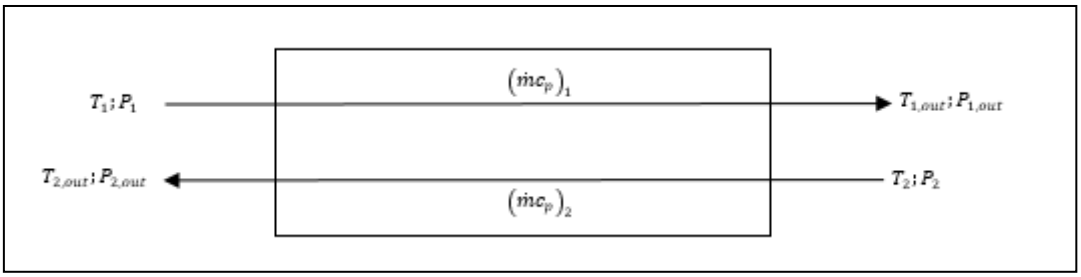

Figure 3.6: Counter-flow Heat Exchanger with specified capacity rates and inlet conditions

The first law of thermodynamics applied to Figure 3.6 yields:

$$C_{min}\left(T_1-T_{1,out}\right)+C_{max}\left(T_2-T_{2,out}\right)=0 \tag{3.44}$$

And given that heat exchanger effectiveness is [84]:

$$\epsilon=\frac{T_{1,out}-T_1}{T_2-T_1} \tag{3.45}$$

$T_{1,out}$ and $T_{2,out}$ can be eliminated and $\dot{S}$ can be expressed in terms of known parameters. Number of entropy production units is defined as:

$$N_s=\frac{\dot{S}}{C_{max}} \tag{3.46}$$

$$N_s=\frac{C_{min}}{C_{max}}\ln\left[1+\epsilon\left(\frac{T_2}{T_1}-1\right)\right]+\ln\left[1-\frac{C_{min}}{C_{max}}\epsilon\left(1-\frac{T_1}{T_2}\right)\right]-\frac{C_{min}}{C_{max}}\left(\frac{R}{c_p}\right)_1\ln\left(1-\frac{\Delta P_1}{P_1}\right)-\left(\frac{R}{c_p}\right)_2\ln\left(1-\frac{\Delta P_2}{P_2}\right) \tag{3.47}$$

Considering counterflow heat exchangers in the following limiting conditions can yield simpler forms of the ‘number of production units’ equation:

- Nearly Ideal Heat Exchangers

- Nearly balanced capacity rate
- Balanced capacity rates

3.5.1.1 Nearly Ideal Heat Exchangers

The assumptions made in this case are that the heat exchanger has small stream-to-stream $\Delta T's$ as well as small frictional $\Delta P's$ such that:

$$1-\epsilon \ll 1 \tag{3.48 a}$$

$$\left(\frac{\Delta P}{P}\right)_{1,2} \ll 1 \tag{3.48 b}$$

The assumption: $1-\epsilon \ll 1$ it can be further assumed as $\epsilon \approx 1$. Expansion of the entropy production number by applying the Taylor series around $\epsilon \approx 1$ yields the following:

$$N_s \cong \frac{C_{min}}{C_{max}} \ln \frac{T_2}{T_1} + \frac{C_{max}}{C_{min}} \ln\left[1-\frac{C_{min}}{C_{max}}\left(1-\frac{T_1}{T_2}\right)\right] + \left(\frac{C_{min}}{C_{max}}\right)^2 \left(1- \frac{C_{min}}{C_{max}}\right) \frac{\left(1-\frac{T_1}{T_2}\right)^2}{1-\frac{C_{min}}{C_{max}}\left(1-\frac{T_1}{T_2}\right)} \left(\frac{e^{\left[-N_{tu}\left(1-\frac{C_{min}}{C_{max}}\right)\right]}}{1-\frac{C_{min}}{C_{max}} e^{\left[-N_{tu}\left(1-\frac{C_{min}}{C_{max}}\right)\right]}} \right) + \frac{C_{min}}{C_{max}} \left(\frac{R}{C_p}\right)_1 \left(\frac{\Delta P}{P}\right)_1 + \left(\frac{R}{C_p}\right)_2 \left(\frac{\Delta P}{P}\right)_2 \tag{3.49}$$

3.5.1.2 Nearly Balanced Capacity Rate

In many gas-to-gas applications, the counter-flow heat exchangers must handle balanced streams or nearly balanced streams. Applying the limit: $C_{min} \rightarrow C_{max}$ reduces the number of entropy production units equation to:

$$N_S \approx N_{S,imbalance} + \left(\sqrt{\frac{T_2}{T_1}} - \sqrt{\frac{T_1}{T_2}}\right)^2 \frac{1}{N_{tu}} + \frac{C_{min}}{C_{max}} \left(\frac{R}{C_p}\right)_1 \left(\frac{\Delta P}{P}\right)_1 + \left(\frac{R}{C_p}\right)_2 \left(\frac{\Delta P}{P}\right)_2 \tag{3.50}$$

Which, in compact form translates to:

$$N_S \approx N_{S,imbalance} + N_{S_1} + N_{S_2} \tag{3.51}$$

Where the overall N_{tu} for each side of the heat transfer surface can be expressed as:

$$\frac{1}{N_{tu}} = \frac{1}{N_{tu_1}} + \frac{C_{min}}{C_{max}} \frac{1}{N_{tu_2}} \tag{3.52}$$

The N_S contribution due to the capacity rate imbalance is represented as:

$$N_{S,imbalance} = \frac{C_{min}}{C_{max}} \ln \frac{T_2}{T_1} + \ln\left[1-\frac{C_{min}}{C_{max}}\left(1-\frac{T_1}{T_2}\right)\right] \tag{3.53}$$

In the limit $C_{min} \rightarrow C_{max}$, the capacity imbalance reduces to:

$$N_{S,imbalance} = \left(\frac{C_{min}}{C_{max}} - 1\right)\left(\frac{T_2}{T_1} - 1 - \frac{C_{min}}{C_{max}} \ln \frac{T_2}{T_1}\right) \tag{3.54}$$

3.5.1.3 Balanced Capacity Rate

At balanced capacity rate: $C_{min} = C_{max}$, the imbalance term falls away and the number of entropy production units for each side is represented identically as:

$$N_{S_1} = \left(\sqrt{\frac{T_2}{T_1}} - \sqrt{\frac{T_1}{T_2}}\right)^2 \frac{1}{N_{tu_1}} + \frac{C_{min}}{C_{max}} \left(\frac{R}{c_p}\right)_1 \left(\frac{\Delta P}{P}\right)_1 \tag{3.55}$$

$$N_{S_2} = \frac{C_{min}}{C_{max}} \left(\sqrt{\frac{T_2}{T_1}} - \sqrt{\frac{T_1}{T_2}}\right)^2 \frac{1}{N_{tu_2}} + \left(\frac{R}{c_p}\right)_2 \left(\frac{\Delta P}{P}\right)_2 \tag{3.56}$$

and:

$$N_{S_{1,2}} = N_{S,\Delta T_{1,2}} + N_{S,\Delta P_{1,2}} \tag{3.57}$$

where:

$$N_{tu_{1,2}} = \left(\frac{L}{r_h}\right) St \tag{3.58 a}$$

$$\left(\frac{\Delta P}{P}\right)_{1,2} = f \left(\frac{L}{r_h}\right) \frac{G^2}{2\rho P} \tag{3.58 b}$$

$\left(\frac{G}{\sqrt{2\rho P}}\right)$ is treated as a dimensionless mass velocity and is represented as $'g'$ in the subsequent equations.

$$N_{S_{1,2}} = \frac{\theta \tau}{(L/r_h) St} + bBf(L/r_h) g^2 \tag{3.59}$$

Where:

$$\theta_1 = 1 \; ; \; \theta_2 = \frac{C_{min}}{C_{max}} \tag{3.60 a,b}$$

$$\tau = \left(\sqrt{\frac{T_2}{T_1}} - \sqrt{\frac{T_1}{T_2}}\right)^2 \tag{3.61}$$

$$b_1 = \frac{C_{min}}{C_{max}} \; ; \; b_2 = 1 \tag{3.62 a,b}$$

$$B_1 = \left(\frac{R}{c_p}\right)_1 ; B_2 = \left(\frac{R}{c_p}\right)_2 \tag{3.63 a,b}$$

Given the balanced capacity rate assumption: $C_{min} = C_{max}$, the θ and b terms in equation (3.60) and (3.61) fall away resulting to:

$$N_{S_{1,2}} = \frac{\tau}{(L/r_h)St} + Bf(L/r_h)g^2 \tag{3.64}$$

The Stanton number for heat transfer is [73]:

$$St = \frac{Nu}{Re*Pr} \tag{3.65 a}$$

And the friction factor can be determined from the Moody chart or the equations below under the assumption that the tubes are smooth and heat transfer occurs in single phase:

For laminar flow, calculated using the Hagen-Poiseuille equation [85]:

$$f = \frac{16}{Re} \quad \text{where:} \quad Re \leq 2100 \tag{3.65 b}$$

For turbulent flow, on the tube side, the Gnielinski correlation was used [86-88]:

$$Nu = \frac{hD}{k} = 0.012(Re^{0.87} - 280)Pr^{0.4} \tag{3.65c}$$

With [89-91]:

$$f = (1.58 \ln Re - 3.28)^{-2} \tag{3.65 d}$$

where $2100 \leq Re \leq 5 \times 10^6$

The above representations of St and f show that the Stanton number and the friction factor are both functions of the Reynolds number Re.

For a given Re and 'L/r_h', the number of entropy generation units increases as 'g' increases. However, unlike g, the ratio 'L/r_h'plays a trade-off role. For a fixed 'g' and 'Re', there exists an optimum 'L/r_h' for which $N_{S_{1,2}}$ is a minimum. Large values of 'L/r_h' result to irreversibilities dominated by fluid friction and low values of 'L/r_h' lead to large ΔT values

and therefore, irreversibilities dominated by heat transfer. On the right hand side of Equation (3.64), the first term varies inversely with the ratio 'L/r_h' whereas the second term varies directly with the same ratio). The optimum 'L/r_h' can therefore be obtained by minimising equation (3.64) [64]:

$$\left(\frac{L}{r_h}\right)_{1,opt} = \frac{\tau^{1/2}}{g_1[Bf_1St_1]^{1/2}} \tag{3.66}$$

Which gives a minimum entropy generation number of:

$$N_{S_{1,min}} = 2(\tau B)^{1/2} g_1 \left(\frac{f_1}{St_1}\right)^{1/2} \tag{3.67}$$

The heat transfer area can be represented as:

$$A = \left(\frac{L}{r_h}\right) \cdot A_c \tag{3.68}$$

Where A_c represents the minimum free-flow area.

The heat transfer area can also be represented as:

$$A\frac{\sqrt{2\rho P}}{\dot{m}} = \frac{(L/r_h)}{g} \tag{3.69}$$

Therefore, the optimum area can be determined by substituting the optimum flow parameter: $(L/r_h)_{opt}$. This yields:

$$A_{opt} = \frac{\dot{m}\cdot(L/r_h)_{opt}}{g\sqrt{2\rho P}} \tag{3.70}$$

At this stage, both the area and the flow parameter (L/r_h) have been obtained for the optimum case. The feedwater heater can then be designed to suit the optimum scenario.

Bejan [83] concluded that the number of entropy generation units $N_{S_{1,2}}$ for each side is a function of three independent flow parameters (degrees of freedom): Re, L/r_h, and g which all depend on the size and geometry of the heat exchanger. The value of N_s can vary from $0\ to\ \infty$.

N_s representing a low or high value depends on the following factors [82]:

- The size of the heat exchanger that can be economically tolerated

- The magnitude of the remanent (flow imbalance) irreversibility
- Entropy generation levels shown by other components that make up the greater system.

There are various constraints that can be applied to the design, depending on the application of the heat exchanger: Area constraint, Volume constraint and Combined Area and Volume constraint. They are discussed below:

Area Constraint

This constraint is applied when there is an economic limitation and specifically where the cost of the heat exchanger surface is a major consideration [64]. Considering that the maximum allowable tube side flow area of the heat exchanger has been specified, the constant-area constraint can be expressed in dimensionless form as:

$$a_1 = \frac{A_1}{\dot{m}}\sqrt{2\rho P_1} \text{ (constant)} \tag{3.71}$$

where a_1 represents the dimensionless area of one side of the heat transfer surface. From (3.54), the following relationship is established:

$$a_1 g_1 = \left(\frac{L}{r_h}\right)_1 \tag{3.72}$$

Where Equations (3.60) and (3.62) are just decoupled forms of Equation (3.63). Substituting (3.63) into (3.55) eliminates one degree of freedom: L/r_h, yielding (considering side 1 to be tube side of the heat exchanger):

$$N_{S_1} = \frac{\tau}{a_1 g_1 St_1} + B f a_1 {g_1}^3 \tag{3.73}$$

Of the two degrees of freedom remaining: 'Re' and 'g', one can be fixed to optimise the other degree of freedom and therefore yield a minimum entropy generation number. In this case, 'Re' is fixed to yield optimal 'g' (Equation 3.74) and then minimise N_{S_1}(Equation 3.75).

$$g_{1,opt} = \left[\frac{\tau}{3Ba_1^2 f_1 St_1}\right]^{1/4} \tag{3.74}$$

$$N_{S_{1,min}} = \left[\frac{256\tau^3 B f_1}{27 a_1^2 St_1^3}\right]^{1/4} \tag{3.75}$$

Volume Constraint

This constraint is applied in cases where space for the heat exchanger is limited [64]. Given a specified volume for the heat exchanger, the constant-volume constraint can be expressed in dimensionless form as:

$$\upsilon_1 = V_1 \frac{8P_1}{\nu \dot{m}} \tag{3.76}$$

With V_1 being the volume of the tubes. Knowing that V_1 can be mathematically expressed as the product of total cross-sectional area of the tubes and the length of the tubes, the following relation is established:

$$\upsilon_1 {g_1}^2 = \left(\frac{L}{r_h}\right)_1 Re_1 \tag{3.77}$$

Which eliminates one degree of freedom: 'L/r_h', and like the area constraint method, allows for the entropy generation minimisation number to be expressed in terms of the 'Re' and 'g' as follows:

$$N_{S_1} = \frac{\tau Re_1}{\upsilon_1 {g_1}^2 St_1} + \frac{Bf\upsilon_1 {g_1}^4}{Re_1} \tag{3.78}$$

As with the constant-area constraint case, the number of entropy generation units can be minimised and 'g' optimised by fixing Reynolds number, yielding:

$$g_{1,opt} = \left[\frac{\tau Re_1^2}{2B\upsilon_1^2 f_1 St_1}\right]^{1/6} \tag{3.79}$$

Which yields a minimum N_{S_1} of:

$$N_{S_{1,min}} = \left[\frac{27\tau^2 BRe_1 f_1}{4\upsilon_1 St_1^2}\right]^{1/4} \tag{3.80}$$

Combined Area and Volume Constraint

In this case, area and volume are constrained simultaneously Constraining two properties greatly limits the design options because it leaves just one degree of freedom to optimise the thermodynamic performance of the heat exchanger.

Combining Equations (3.64), (3.71), (3.76) yields an expression for the entropy generation number:

$$N_{S_1} = \frac{\tau v_1}{a_1^2 St_1 Re_1} + \frac{Ba_1^4 f_1 {Re_1}^3}{v_1^3} \tag{3.81}$$

With Re being the only degree of freedom, it can be optimised to give minimum N_{S_1}:

$$Re_{opt} = \frac{v_1}{a_1^{3/2}} \left[\frac{\tau}{3Bf_1 St_1}\right]^{1/4} \tag{3.82}$$

3.7.2 Downhole Coaxial Heat Exchanger (DCHE)

The geothermal heat exchanger was modelled as a downhole co-axial heat exchanger. The method of entropy generation minimisation, developed by Bejan [73] was used to optimise the DCHE. Once the stream reaches the bottom of the well, it is heated and then returned to the surface by flowing through the inner pipe which is well insulated to minimise heat loss to the annulus (Figure 3.7).

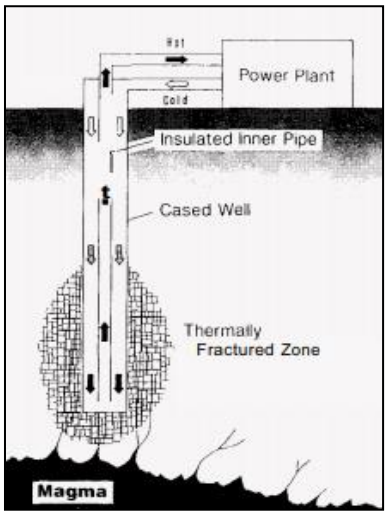

Figure 3.7: A concept of the Downhole Coaxial Heat Exchanger [26]

The low-pressure feedwater heater is replaced with a geothermal heat exchanger which aims to transfer geothermal heat to the feedwater (preheating the feedwater). Modelling this geothermal preheater as a DCHE has several appealing features and advantages. Environmental and institutional restrictions require geothermal water to be returned underground from where it came from. Therefore, heat extraction techniques that involve the physical removal of water from underground need a second well to dispose of the water. Thus, from an economic perspective, the DCHE is preferred because the cost of keeping a pump running in the corrosive geothermal fluid is far greater than that of maintaining a DCHE.

From the first and second laws of thermodynamics, for a duct of arbitrary cross section 'A' and wetted perimeter 'p', the entropy generation rate is derived as follows [82]:

$$\dot{S}'_{gen} = \frac{d\dot{S}_{gen}}{dx} = \frac{\dot{Q}'\Delta T}{T_m^2(1+\tau)} + \frac{\dot{m}}{\rho T_m}\left(-\frac{dP}{dx}\right) \tag{3.83}$$

Where $\dot{Q}' = \dot{m} \cdot C_p \cdot \left(\frac{dT}{dx}\right)$; τ represents the dimensionless temperature difference; T_m the mean stream temperature; and ΔT, the difference between the outer wall temperature and the mean stream temperature.

$$\dot{S}'_{gen} = \dot{m} \cdot C_p \cdot \frac{\Delta T}{T_m^2(1+\tau)}\left(\frac{dT}{dx}\right) + \frac{\dot{m}}{\rho T_m}\left(-\frac{dP}{dx}\right) \tag{3.84}$$

Assuming a control volume of length dx of the co-axial pipes, the energy balance of the DCHE was considered. The total rate of convective heat transfer given by Bejan [80] is as follows:

$$\dot{Q} = \dot{m} \cdot C_p \cdot dT = h \cdot \pi D_0 dx \cdot \Delta T_{lm} \tag{3.85}$$

And ΔT_{lm} was further defined as:

$$\Delta T = \Delta T_{lm} = \frac{\dot{m}C_p}{h\pi D_0}\left(\frac{dT}{dx}\right) \tag{3.86}$$

Assuming that: $\tau = {}^{\Delta T}/_{T_m} \ll 1$ yields the following entropy generation rate:

$$\dot{S}'_{gen} = \frac{\dot{m}^2 C_p^2 \Delta T}{h\pi D_0 T_m^2}\left(\frac{dT}{dx}\right)^2 + \frac{\dot{m}}{\rho T_m}\left(-\frac{dP}{dx}\right) \tag{3.87}$$

The equation above is an expansion of: $\left[\dot{S}_{gen} = \dot{S}_{gen,\Delta T} + \dot{S}_{gen,\Delta P}\right]$ where:

$\dot{S}'_{gen,\Delta T}$: represents the entropy generation per unit length of the DCHE due to the heat transfer irreversibility across a finite temperature difference along the outer wall of the annular space, while the inner pipe, through the insulation, minimises heat loss to the surroundings.

$\dot{S}'_{gen,\Delta P}$: represents the total fluid friction irreversibility owing to the downward flow of the water through the annular region and then after through the inner pipe.

Heat transfer occurs only across the outer wall of the annular space and therefore, the following heat transfer principles apply [92]:

$$h_a = St \cdot \rho \cdot C_p \cdot u_a \tag{3.88}$$

$$Nu_a = \frac{hD_h}{k} = St \cdot Re_a \cdot Pr \tag{3.89}$$

$$u_a = \frac{4\dot{m}}{\pi \rho D_h^2} \tag{3.90}$$

where:

$$D_h = D_o - D_i = D_o(1 - r) \tag{3.91}$$

The entropy generation rate per unit length can be expressed as:

$$\dot{S}'_{gen} = \frac{\dot{m} C_p Re_a Pr D_o (1-r)^2}{4 Nu_a T_m^2} \left(\frac{dT}{dx}\right)^2 + \frac{\dot{m}}{\rho T_m} \left(-\frac{\Delta P}{L}\right)_{total} \tag{3.92}$$

For flow through a straight pipe in terms of the outer diameter, Reynolds number can be represented as follows:

$$Re_a = \frac{4\dot{m}}{\pi \mu D_o (1-r)} \quad and \quad Re_i = \frac{4\dot{m}}{\pi \mu D_o} \tag{3.93 a,b}$$

3.5.1.4 Turbulent flow

In the annular space of the co-axial pipes, the Nusselt number of the flowing geothermal fluid was approximated by the Petukhov and Roizen [59] correlation for heat transfer at the outer wall of a concentric annular duct with its inner wall well-insulated as [93] :

$$\frac{Nu_a}{Nu_i} = 1 - 0.14 \left(\frac{D_i}{D_o}\right)^{0.6} \tag{3.94}$$

Where the Nusselt number of the hot stream of fluid flowing up the inner pipe is represented as [92]:

$$Nu_i \approx 0.023 \cdot {Re_i}^{0.8} \cdot Pr^{0.4} \ \textbf{for}\ 0.7 < Pr < 160,\ Re_i > 10^4 \tag{3.95}$$

The following equation was obtained [57]:

$$\dot{S}'_{gen} = \frac{13.84\dot{m}^2 C_p Pr^{0.6}(1-r)^{0.2}}{\mu\left(\frac{1}{r^{0.8}}-\frac{0.14}{r^{0.2}}\right)T_m^2 Re_a^{0.8}}\left(\frac{dT}{dx}\right)^2 + \frac{0.0446 Re_a^{4.8}\mu^5(1-r)^{4.8}}{\rho^2 T_m \dot{m}^2}\left(\frac{1}{(1-r)^{2.8}(1+r)^2}+\frac{1}{r^{4.8}}\right) \quad (3.96)$$

The equation above was then differentiated with respect to the mass flow rate of the water and equated to zero. The optimum mass flow rate under turbulent conditions was then obtained to be:

$$\dot{m}_{opt,turb} = 0.238 \cdot Re_a^{1.4} \cdot C_{turb}^{0.25} \quad (3.97)$$

Where:

$$C_{turb} = \frac{\mu^6 T_m}{\rho^2 C_p Pr^{0.6}\left(\frac{dT}{dx}\right)^2}(1-r)^{4.6}\left(\frac{1}{r^{0.8}}-\frac{0.14}{r^{0.2}}\right)\left(\frac{1}{(1-r)^{2.8}(1+r)^2}+\frac{1}{r^{4.8}}\right) \quad (3.98)$$

3.5.1.5 Laminar Flow

Equation (3.99) represents the approximation made by Martin's correlation of the Nusselt number of the geothermal fluid in the annular space of the DCHE with the inner pipe well insulated and heat transfer occurring on the outer wall:

$$Nu_a = 3.66 + 1.2\left(\frac{D_i}{D_o}\right)^{0.5} \quad (3.99)$$

For: $0.1 < Pr < 10^3, Re_D < 2300, 0 < \frac{D_i}{D_o} < 1$

Substituting the above Nusselt number relationship into the equation for the entropy generation rate per unit length and eliminating D_o yields [57]:

$$\dot{S}'_{gen} = \frac{0.318\dot{m}^2 CpPr(1-r)}{\mu(3.66+1.2r^{0.5})T_m^2}\left(\frac{dT}{dx}\right)^2 + \frac{15.50 Re_a^4\mu^5(1-r)^4}{\rho^2 T_m \dot{m}^2}\left(\frac{\frac{1-r}{1+r}}{1-r^4-\frac{(1+r^2)}{\ln\left(\frac{1}{r}\right)}}+\frac{1}{r^4}\right) \quad (3.100)$$

To obtain the mass flow rate, the above equation is differentiated with respect to the mass flow rate $\dot{m}$ and then equated to zero yielding:

$$\dot{m}_{opt,lam} = 0.2642 \cdot Re_a \cdot C_{lam}^{0.25} \quad (3.101)$$

Where:

$$C_{lam} = \frac{\mu^6 T_m}{\rho^2 C_p Pr\left(\frac{dT}{dx}\right)^2}(1-r)^3(3.66+1.2r^{0.5})\left(\frac{\frac{1-r}{1+r}}{1-r^4-\frac{(1+r^2)}{\ln\left(\frac{1}{r}\right)}}+\frac{1}{r^4}\right) \quad (3.102)$$

From the mass flow rates obtained for laminar flow and turbulent flow, the diameter was determined to be:

$$D_o = \frac{4\dot{m}_{opt}}{\pi\mu(1-r)Re_a} \quad (3.103)$$

3.8 Design and Sizing of Components

A water-cooled condenser was used over an air-cooled condenser to condense the feedwater heater. Although an air-cooled condenser has low maintenance costs and minimal fouling, it would require very large volume rates because of its very low specific heat and density relative to water.

The condenser and feedwater heaters were all modelled as horizontal single pass shell and tube counter-flow heat exchangers. In the condenser, the working fluid was allowed to flow through the tube and the cooling fluid allowed to flow in the shell side.

In the feedwater heaters, the cold fluid was allowed to flow through the tubes and the hotter fluid on the shell side.

3.8.1 Condenser and Feedwater Heaters Design

Tubes can be arranged in different layouts or patterns: square pitch layout; triangular-pitch layout (both shown in Figure 3.8) or even rotated square-pitch layout.

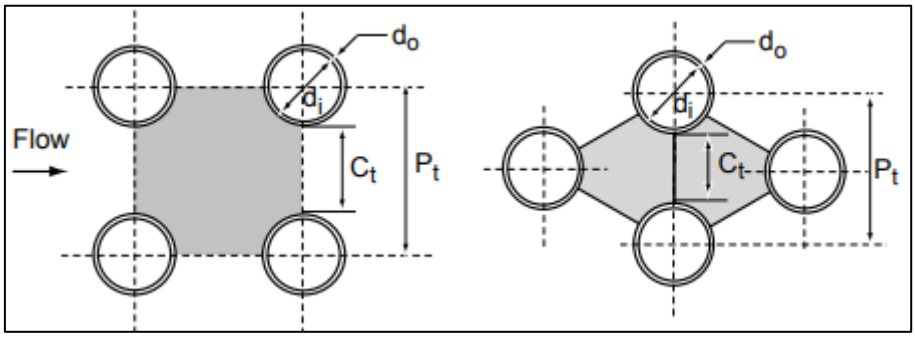

Figure 3.8: Tube arrangements [94]

For the squared-pitch tube layout, the equivalent diameter was defined as [75], [94], [95]:

$$D_e = \frac{4\left(P_t^2 - \frac{\pi d_o^2}{4}\right)}{\pi d_o} \tag{3.104}$$

And for the triangular-pitch layout, it was defined as:

$$D_e = \frac{4\left(\frac{\sqrt{3}P_t^2}{4} - \frac{\pi d_o^2}{4}\right)}{\frac{\pi d_o}{2}} \tag{3.105}$$

The cross-flow area of the shell is defined as:

$$A_s = \frac{D_s C_t B}{P_t} \tag{3.106}$$

where: $B = baffle\ spacing$

The diameter and tube pitch ratios were defined respectively as:

$$d_r = \frac{d_o}{d_i} \text{ and } P_r = \frac{t}{d_o} \tag{3.107 a,b}$$

The tube pitch and clearance were obtained from Figure 3.8 as:

$$P_t = C_t + d_o \tag{3.108}$$

The number of tubes were then predicted in approximation with the shell side diameter D_s:

$$N_t = (CTP)\frac{\frac{\pi D_s^2}{4}}{Shade\ Area} \tag{3.109 a}$$

With: $CTP = 0.93$ for a single-pass heat exchanger.

$$Shade\ Area = CL \cdot P_t^2 \tag{3.109 b}$$

with:

$CL = 1$ for a square-pitch layout

$CL = 0.866$ for a triangular-pitch layout

This yields the following equation for the number of tubes [94], [95]:

$$N_t = \frac{\pi}{4}\left(\frac{CTP}{CL}\right)\frac{D_S^2}{P_t^2} = \frac{\pi}{4}\left(\frac{CTP}{CL}\right)\frac{D_S^2}{P_r^2 d_0^2} \tag{3.110}$$

A recommended baffle spacing and baffle cut corresponding to about 40-60 % and 25-35 % of the shell diameter were assumed, respectively [57].

3.8.2 Turbine Design

The turbines used in thermal power plants are based on application and conditions. There are various types including: axial or radial (regarding steam flow direction); Impulse or reaction (regarding working principal). In this research, the turbine was assumed to be an axial single-stage expander. The actual turbine dimension were estimated by a turbine size parameter [96]:

$$SP = \frac{\sqrt{V_{out}}}{\Delta H_{is}^{\frac{1}{4}}} \tag{3.102}$$

which takes into account the turbine outlet volume flow rate and the enthalpy drop during the expansion process.

4 RESULTS AND DISCUSSION

4.1 Thermodynamic Analysis

Two systems were designed and compared against each other. The difference between the two systems is the use of the geothermal heat exchanger. In one system, a low pressure feedwater heater makes use of steam extracted from the low pressure turbine to preheat the feedwater and in the second system, the geothermal heat exchanger replaces the low pressure feedwater heater and instead of using extracted steam from the LP turbine, makes use of geothermal energy to preheat the feedwater.

The two systems are shown schematically in Figures 4.1 and 4.3. Tables 4.1 and 4.3 show the process parameters of the two systems that were designed. These process parameters include: enthalpy (h); pressure (P); entropy (s); temperature (T); mass flow rate and flow specific exergy, also known as exergy (**ψ)**

4.1.1 Low Pressure Feedwater Heater System

A schematic of a Rankine cycle with single reheat and regeneration is shown (Figure 4.1). This model has been designed with one low pressure feedwater heater and two high pressure feedwater heaters which make use of extracted steam from the low and high-pressure turbines, respectively. The deaerator mixes steam bled from the low-pressure turbine, feedwater that has been preheated in the low-pressure feedwater heater and the condensate that exits the first high pressure feedwater heater. The feedwater then exits the deaerator as a saturated liquid at the deaerator pressure.

The two high pressure feedwater heaters extract steam from the high pressure turbine and use this extracted steam to further preheat the feedwater before it enters the boiler [97].

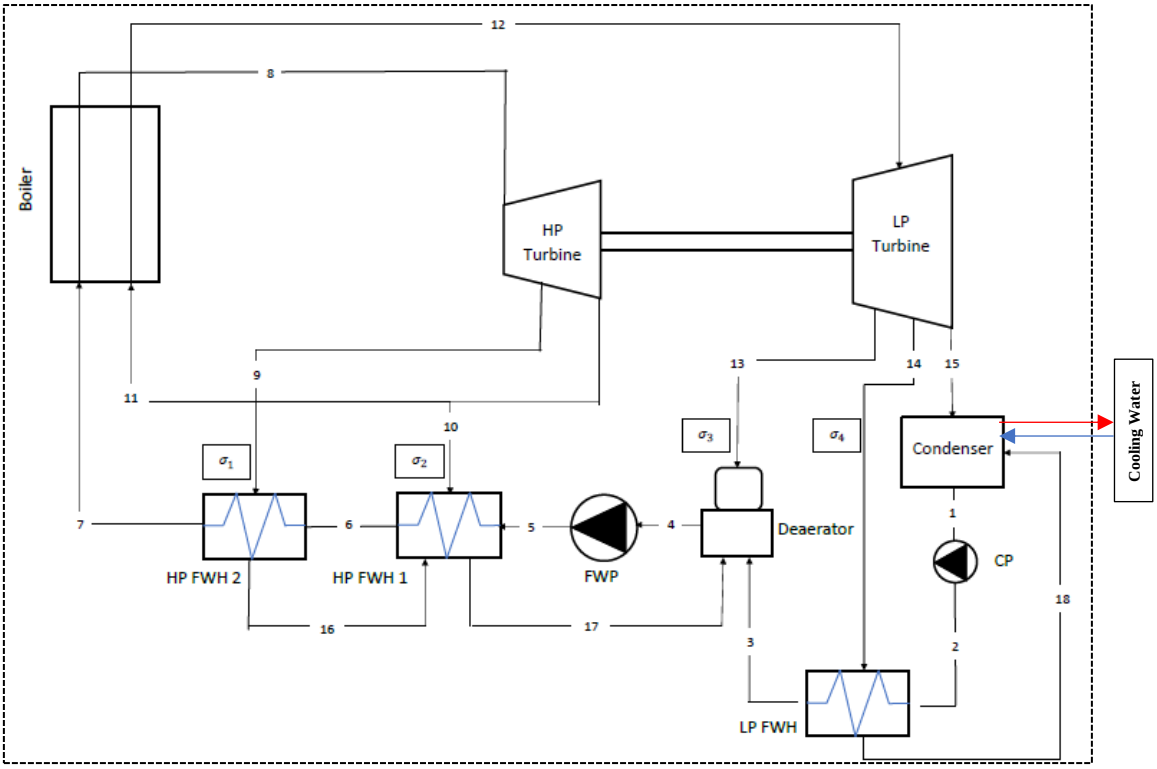

Figure 4.1: Schematic of Rankine Cycle with reheat, regeneration (including low pressure feedwater heater)

The T-s diagram of the Rankine cycle is illustrated in Figure 4.2. The system shown in Figure 4.1 was modelled on the EES Software, based on the assumptions stated in the Methodoology, to produce the T-s diagram illustrated in Figure 4.2. The solid and dotted lines that cut across the isobaric lines represent the ideal and actual system, respectively. The deviation of the dotted lines from the isentropic lines (solid lines) represents the irreversibilities within the system.

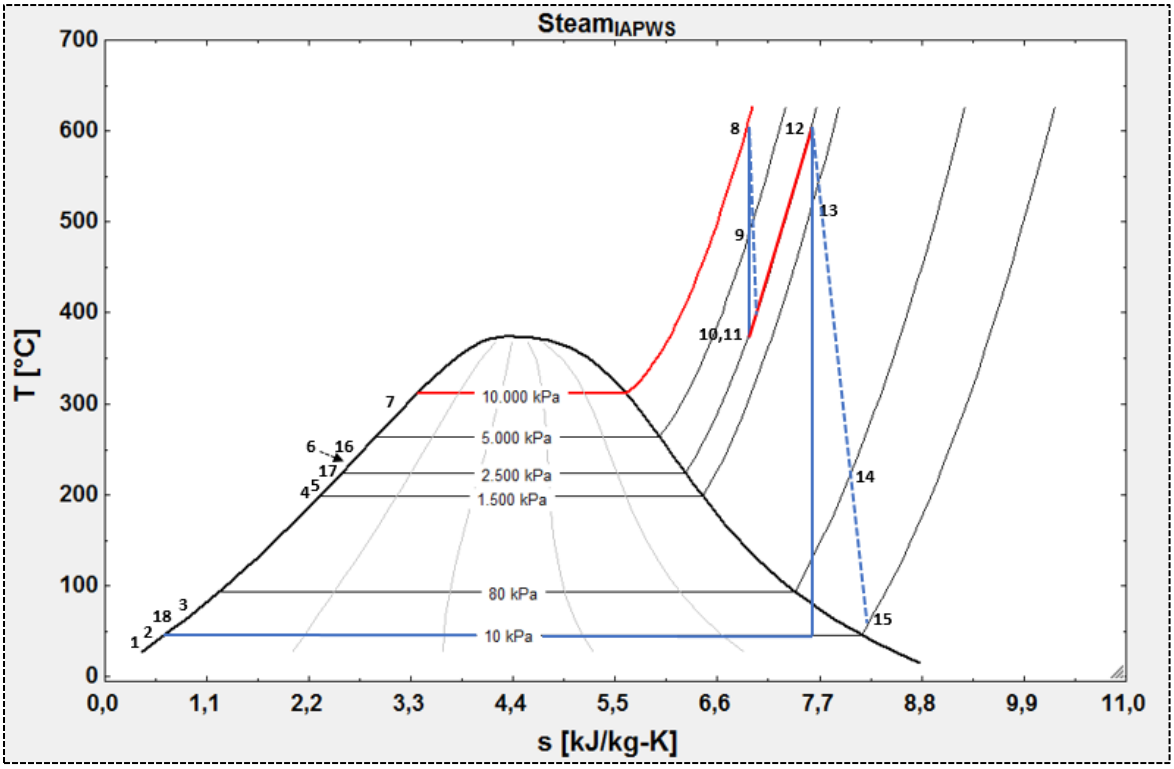

Figure 4.2: T-s diagram of Rankine cycle with single reheat, regeneration (including low pressure feedwater heater)

Table 4.1 shows the process parameters at the inlets and outlets of every component that forms the Rankine cycle depicted in Figure 4.1. The mass flow rates are represented as fractions of the mass flow rate of the feedwater entering the boiler. Therefore, they can be scaled up to produce the required power.

Table 4.1: Process parameters of Rankine Cycle with reheat, regeneration and LP feedwater Heater

	h (kJ/kg)	**P (kPa)**	**s (kJ/kg/K)**	**T (°C)**	$\dot{m}\left(\frac{kg}{s}\right)$	$\psi\left(\frac{kJ}{kg}\right)$	$\dot{X}\left(\frac{kJ}{s}\right)$
1	191,7	10	0,6489	45,79	0,685	2,822	1,933
2	193,6	1500	0,6501	45,93	0,685	4,364	2,989
3	432,8	1500	1,34	93,7	0,685	37,87	25,94

4	844,8	1500	2,315	198,3	1	159,17	159,2
5	857,2	10000	2,32	200,3	1	170,08	170,1
6	1029	10000	2,67	238,1	1	237,53	237,5
7	1381,4	10000	3,315	306,7	1	397,62	397,6
8	3625	10000	6,902	600	1	1571,8	1571,7
9	3415	5000	6,951	491,9	0,15	1347,2	202,1
10	3234	2500	7,007	397,7	0,0725	1149,5	83,34
11	3234	2500	7,007	397,7	0,7775	1149,5	893,7
12	3686	2500	7,596	600	0,7775	1425,8	1108,6
13	3522	1500	7,632	522,3	0,0925	1251,1	115,7
14	2868,6	80	7,923	196,4	0,062	511,0	31,68
15	2599	10	8,195	53,72	0,623	160,3	99,84
16	1066	5000	2,754	246,1	0,15	249,5	37,42
17	890,2	2500	2,408	208,3	0,2225	176,8	39,35
18	225,8	80	0,7543	53,93	0,062	5,500	0,341
Cold water	104,8	101	0,3669	25	30	0	0
Hot water	154,8	101	0,5312	37	30	1,00	30

The power balance of the major components is shown in Table 4.2, where the power balance of the boiler represents the power required to superheat and reheat the feedwater heater. The condenser power balance represents the power required to condense the residual steam from the low-pressure turbine to saturated liquid at the condenser pressure. The turbine power balance is essentially the combined work produced by the low and high-pressure turbines. And

finally, the power balance of the two pumps represents the work that must be supplied to the pumps to increase the feedwater pressure to the required pressure at the two respective points.

Table 4.2: Power Balance of the main power plant components

Component	Power Balance (kW)
Boiler	2595,0
Condenser	1501,9
Turbine	1106,9
FWP	12,4
CP	1,30
Total	**5217,5**
Thermal Efficiency	**42.13** -

4.1.2 Geothermal Preheater System

Figure 4.3 is a schematic of the geothermal preheat system that was modelled. Comparing it to Figure 4.1, the geothermal heat exchanger replaced the low-pressure feedwater heater. The geothermal heat exchanger uses geothermal energy to preheat the feedwater at low pressure and thus eliminates the need to extract steam from the low-pressure turbine. This means that less steam is extracted from the low-pressure turbine which allows the low-pressure turbine to generate more power. The rest of the system was constructed very similarly to the one depicted in Figure 4.1: The condensate pump pressurises the saturated feedwater from the condenser. The feedwater is then preheated through the geothermal preheater. When it enters the deaerator, it is heated to a saturated liquid phase to allow the removal of oxygen. Thereafter, the feedwater is pressurised by the feedwater pump and is then heated further by the two serial high pressure feedwater heaters before it enters the boiler. In the boiler, the pressurised feedwater is superheated. Upon exiting the boiler, the superheated feedwater enters the high-pressure turbine. The feedwater expands in the turbine and power is generated. A portion of the bled

steam is sent back to the boiler to be reheated. This reheated steam is then used to generate more power through the low-pressure turbine. Finally, a portion of the steam bled from the low-pressure turbine is condensed in the condenser and the cycle begins again.

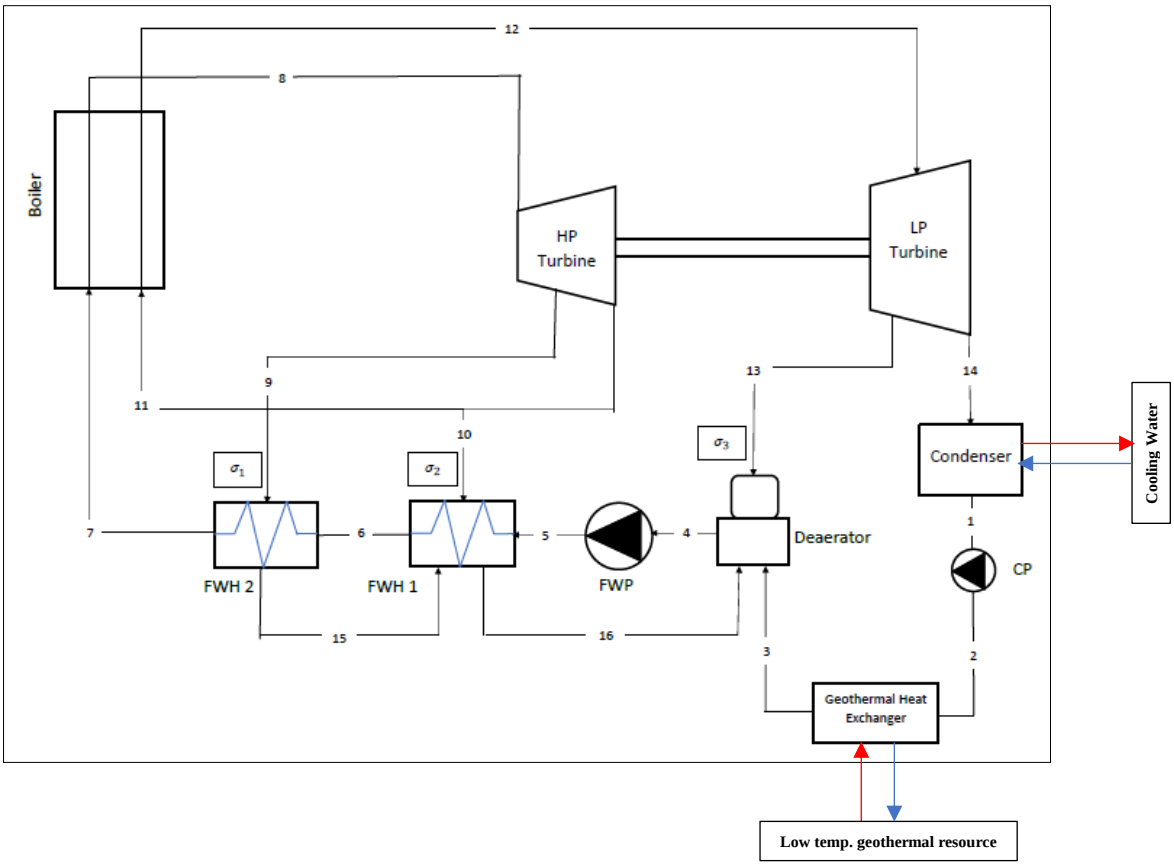

Figure 4.3: Rankine Cycle with reheat, regeneration and geothermal preheater

The T-s diagram depicted below is identical to the one depicted in Figure 4.2. TheT-S diagram was drawn using the EES Software as well.

The main difference between Figure 4.2 and Figure 4.4 is that Figure 4.4 shows two extraction points (13 & 14) from the low-pressure turbine stream unlike the three extraction points shown in Figure 4.2 (13,14 & 15). As discussed before, the reason for this is that the Geothermal Heat Exchanger does not make use of steam bled from the turbine.

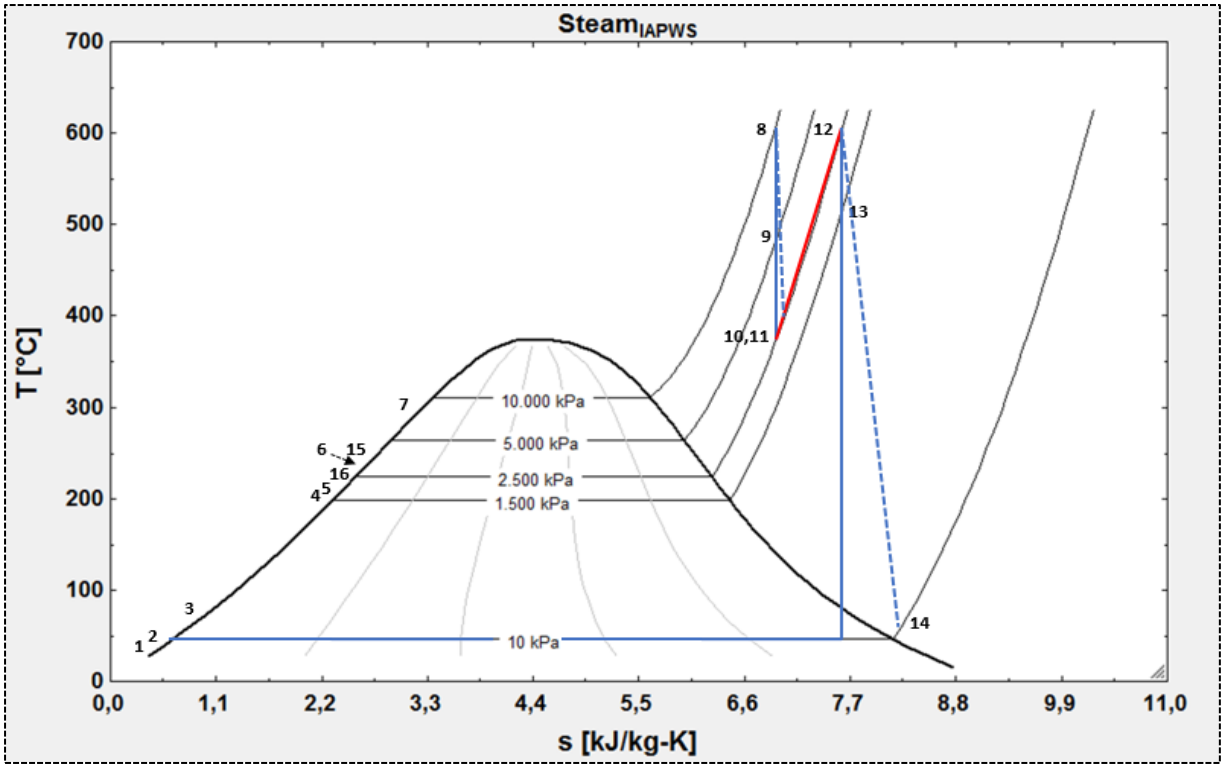

Figure 4.4: Schematic of Rankine Cycle with reheat, regeneration (with geothermal preheater)

Analysis of the T-s diagrams in Figures 4.2 and 4.4 in conjunction with their respective schematics (Figures 4.1 and 4.3) shows that the greatest energy losses occurred in the condenser. More energy was lost to the environment through the condenser than the boiler. These results were validated by Isam H. Aljundi's study of the Energy and Exergy analysis of a steam power plant in Jordan [65].

The process parameters of the geothermal preheat system are tabulated in Table 6. Compared to table 4, there are a reduced number of points due to the elimination of the extracted steam from the low-pressure turbine.

Table 4.3: Process parameters of Rankine cycle with geothermal preheater in place of low-pressure feedwater heater

	h (kJ/kg)	**P (kPa)**	**s (kJ/kg/K)**	**T (°C)**	$\dot{m}\left(\frac{kg}{s}\right)$	$\psi\left(\frac{kJ}{kg}\right)$	$\dot{X}\left(\frac{kJ}{s}\right)$
1	191,7	10	0,6489	45,79	0,685	2,822	1,93

2	193,6	1500	0,6501	45,93	0,685	4,364	2,99
3	432,8	1500	1,34	93,7	0,685	37,87	25,94
4	844,8	1500	2,315	198,3	1	159,2	159,2
5	857,2	10000	2,32	200,3	1	170,1	170,1
6	1029	10000	2,67	238,1	1	237,5	237,5
7	1381,4	10000	3,315	306,7	1	397,6	397,6
8	3625	10000	6,902	600	1	1572	1572
9	3415	5000	6,951	491,9	0,15	1347	202,1
10	3234	2500	7,007	397,7	0,0725	1150	83,34
11	3234	2500	7,007	397,7	0,7775	1150	893,7
12	3686	2500	7,596	600	0,7775	1426	1109
13	3522	1500	7,632	522,3	0,0925	1251	115,7
14	2599	10	8,195	53,72	0,685	160,3	109,8
15	1066	5000	2,754	246,1	0,15	249,5	37,42
16	890,2	2500	2,408	208,3	0,2225	176,9	39,35
Cold water	104,8	101	0,3669	25	33	0	0
Hot water	154,8	101	0,5312	37	33	1,00	30,00

The power balance of the different components in the geothermal preheater system are displayed in Table 4.4 below. Comparing these values to those tabulated in Table 4.2 reveals the boiler heat loads for both systems remains unchanged. As discussed earlier that there are two functional modes of the geothermal preheat system: The Power Boosting mode and the

Fuel Saving mode. The system in Figure 4.3 was modelled in power boosting mode given that the boiler heat load was fixed. This means that the same amount of fuel was supplied to the boiler in both systems. Because of this, the geothermal preheat system has the capacity to generate more work from the low-pressure turbine (as is illustrated by comparing turbine power balances displayed in Tables 4.3 and 4.5 for the LPFWH system and the GP system, respectively).

Table 4.4: Power Balance of the main power plant components in hybrid system

Component	Power Balance (kW)
Boiler	2595
Condenser	1649
Turbine	1136,9
GPH	239,2
CP	1,30
FWP	12,4
Total	**5381,7**
Thermal Efficiency	**40,2**

4.1.3 Model Validation of Fossil-Geothermal Hybrid Power Plant

In their study, Qin and Hu [62] assessed the effects of replacing various proportions of the feedwater with renewable energy and plotted the results in the graph below (Figure 4.5). They assessed different scenarios but scenario 4 is the one that is applicable to this research since it involves the replacement (partial or complete) of the low-pressure feedwater heater. Each plot represents a different scenario, the difference between the scenarios being the location of the renewable assisted preheater.

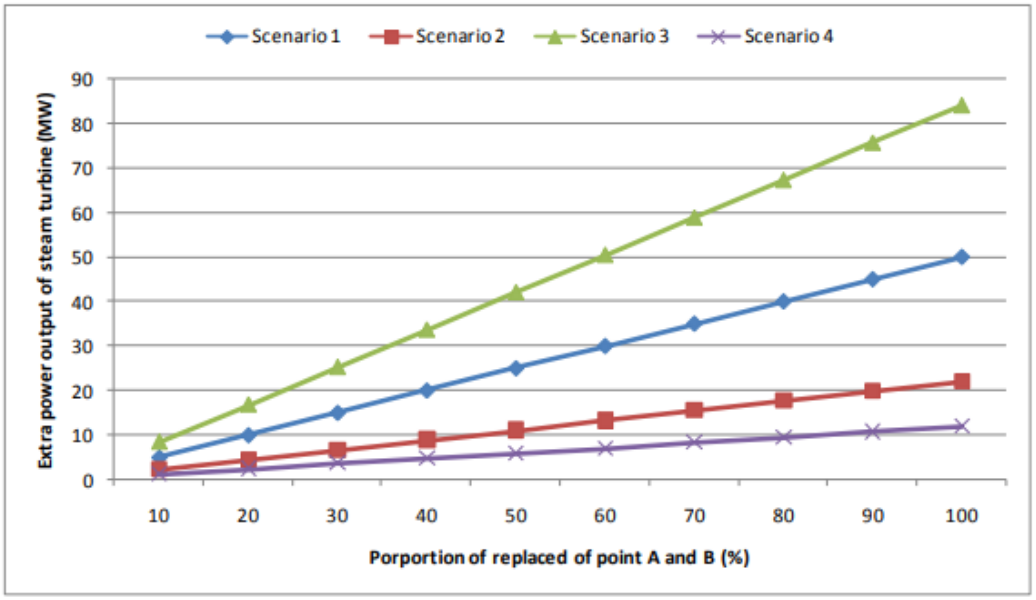

Figure 4.5: Extra power generated for different proportions of replaced bled steam [61]

Figure 4.6 displays a graph showing the power boosting effects of replacing the feedwater heater in various portions for this research. Comparing Figure 4.6 to the scenario 4 in Figure 4.5 shows some similarities. The main one being that both graphs have relatively low gradients but most importantly, the greater the portion of feedwater heating replaced, the greater the power boost.

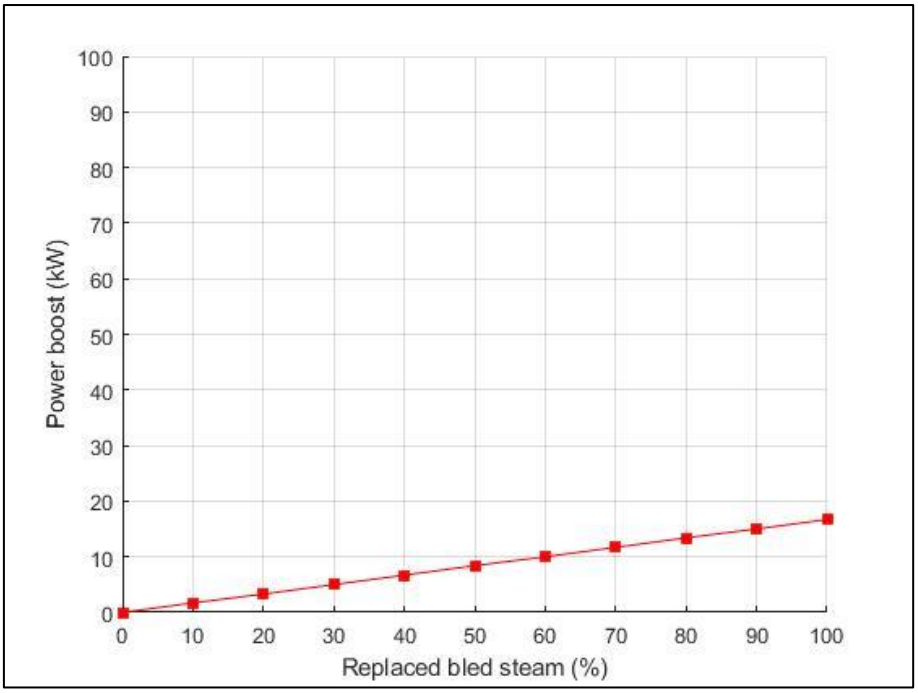

Figure 4.6: Extra power generated for different proportions of replaced bled steam in hybrid system

Results of Energy and Exergy Analysis As discussed previously, in the T-s diagram, the two dotted blue lines are representatives of the actual cycle whereas the two blue solid lines show isentropic processes which are representative of an ideal cycle; where the deviation of the dotted lines from the solid lines is representative of the irreversibilities within the system.

In the two systems illustrated previously (Figures 4.1 and 4.3), the parameter values (temperature and pressure) at the boiler outlet were assumed to be constant. This helped to highlight the effect of replacing the low-pressure feedwater heater in Figure 4.1 with a geothermal preheater in Figure 4.3 in power boosting mode.

4.2 Results of Energy and Exergy Analysis

4.2.1 Results of First Law Efficiency

Two major observations were made regarding the first law thermodynamic efficiency of the two systems:

- In the geothermal preheat system, there are two external sources of heat: coal combustion in the boiler (primary heat and reheat) and the geothermal preheater.

- In the system with a low pressure feedwater heater, there is just one external source of heat: coal combustion in the boiler (primary and reheat). The low-pressure feedwater heater uses steam extracted from the low-pressure turbine to preheat the feedwater heater. This means that the work output from the low-pressure turbine is reduced.

The system with the geothermal preheater will have a higher value of Q_{in} in comparison to the low-pressure feedwater heater system. This is because the geothermal heat required to preheat the feedwater heater is considered an external source of heat, the same way that the fossil fuel resource in question is. The heat lost in the condenser, Q_{out}, is nearly equal in both systems.

The ratio of electrical output to total heat supply is known as the thermal efficiency: $\eta_{th} = \frac{W_{net}}{Q_{in}}$. It is lower for the system with the geothermal preheater than it is for the system with a LPFWH (Tales 4.2 and 4.4). This can be attributed to the geothermal energy resource. The geothermal energy is supplied from a low temperature resource which is at a much lower temperature than the boiler as well as the steam extracted from the LPT to preheat the feedwater in the LPFWH system.

Because of the additional external heat source (geothermal energy), the denominator in the thermal efficiency equation, Q_{in}, is higher for the geothermal preheater system than it is for the LPFWH system. The nominator in the thermal efficiency equation, W_{out}, is also higher for the geothermal preheat system than it is for the LPFWH system because the geothermal preheat system eliminates the need to extract steam from the low-pressure turbine, thereby generating more electrical power. However, W_{out} does not increase at the same rate as Q_{in} resulting to an overall reduced ratio (owing to the geothermal resource temperature as discussed before).

Despite this, if the electricity generation of each system is compared only to the fossil-fuel primary supply, a numerical analysis of the efficiencies showed a 4% increase in the energetic efficiency of the hybrid system which is a quantification of the power boosting capacity of the hybrid system.

In Figure 4.7, the first law efficiency of the two systems was plotted with a variation in the high-pressure turbine inlet pressure. The graph shows the effect that pressure has on the first law efficiency. The efficiency increases because the pressure drop across the turbine increases along with the extraction mass flow rate. This increase reaches a peak at an optimum operating pressure after which it begins to drop. This behaviour can be attributed to the change of the

gradient of the saturated vapour line water. It is also clear that the hybrid system is less efficient than the non-hybrid system. This is because, as discussed previously, the first law efficiency includes the heat input from the low temperature geothermal resource.

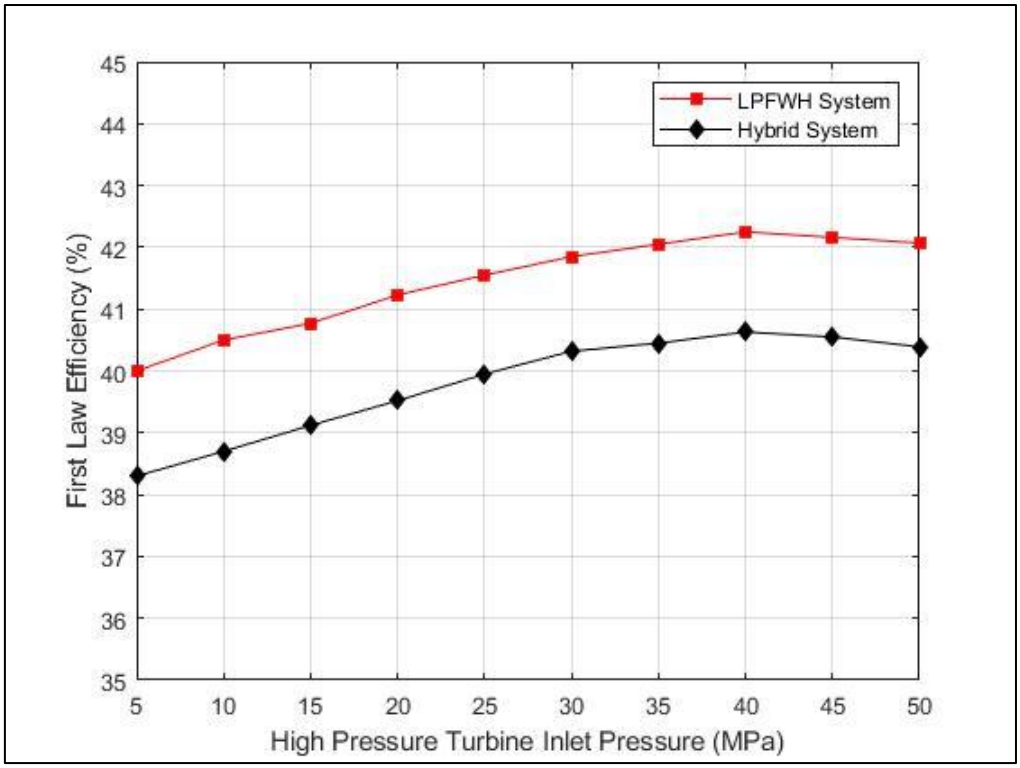

Figure 4.7: Effect of High Pressure Turbine Inlet Pressure on First Law Efficiency

It is important to note that in both systems, the heat input from the geothermal preheater is equated to the heat input from the low-pressure feedwater heater (through regeneration). However, this may not always be the case because the heat supplied from the geothermal preheater is dependent on the geothermal resource and the mass flow rate of the feedwater heater flowing through the geothermal preheater (modelled as DCHE).

A second system was designed where an additional LPFWH was added (see in appendices). This distributes the required preheat load across two FWHs which means more steam is extracted from the LPT. Therefore, as expected, a decreased efficiency was noted (compared to the system with a single LPFWH). But, it was still more efficient than the hybrid system.

If the geothermal resource temperature happens to be greater than 200°C (medium to high temperature resource), then it is advisable to change the location and instead of replacing the low-pressure feedwater heater, use the geothermal preheater in place of one of the high-pressure feedwater heaters. This would yield a greater power boosting capacity.

Fuel Saving Mode

In the two systems designed, Q_{in} was assumed to be constant. This means that the boilers in the two systems have different heating loads. In the GP system, the GP carries a portion of the heat load whereas in the LPFWH system, the boiler carries the total heat load. This however does not translate to improved efficiency in the GP system, given that the GP does not use steam bled from the LPT. This is because decreasing the boiler heat load results to a decrease in the enthalpy and therefore, an overall decrease in the work produced by the turbines. Therefore, for the GP system to be more efficient, the decrease in the work generated in the turbines must be less than the work lost in the LPT (LPFWH system) as a result of steam extraction for feedwater preheating in the LPFWH.

4.2.2 Results of Second Law Efficiency

The second law efficiency of the hybrid system is superior to that of the fossil-fuelled system. Exergy destruction analysis shows that there is a higher rate of exergy destruction in the system that uses a low-pressure feedwater heater to preheat the feedwater.

Entropy generation occurs in all the cycle components due to the various irreversibilities within the system, as shown in Tables 4.5 and 4.6. Optimisation is necessary for the minimisation of these irreversibilities. Although the boiler is the component with the largest irreversibility (as indicated by the entropy generated in the boiler), it is a very expensive and complex component. As pointed out previously, entropy generation is principally defined as the destruction of exergy, so there is a major source of exergy destruction within the boiler. The chemical process involved in the combustion of energy is the biggest contributor to exergy destruction in the boiler. Table 8 below shows the exergy destroyed in each major component of the fossil fuelled power plant.

Table 4.5: Exergy destruction rate of the power plant components

COMPONENT	EXERGY DESTRUCTION (KW)	PERCENT RATIO	EXERGY EFFICIENCY
Boiler	319,6	54,8	54,6
Condenser	67,63	11,6	32,3
Turbine	147,03	25,2	88,3
FWP	1,49	0,26	88
CP	0,245	0,04	81,2
LP heater	8,39	1,44	75,8
Deaerator	19,92	3,42	89
First HP heater	13,96	2,40	95,2
Second HP heater	4,56	0,78	98
Total	**582,8**	**100**	-

The exergy analysis of the main power plant components of the hybrid system is displayed in Table 4.6. The table reveals the boiler and turbines to have the highest entropy generation rates. The exergy destruction rate in the boiler accounts for nearly half of the cycle exergy destruction rate. This means that irreversibility is greatest in the boiler where chemical reaction can account for a significant portion. However, optimisation of the boiler becomes a challenging task and therefore, other components in the system can be optimised to reduce the overall system irreversibility.

Table 4.6: Exergy destruction rate of the power plant components in hybrid system

COMPONENT	EXERGY DESTRUCTION (kW)	PERCENT RATIO	EXERGY EFFICIENCY (%)
Boiler	319,6	54,26	54,6

Condenser	74,34	12,62	32,3
Turbine	152,1	25,82	88,1
FWP	1,49	0,253	88,0
CP	0,245	0,042	81,2
Geothermal PH	0,85	0,145	80,5
Deaerator	21,84	3,709	87,9
First HP heater	13,96	2,371	95,2
Second HP heater	4,556	0,774	96,9
Total	**588,9**	**100**	**-**

Tables 4.4 and 4.6show the importance of performing an energy and exergy analysis. Table 4.4shows that 30% of the energy is lost to the environment through the condenser. Table 4.6 goes on to show the quality of the energy that is lost in the condenser. Although the energy losses are very high, the quality is lower in comparison to other components. This can be attributed to the temperature of the working fluid when it gets to the condenser. It has a lower potential to do work, compared to the high potential of superheated steam at high temperatures that is found in the boilers. This highlights the need for both energy and exergy analysis because high energetic efficiency does not translate to high exergetic efficiency.

Figure 4.8 below shows the effect of the inlet pressure of the high-pressure turbine on the second law efficiency. The graph reflects a similar profile to the graph in Figure 4.7. This is because the second law efficiency is a function of the first law efficiency. However, unlike the

first law efficiency (Figure 4.7), the hybrid system has a greater second law efficiency, evidence of its superiority according to the second law.

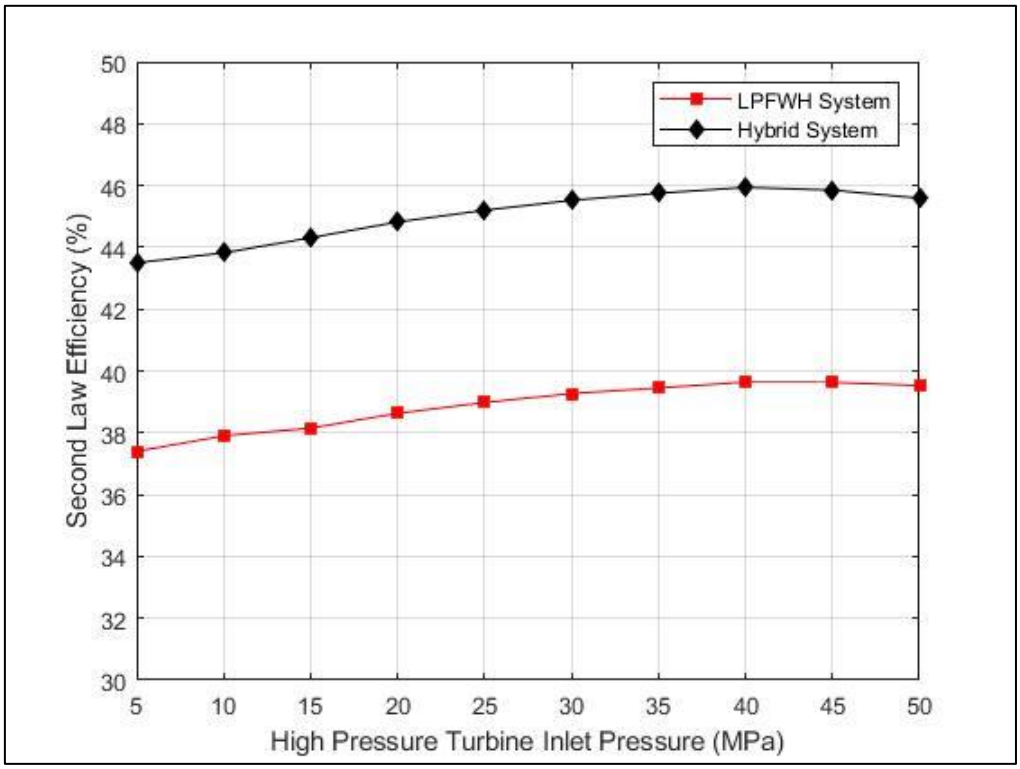

Figure 4.8: Effect of High Pressure Turbine Inlet Pressure on Second Law Efficiency

4.2.3 Results of Organic Rankine Cycle

The energetic and exergetic potential of a low temperature geothermal resource are presented by analysing the behaviour of an Organic Rankine Cycle that utilises the same geothermal resource used in the hybrid system. An Organic Rankine Cycle makes use of the low temperature geothermal resource as a secondary fluid to heat the primary fluid (normally an organic fluid with a very low boiling point).

Figure 4.9shows the behaviour of the first law efficiency with respect to rejection temperature. It is clear from the graph that a higher geothermal resource temperature will have a higher efficiency. The greater the difference between the resource temperature and the rejection temperature, the higher the first law efficiency because it means that a greater amount of heat was transferred to the binary working fluid and therefore, more work was generated. The geothermal power plant, as a stand-alone, assuming the geothermal resource in question is 135°C has an efficiency that is no more than 10,8%. However, hybridising it with another

energy resource (such as the fossil fuelled power plant case presented), enables an increase in efficiency.

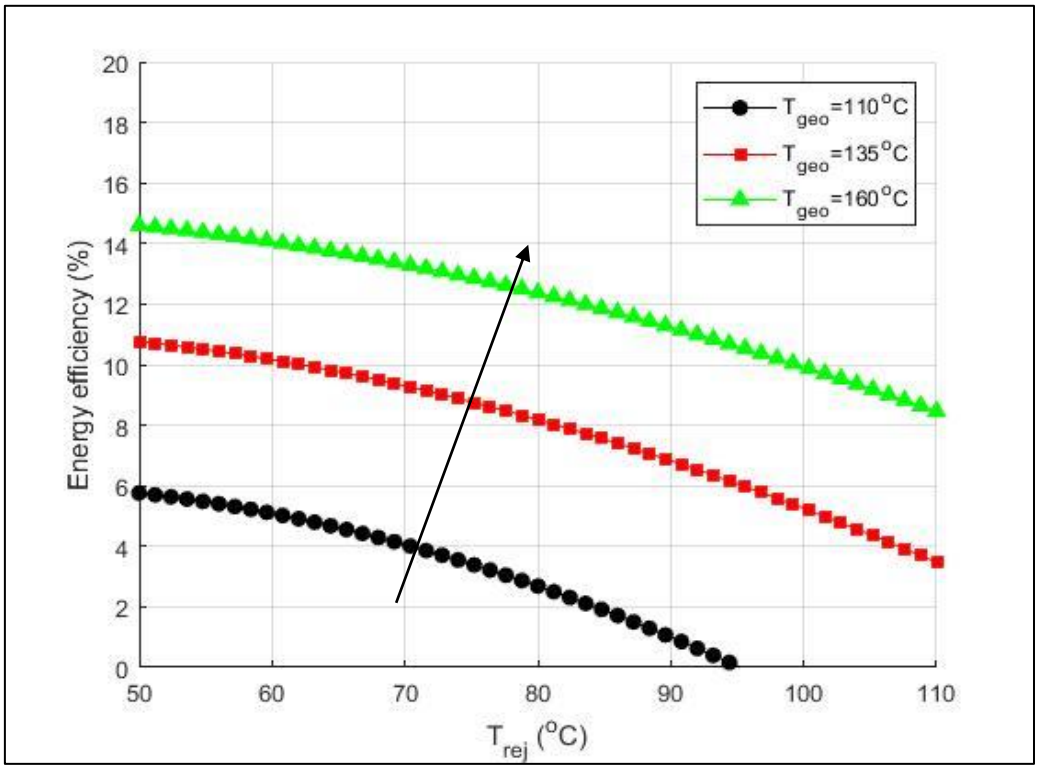

Figure 4.9: Maximum first law efficiency of geothermal power plant (Organic Rankine Cycle) as a function of rejection temperature and with variation in resource temperature

Figure 4.10shows the exergetic efficiency or second law efficiency of the Organic Rankine Cycle that was discussed earlier in this report. Similar to Figure 4.9, the graph shows that the difference between resource temperature and rejection temperature is directly proportional to the exergetic efficiency.

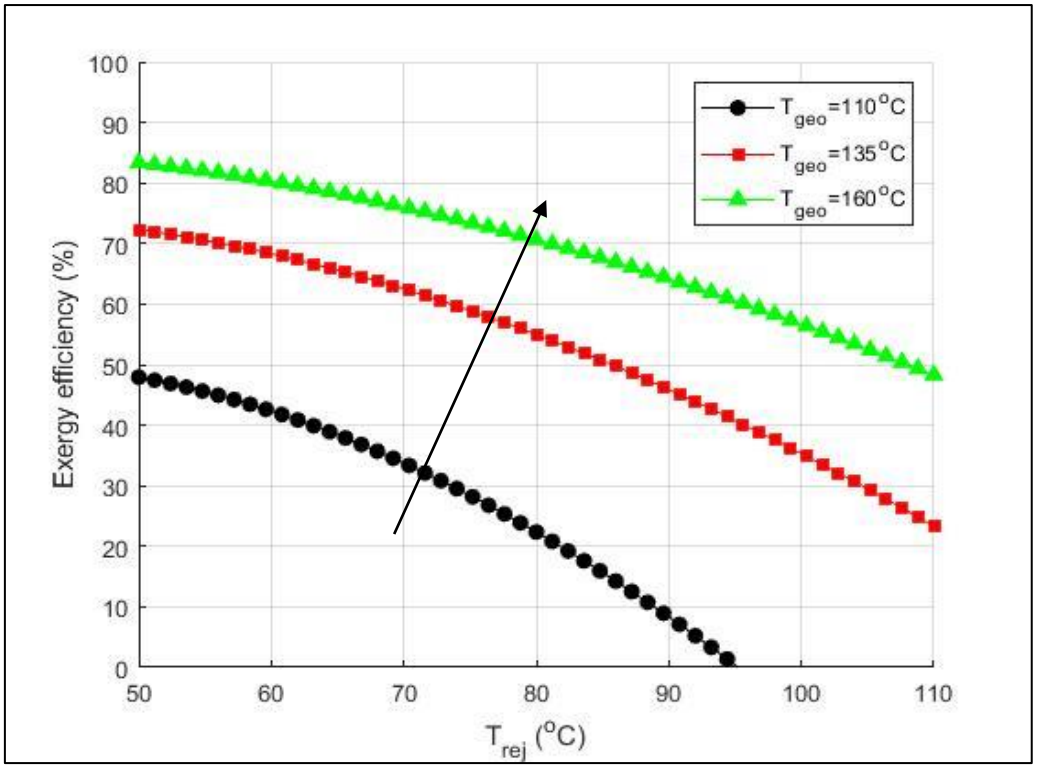

Figure 4.10: Maximum second law efficiency of geothermal power plant (Organic Rankine Cycle) as a function of rejection temperature and with variation in resource temperature

The heat exchangers in the system are the preferred component for optimisation. Therefore, an entropy generation minimisation analysis (EGM) can be used to optimise them. The feedwater heaters as well as the condenser are all examples of heat exchangers within the system.

The feedwater heaters were selected to undergo optimisation. Feedwater heaters are good examples of counterflow heat exchangers and were therefore modelled as such. In counter-flow heat exchangers, as the name suggests, the two fluid streams flow in opposite directions. The optimisation results are discussed below.

4.3 Optimisation

The following optimisation was performed on the hybrid system. Two components were optimised: one of the high pressure feedwater heaters and the geothermal preheater.

4.3.1 Feedwater Heater

The second high-pressure feedwater heater was optimised and the graphs to follow display the results of the optimisation. Two conditions were analysed: optimum (L/r_h) as well as the area

constraint condition which is applied when the cost of the heat exchanger is of major consideration.

The mass flow rate was set as 92 kg/s to give the power plant a 100 MW rating. The minimum tube flow area used to plot the graphs that follow is 0.01 m^2 and the maximum 0.02 m^2. For the mass flux, the mass flow rate was fixed, and the tube flow area range of 0.01 m^2 to 0.02 m^2 resulted to a minimum and maximum mass flux of 4600 kg/s.m^2 and 9200 kg/s.m^2 respectively.

Area Constraint

In Figures 4.11, 4.12 and 4.13, the pressure was fixed at 10 MPa, and the tube side flow area was varied from 0.01 m^2 to 0.02 m^2. The optimum dimensionless mass flow rate and minimum entropy generation number based on the optimum 'g', were both plotted against Reynolds number.

Figure 4.11 shows the effect that fluid flow has on the optimal mass velocity. From the graph, an inverse parabolic relationship between the dimensionless mass velocity and Reynolds number which is representative of the equation: $g_{1,opt} = \left[\frac{\tau}{3Ba_1^2 f_1 St_1}\right]^{1/4}$ can be observed. As the flow area of the tube increases, the optimum mass velocity decreases which reflects the equation: $g = \frac{G}{\sqrt{2\rho P}} = \frac{\dot{m}/A}{\sqrt{2\rho P}}$ (assuming fixed density). In physical terms, increasing the flow area could mean increasing the shell flow area which allows for either:

- An increase in the cross-sectional area of each tube or;
- An increase in the number of tubes within the shell.

Note the inconsistent difference between subsequent plots for the various areas. As the area decreases, the optimum mass velocity number (g) becomes more sensitive to changes in area.

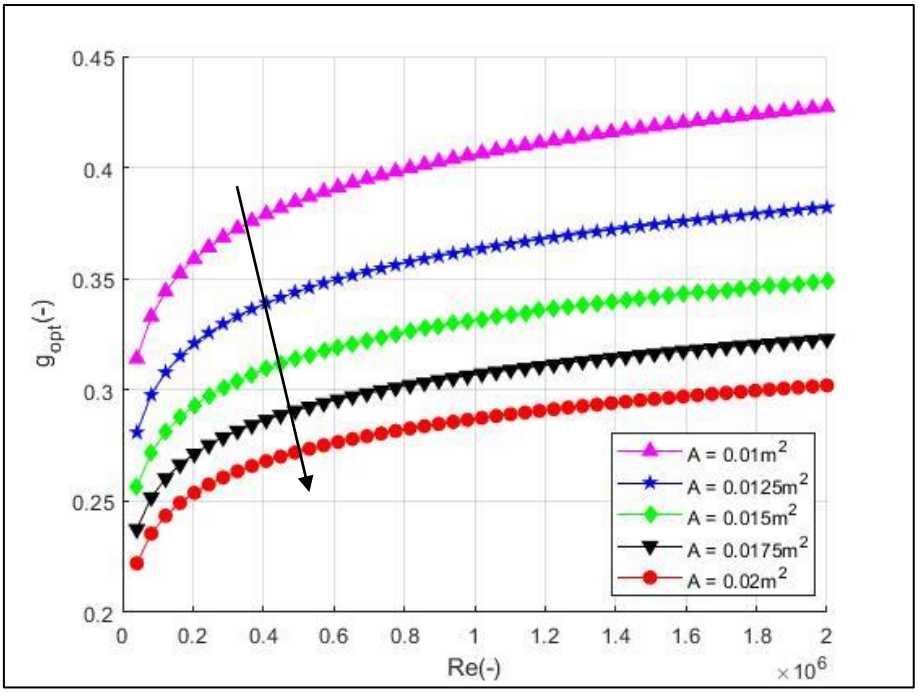

Figure 4.11: Optimal dimensionless mass velocity with variation in cross sectional area

Figure 4.12 depicts the effect that the fluid flow has on the minimum entropy generation rate. This reflects similar behaviour to that of the optimum mass velocity in Figure 4.11. Observing the magnitudes of the scale on the dependent axis (g_{opt} in Figure 4.11 and N_{Smin} in Figure 4.12), shows that Reynolds number has a greater effect on the optimum g than it does on the minimum entropy generation. Similar to Figure 4.11: decreasing the area leads to an exponential increase in the minimum entropy generation number.

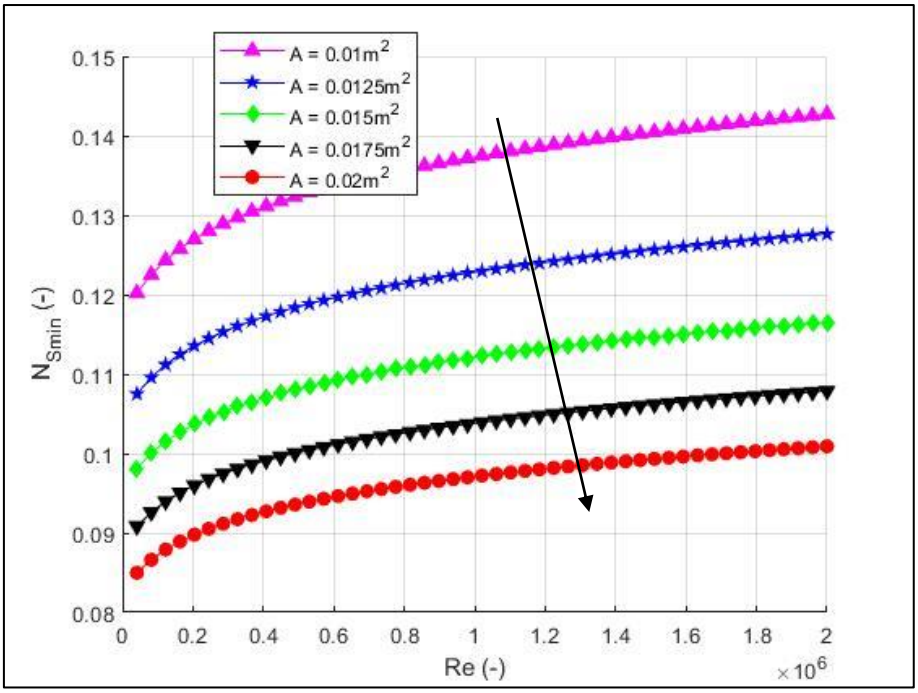

Figure 4.12: Minimum entropy generation number with variation in cross sectional area

Figure 4.13 shows a graph that represents the relationship between the minimum entropy generation number and the optimum dimensionless mass flux, g. From the similarities observed in Figures 4.11 and 4.12, a relationship of direct proportion is expected between the minimum entropy generation number and the optimum mass flux number. Figure 4.13 represents the equation below:

$N_{S_1} = \frac{\tau}{a_1 g_1 St_1} + Bf a_1 {g_1}^3$, with the first term on the right-hand side being the entropy generation contribution due to a finite temperature difference and the second term being the contribution due to fluid friction caused by pressure drop.

Another observation made from Figure 4.13 is how concentrated the points become as g_{opt} increases.

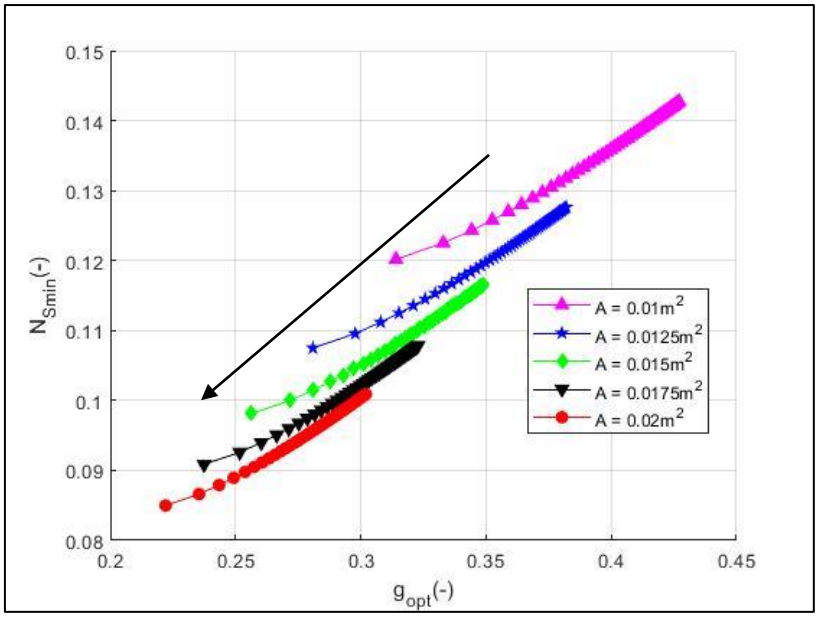

Figure 4.13: Minimum entropy generation number versus optimal dimensionless mass velocity with variation in cross sectional area

In Figure 4.14, the entropy generation contributions of heat transfer and fluid friction are plotted separately. Figure 4.13 above is a combination of the two contributions. The graph in Figure 4.14 shows that irreversibility is mostly driven by heat transfer because the set of graphs representing heat transfer irreversibility lie above those representing fluid friction irreversibility.

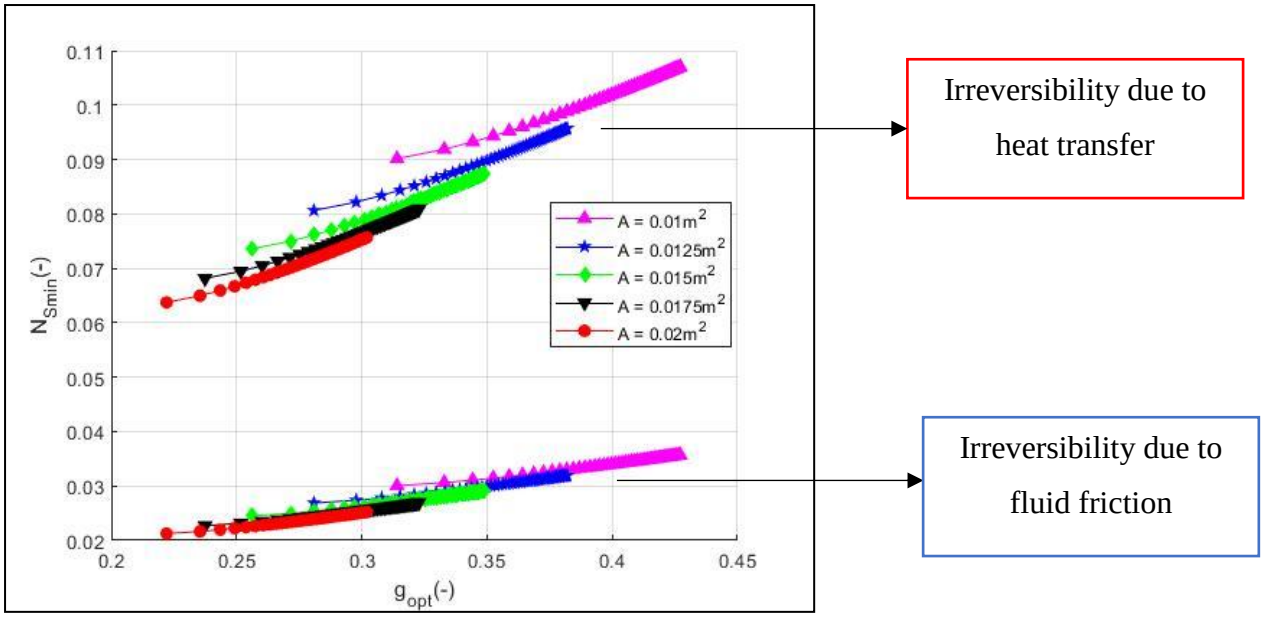

Figure 4.14: Heat transfer and fluid friction contributions to minimum entropy generation number versus optimal dimensionless mass velocity with variation in cross sectional area

Optimisation of tube length to tube radius ratio $\left(\frac{L}{r_h}\right)$

Figures 4.15, 4.16 and 4.17show the L/r_h feature of the minimum entropy generation rate qualitatively. Again, the pressure is fixed at 10 MPa and the mass flux is varied according to the area limits from the previous graphs, ranging between a minimum and maximum of 4600 kg/s.m^2 and 9200 kg/s.m^2 respectively.

In Figure 4.15, the L/r_h ratio is plotted against Reynolds number, Re, displaying:

$\left(\frac{L}{r_h}\right)_{1,opt} = \frac{\tau^{1/2}}{g_1[Bf_1St_1]^{1/2}}$ graphically. It shows the L/r_h ratio increases as Re increases, mimicking inverse parabolic behaviour, similar to the optimum mass flux number analysed in Figure 4.11 above.

Two assumptions can be made regarding the mass flux, given $G = \frac{\dot{m}}{A}$:

- Assuming cross-sectional flow area, A is fixed, an increase in G implies an increase in mass flow rate, $\dot{m}$.

- Assuming mass flow rate, $\dot{m}$ is fixed, an increase in G implies a decrease in the cross-sectional flow area, A.

Figure 4.15 shows that increasing the mass flux reduces the optimum L/r_h ratio. An inconsistent difference between the graphs at varying mass flux is noted and this is representative of the sensitive nature of the L/r_h ratio at lower mass flux values.

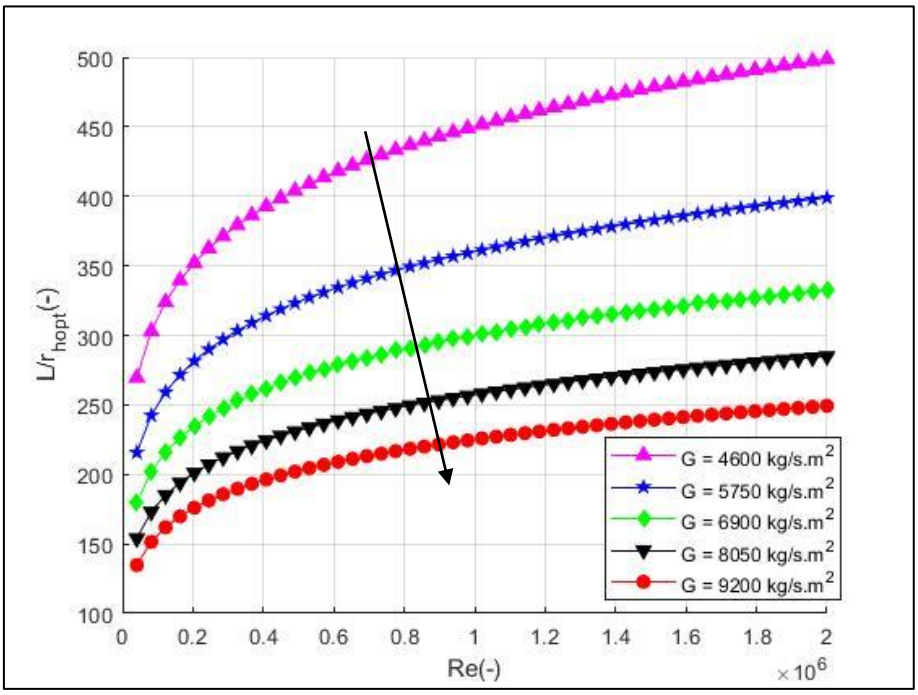

Figure 4.15: Optimum tube length to tube radius ratio versus Reynolds number at varying mass velocity

Figure 4.16 shows the effect of Reynolds number on the minimum entropy generation number at varying mass flux rates. Comparing Figure 4.16 to Figure 4.15, it is clear that the L/r_h ratio is more responsive to changes in Reynolds number than minimum entropy generation number is. This can be explained through the following equation: $N_{S_{1,min}} = 2(\tau B)^{1/2} g_1 \left(\frac{f_1}{St_1}\right)^{1/2}$ which shows a different relationship between minimum entropy generation and Reynolds number (contained in the factor: $\left(\frac{f_1}{St_1}\right)^{1/2}$) compared to the area constraint relationship:

$N_{S_{1,min}} = \left[\frac{256\tau^3 B f_1}{27 {a_1}^2 {St_1}^3}\right]^{1/4}$. From Figure 4.16, it can also be concluded that increasing G increases the minimum entropy generation number.

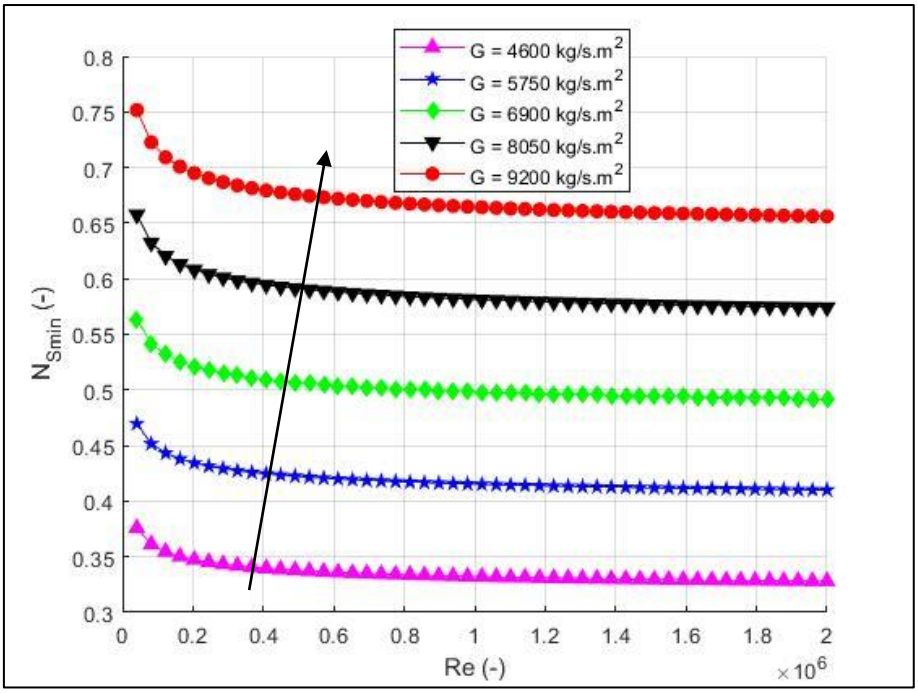

Figure 4.16: Minimum entropy generation number with variation in cross sectional area

Figure 4.7 shows the relationship between the minimum entropy generation number and the L/r_h ratio. It shows that increasing the L/r_h ratio results to a decrease in the minimum entropy generation number. To plot the minimum entropy generation number, the optimum L/r_h ratio was plugged into the equation*:* $N_{S_{1,2}} = \frac{\tau}{(L/r_h)St} + Bf(L/r_h)g^2$ with the first term on the right hand side representing the entropy generated due to heat transfer (owing to a finite temperature difference) and the second representing entropy generated due to fluid friction. Figure 4.17 shows a relatively inverse proportion relationship between the minimum entropy generation number and the L/r_h ratio.

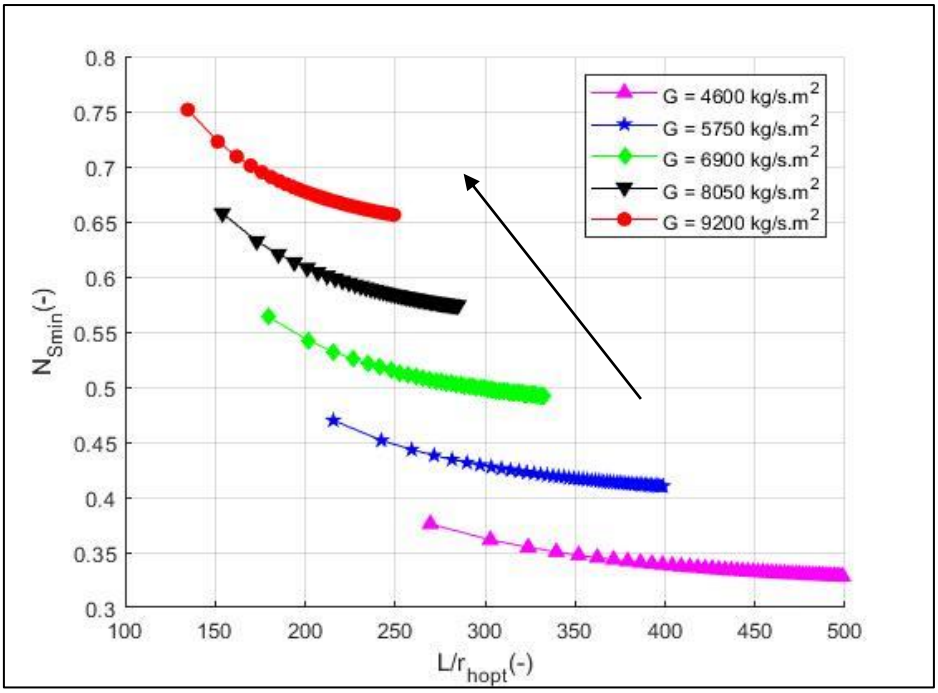

Figure 4.17: Minimum entropy generation number versus optimal length to radius ratio at varying mass flow rates

Figure 4.18 below shows the irreversibility contribution due to heat transfer and fluid friction. It was noted that the irreversibility contribution from each component is equal. The top set of graphs is the combination of the two contributions and the plots mimic those in Figure 4.17. The bottom set of plots represents the contribution due to heat transfer and fluid friction, individually since they are equal in magnitude.

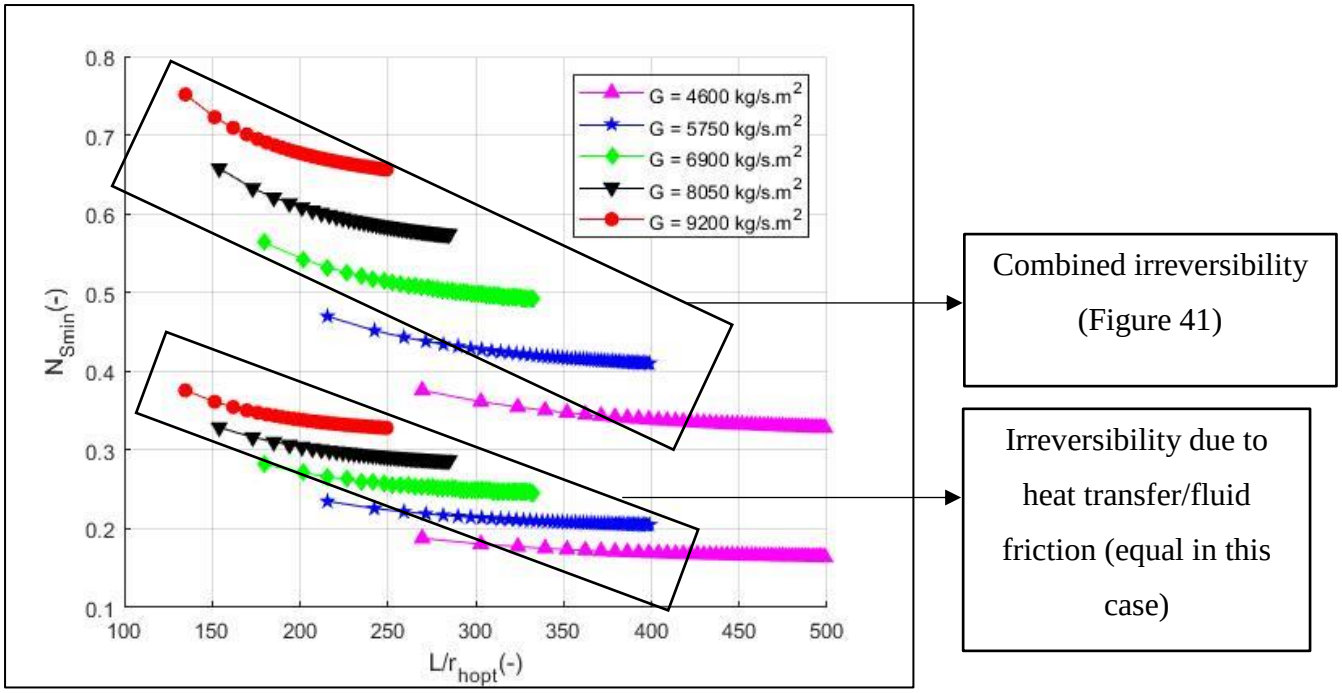

Figure 4.18: Heat transfer and fluid friction contributions to minimum entropy generation number versus optimal L/r_h ratio with variation in mass velocity number

4.3.2 Model Validation of Feedwater Heater Optimisation

The three dimensional logarithmic plot shown in Figure 4.19 was plotted by Adrian Bejan [83]. It is based on turbulent flow in round tubes.

The graph shows that an increase in the entropy generation number is driven by increases in 'g'. Also shown on the three-dimensional plot below is the relative weak effect of the Reynolds number on the number of entropy generation units.

Large values of the L/r_h ratio leads to irreversibilities dominated by fluid friction whereas small values of the L/r_h ratio lead to large stream to stream temperatures and large and therefore, the irreversibilities are dominated by heat transfer.

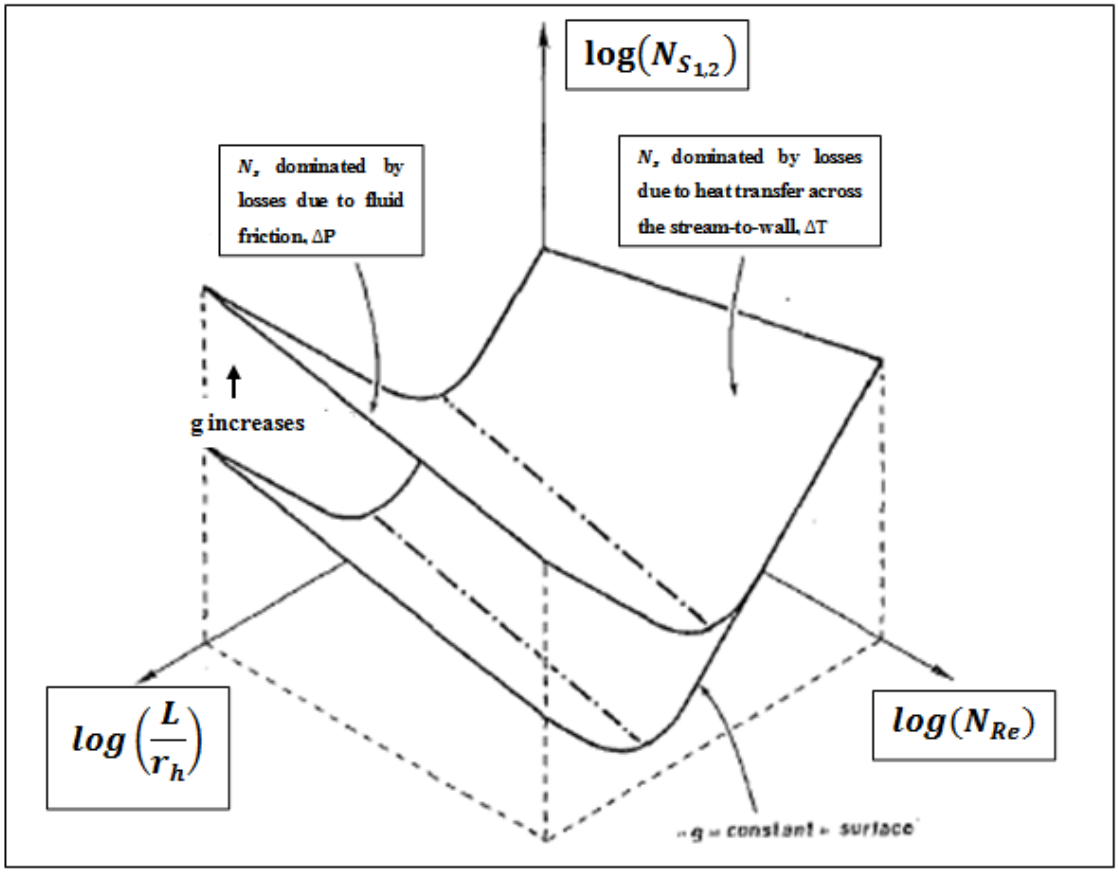

Figure 4.19: Number of entropy generation units per side as a function of Reynolds number, dimensionless mass velocity, and tube length to tube radius ratio [83]

4.3.3 Sensitivity Analysis of Feedwater Heater Optimisation

In the optimisation of the feedwater heater that is modelled as a counter-flow heat exchanger, it is evident that the minimum entropy generation number is relatively insensitive to Reynolds number, particularly high Reynolds numbers (turbulent flow) in the case where the L/r_h ratio is being optimised. This is evident from the way the graph flattens out when the flow becomes turbulent (Figure 4.16).

In Figures .11 and 4.12, observing the axis where g_{opt} and $N_{S_{min}}$ are plotted (with the g_{opt} scale being three times greater) shows that Reynolds number has a greater effect on the mass velocity than it does on the entropy generation.

4.3.4 Geothermal Preheater

An optimised geothermal system consists of an optimal geothermal mass flow rate that ensures minimum pressure drop and minimum entropy generation, while extracting maximum heat [99]. In the extreme cases of a very large flow rate or a very small flow rate, there is no temperature rise in the fluid. Therefore, it is essential to obtain an optimal mass flow rate. In Figures 4.20 and 4.21, an exponential relationship between laminar flow and optimum mass flow rate can be observed. As the flow transitions to turbulent, both graphs reveal a more linear relationship. This can be attributed to the friction factor being:

- Dependent on Re in laminar flow.
- Independent of Re in turbulent flow.

Another important observation to note is that in Figure 4.20, the higher the temperature gradient, the lower the mass flow rate required to extract maximum heat. Similarly, in Figure 4.21. The higher the geothermal resource temperature, the lower the mass flow rate required to extract maximum heat. Hence, high temperature gradients and resource temperatures are expected to generate a higher power output.

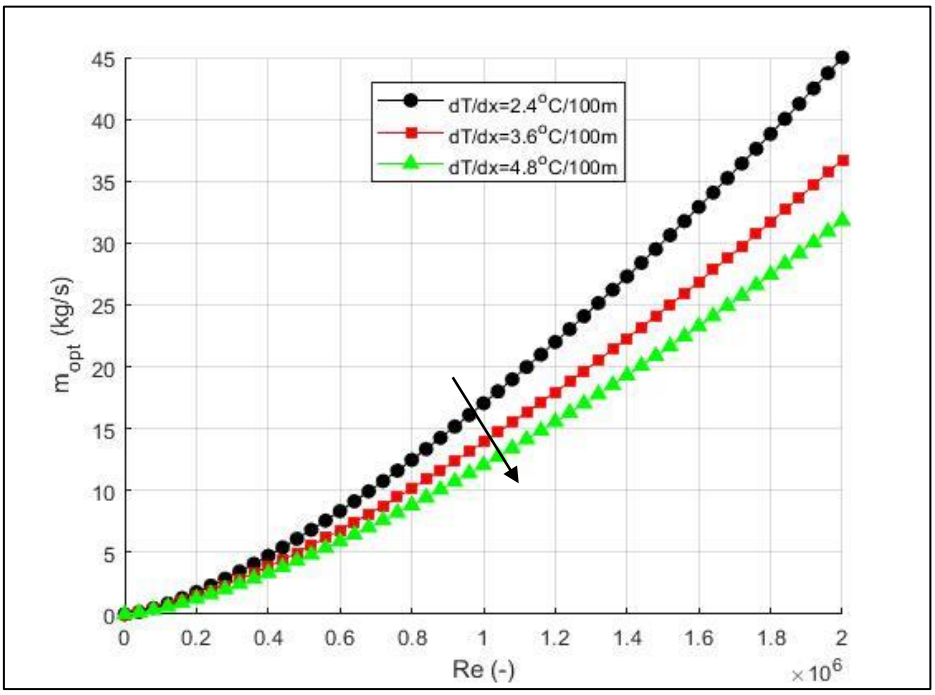

Figure 4.20: Optimal mass flow rate of geothermal fluid with variation in temperature gradient

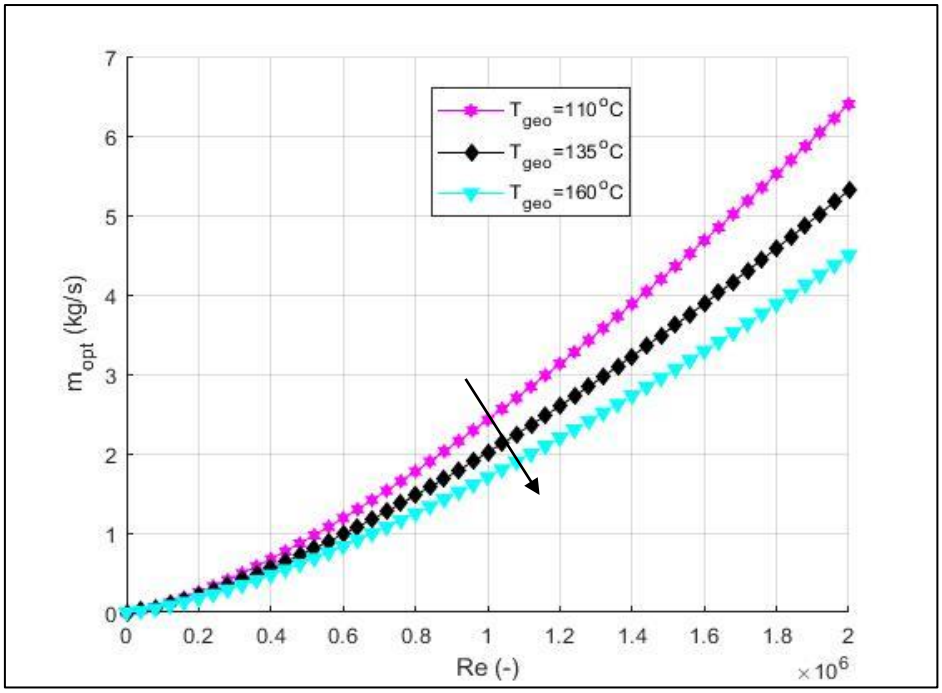

Figure 4.21: Optimal mass flow rate of geothermal fluid with variation in resource temperature

Figures 4.22 and 4.23 show the inverse exponential relationship between the outer diameter of the DCHE and Reynolds number. Figure 4.22 shows a greater change in the outer diameter at different temperature gradients compared to the slight changes in Do at different resource temperatures depicted in Figure 4.23. This indicates that temperature gradient has a greater influence on the outer diameter of the DCHE. Also, similar to the analysis of Figures 4.20 and 4.21, a higher temperature gradient and a higher resource temperature are highly recommended. In this particular case, regarding the outer diameter, D_o, of the DCHE, a geothermal site with the highest temperature gradient and/or resource temperature will require a smaller DCHE and therefore, reduce the overall cost of the power plant.

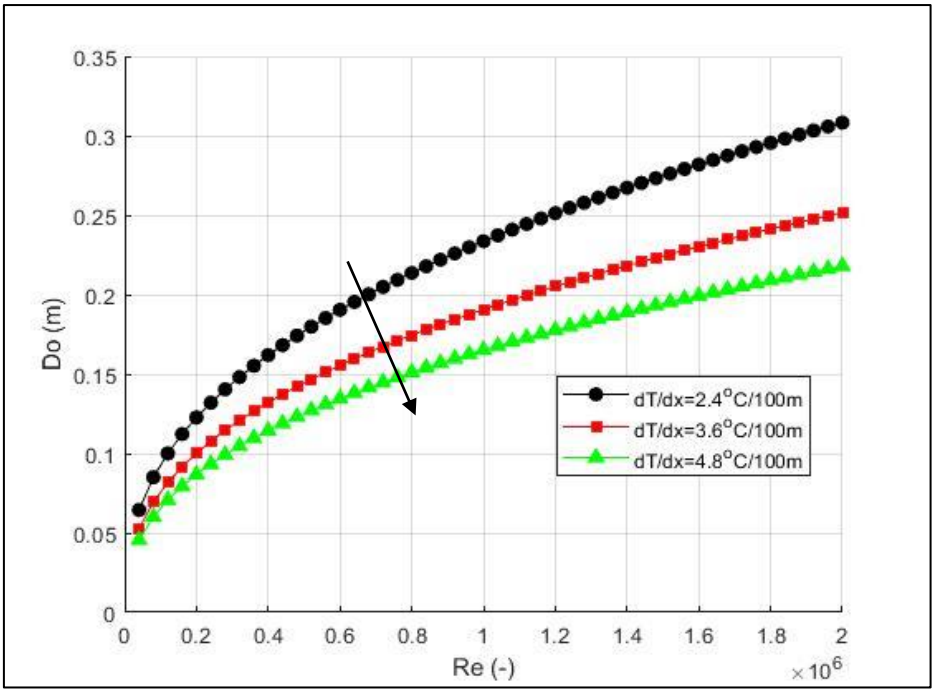

Figure 4.22: Optimal DCHE outer diameter with variation in temperature gradient

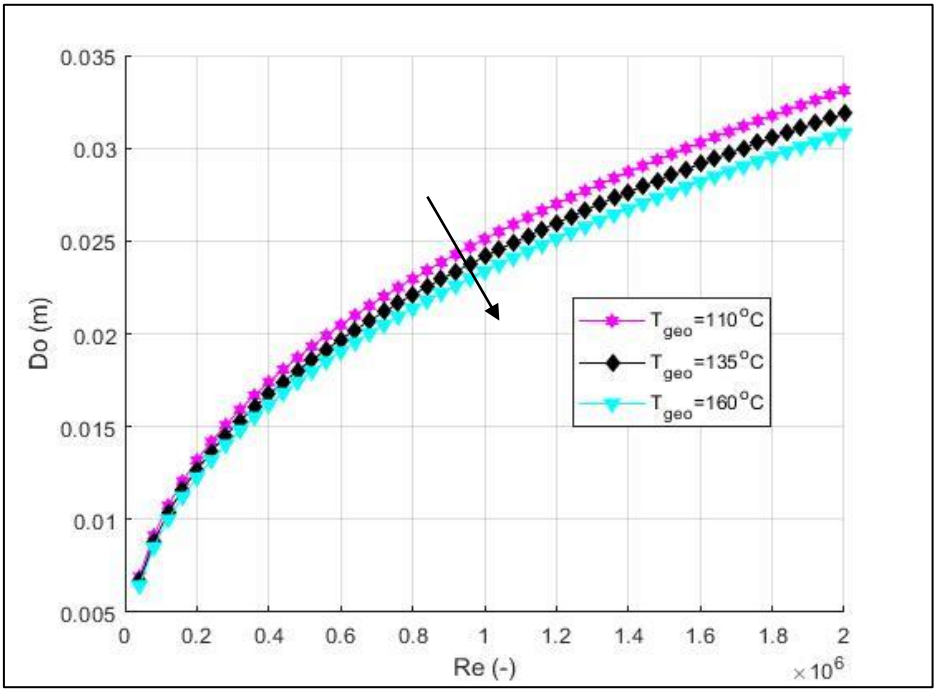

Figure 4.23: Optimal DCHE outer diameter with variation in resource temperature

Figure 4.24 is essentially a combination of the graphs shown in Figures 4.20 and 4.22. Similarly, Figure 4.25 is representative of the graphs illustrated in Figures 4.21 and 4.23. An inverse exponential relationship between the optimum outer diameter and the mass flow rate is observed in both cases. Bearing resemblance to the analysis done by the comparison of Figures

4.22 and 4.23, a greater change in outer diameter with varying temperature gradient is observed compared to the slight change with varying resource temperature.

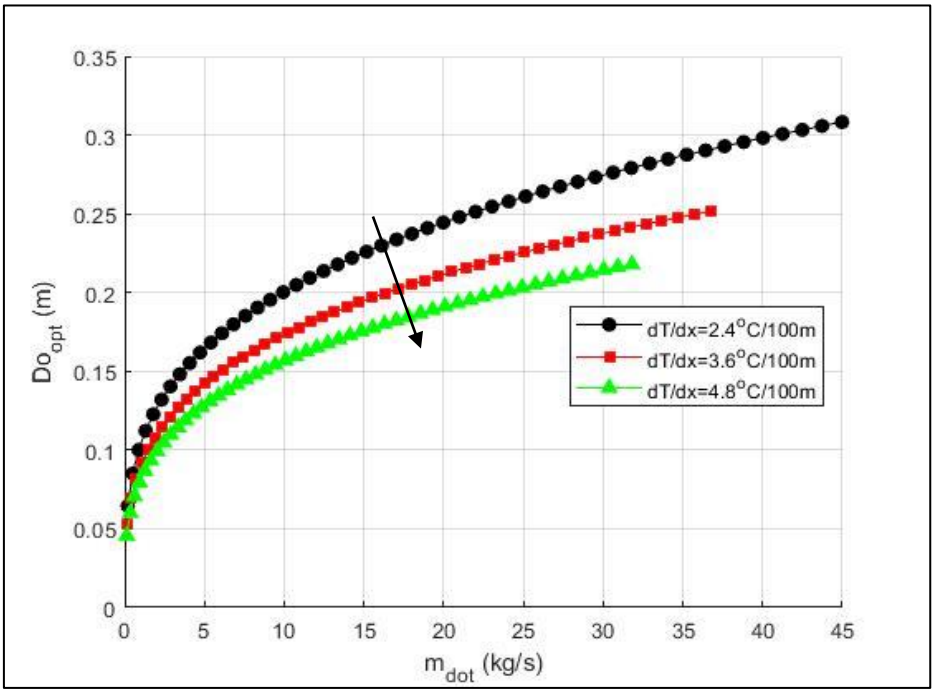

Figure 4.24: Optimal DCHE outer diameter at varying mass flow rates with variation in temperature gradient

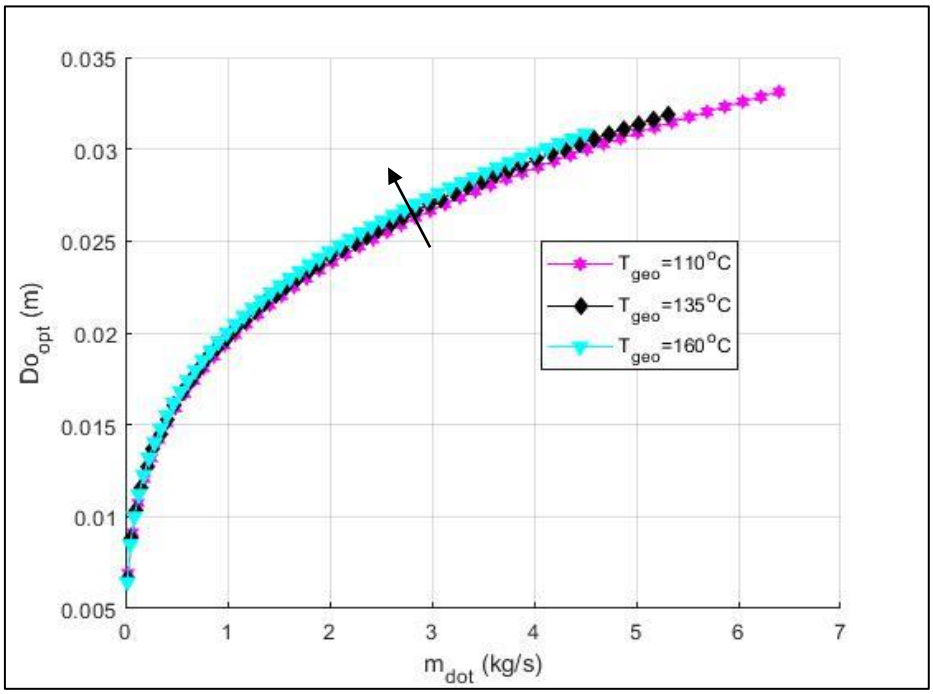

Figure 4.25: Optimal DCHE outer diameter at varying mass flow rates with variation in resource temperature

Figures 4.22 - 4.25 show that the outer diameter is relatively independent of the resource temperature but dependent on the temperature gradient.

Figure4.26shows the relationship between the minimum generated entropy and Reynolds number. The graph shows an exponential relationship in both laminar and turbulent regions. The previous graphs highlighted the advantages of having a geothermal resource with a high temperature gradient and resource temperature. The downside to ensuring that these design parameters are a maximum is that the higher they are, the greater the entropy generated in the system. Therefore, a trade-off is necessary to achieve the optimum design case.

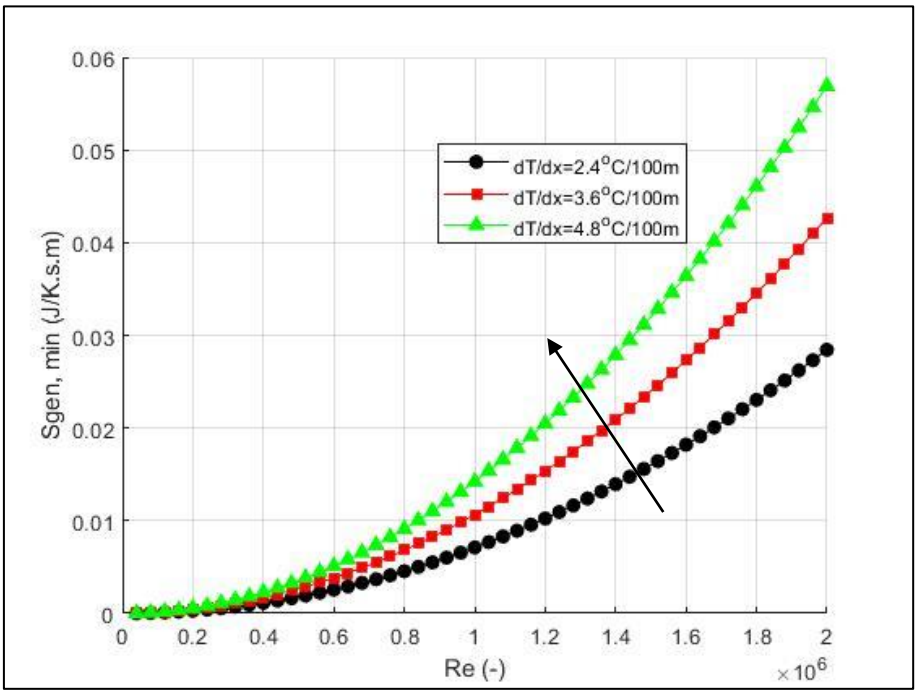

Figure 4.26: Minimum entropy generated with variation in temperature gradient

4.3.5 Sensitivity Analysis of Geothermal Preheater Optimisation

From the graphs plotted to display the optimal geothermal preheater characteristics, a comparable observation is made regarding the effects of changing the geothermal resource temperature and changing the effects of varying the temperature gradient. In the graphs showing the optimum outer diameter of the downhole coaxial heat exchanger (DCHE), it can be observed that the optimum outer diameter is more sensitive to changes in the underground temperature gradient than it is to the geothermal resource temperature. This is depicted by the greater differences between the graphs with varying temperature gradient than varying geothermal resource temperature (compare Figures 4.19 and 4.20).

5 Conclusion and Recommendations

The energy crisis that is being experienced is a consequence of the misuse and overuse of fossil fuels both at a government level and a community level. The use of renewable energy is a solution that is being explored extensively in various capacities. This research looks at one type of renewable energy: geothermal energy and presents the technical advantages of integrating it into already existing fossil-fuelled power plants.

Two cycles were designed: a steam Rankine cycle with single reheat and regeneration as well as a steam Rankine cycle with single reheat and regeneration that makes use of hybridisation (integration of geothermal energy to preheat feedwater) with the latter being designed as a power boosting cycle. The geothermal resource was assumed to be of low temperature ranging from 110°C to 160°C. A reference temperature and atmospheric pressure of 25°C and 101.3 kPa was considered for the environment ambient conditions.

Heat exchangers are very critical components in a power plant. They are used for a variety of applications, from preheating to regeneration and deaeration. For this reason, heat exchangers will always be a very important issue to consider in energy conservation. FWHs are a practical example of counterflow heat exchangers and they were designed as such in this project. The geothermal preheater was designed as a downhole coaxial heat exchanger. First law efficiency shows that the system with a geothermal preheater is about 4% more efficient when the efficiency is based on only the heat input from the fossil fuel resource.

From an exergy efficiency stand point, the hybrid system was found to be superior to the fossil fuelled power plant. The exergy analysis revealed that the greatest exergy destruction occurs in the boiler for both systems which parallels the results from the thermodynamic analysis that showed the boiler to be the greatest source of irreversibility in the system (regardless of a change in the reference environment temperature). The hybrid system was also compared to a stand-alone geothermal power plant making use of a low temperature source. The analysis revealed that the hybrid system is far superior according to both the first and the second law.

Entropy generation minimisation and analysis is an effective approach to use for the optimisation of engineering systems and components. The feedwater heaters were optimised using the method of number of entropy generation units. They were modelled as counter-flow shell and tube heat exchangers. By minimising generated entropy in the feedwater heaters, the

entropy generated in the overall system was minimised. For the optimisation of the counter-flow heat exchanger, all losses were assumed to occur through entropy generation. Optimisation of the tube side was presented in this work where shell side optimisation would follow a very similar method. Two main design parameters that were varied: tube side cross-sectional flow area as well as the mass flow number, G. In the constant area case, the losses were dominated by heat transfer losses and in the L/r_h case, the losses due to heat transfer across a finite temperature difference and due to fluid friction were determined to be equivalent. The optimisation results obtained in this project could subsequently be used to model the FWHs.

The geothermal preheater was modelled as a downhole co-axial heat exchanger and it was optimised using a method similar to the FWHs: the entropy generation minimisation. Where the optimisation method used for the counter-flow heat exchanger is a non-dimensionalising technique, the optimisation of the geothermal preheater is not.

Many developing countries rely on imports for their energy needs and thus purchase fossil fuel from imports. This weakens their financial potential and plays a major role in restraining healthy economic growth. Making use of renewable resources for power generation or integrating them into already existing power plants can help boost economic growth and gradually reduce dependence on imports to meet energy needs. Unfortunately, high installation costs and longer development periods (compared to solar and wind energy) are factors that continue to impede the exploration of geothermal energy globally.

There is major potential for the development of low to moderate enthalpy geothermal direct and indirect use. Financial constraints as well as low price of competing energy sources are two primary reasons why this potential is not being exploited. However, as oil and gas supplies run out over time, geothermal energy will provide a competitive and economic alternative to renewable energy. Therefore, it is important to perform a thermoeconomic/exergoeconomic analysis to assess the viability and economic feasibility of investing in advanced geothermal energy technologies.

This research project aims to address the ongoing energy crisis as far as renewable energy (specifically geothermal energy) is concerned. The rapid rise in urban population is increasing the energy demand which emphasises the need for increased energy supply. What makes it difficult currently, to supply more energy, is the huge risk posed on the climate through the use

fossil fuels. Therefore, it has become imperative to explore other sources of energy that will satisfy the demand while causing zero harm to the climate. This research project optimises a system that integrates a renewable energy source (geothermal energy) within a currently existing fossil fuelled power plant.

6 REFERENCES

[1] World Energy Council, “World Energy Resources 2016,” *World Energy Resour. 2016*, 2016.

[2] World Energy Council, *World Energy Scenarios 2016*. 2016.

[3] World Energy Council, “WEC Trilemma: Pathway calculator,” *Pathway Calculator*, 2017. .

[4] G. Axelsson, “Sustainable geothermal utilization - Case histories; definitions; research issues and modelling,” *Geothermics*, 2010.

[5] G. Power, “Why Support Geothermal Energy ?,” no. February, pp. 1–8, 2012.

[6] K. C. Lee, “Geothermal Power Generation,” *Encyclopedia of Energy*. Auckland Academic Press, pp. 875–893, 2004.

[7] Various, A. Kagel, D. Bates, and K. Gawell, “A Guide to Geothermal Energy and the Environment,” *Geotherm. Energy Assoc.*, 2007.

[8] H. Perlman, “Land Subsidence,” 2017. [Online]. Available: https://water.usgs.gov/edu/earthgwlandsubside.html. [Accessed: 03-Apr-2017].

[9] M. Diesendorf and D. Nuccitelli, “Renewable energy can provide baseload power - here’s how,” *The Conversation*, 2011. [Online]. Available: https://theconversation.com/renewable-energy-can-provide-baseload-power-heres-how-2221. [Accessed: 10-Jun-2017].

[10] E. Nawawi and M. Prihatini, “Geothermal Power Plant.” 2007.

[11] R. Mogg, “The ring of fire: The use of geothermal energy in Indonesia,” *Refocus*, 2001.

[12] REN21, “Renewables 2017 Global Status Report,” 2017.

[13] S. Ishita, “Types of Geothermal Energy.” [Online]. Available: http://www.engineeringenotes.com/essay/geothermal-energy/geothermal-energy-types-advantages-essay-energy-management/20041. [Accessed: 24-Apr-2017].

[14] J. W. Lund, “Development and utilization of geothermal resources,” in *International Solar Energy Society Solar World Congress 2007, ISES 2007*, 2007.

[15] G. Cappetti, “Geothermal Energy Technologies and Strategies for a Sustainable Development: the Lardarello Case Hystory,” in *International Geothermal Days Poland 2004*, 2004.

[16] E. T. Eliasson, S. Thorhallsson, and B. Steingrímsson, “Geothermal Power Plants and Main Components,” *Geotherm. Drilling, Resour. Dev. Power Plants*, p. 24, 2011.

[17] R. DiPippo, “Geothermal power plants,” in *Comprehensive Renewable Energy*, 2012.

[18] M. Mburu, “Geothermal Energy Utilisation,” *Explor. Geotherm. Resour.*, pp. 1–11, 2012.

[19] J. Kestin, R. DiPippo, and H. E. Khalifa, “HYBRID GEOTHERMAL-FOSSIL POWER PLANTS.,” *Mech Eng*, 1978.

[20] H. E. Khalifa, R. DiPippo, and J. Kestin, “Geothermal Preheating In Fossil-Fired Stew Power Plants,” in *Society of Automotive Engineers. Inc.*, 1978.

[21] R. DiPippo and E. M. Avelar, “Compound Hybrid Geothermal-Fossil Power Plants,” 1979.

[22] R. DiPippo, H. E. Khalifa, R. J. Correia, and J. Kestin, “FOSSIL SUPERHEATING IN GEOTHERMAL STEAM POWER PLANTS.,” *Geotherm Energy*, 1979.

[23] R. DiPippo, “ANALYSIS OF AN EARLY HYBRID FOSSIL-GEOTHERMAL POWER PLANT PROPOSAL.,” *Geotherm Energy*, 1978.

[24] P. Seibt, P., Kabus, F., Hoth, “The Neustdt-Glewe Geothermal Power Plant - Practical Experience in the reinjection of cooled thermal waters into sandstone aquifers,” in *Proceedings World Geothermal Congress 2005 Antalya, Turkey, 24-28 April 2005*, 2005.

[25] C. Zhou, E. Doroodchi, and B. Moghtaderi, “An in-depth assessment of hybrid solar-geothermal power generation,” *Energy Convers. Manag.*, 2013.

[26] K. F. Beckers, M. Z. Lukawski, G. A. Aguirre, S. D. Hillson, and J. W. Tester, “Hybrid Low-Grade Geothermal-Biomass Systems for Direct-Use and Co-Generation: from Campus Demonstration to Nationwide Energy Player,” *Fortieth Work. Geotherm. Reserv. Eng.*, pp. 1–11, 2015.

[27] A. Stodola, “Steam and Gas Turbines. Vol. I,” *IIMcGraw-Hill, New York*, 1927.

[28] A. Nelson, “2017 Outlook: Geothermal Is Trending Upwards.” Renewable Energy World, 2017.

[29] P. Duddu, “The top 10 biggest geothermal power plants in the world.” Power-technology.com, 2013.

[30] A. Eberhard, K. Gratwick, E. Morella, and P. Antmann, “Independent Power Projects in Sub-Saharan Africa: Investment trends and policy lessons,” *Energy Policy*, 2017.

[31] African Development Bank Group, “In Kenya, African Development Bank marks a milestone in financing clean energy on the continent,” 2018. [Online]. Available: https://www.afdb.org/en/news-and-events/in-kenya-african-development-bank-marks-a-milestone-in-financing-clean-energy-on-the-continent-18359/. [Accessed: 25-Jul-2018].

[32] E. Barbier, “Geothermal energy technology and current status: An overview,” *Renewable and Sustainable Energy Reviews*. 2002.

[33] IRENA, “Renewable Power Generation Costs in 2017,” 2018.

[34] P.A. Omenda, “The geology and geothermal activity of the East African Rift System,” *Work. Decis. Makers Geotherm. Proj. Manag.*, 2005.

[35] M. Teklemariam and A. Ababa, “Overview of Geothermal Resource Utilization and Potential in East African Rift System,” *Explor. Geotherm. Resour.*, 2007.

[36] K. Saemundsson, “East African Rift System - An overview,” in *East African Rift System-An Overview, Short Course V on Exploration for Geothermal Reservoirs, United Nations Geothermal Training Programme-KenGen, Lake Bogoria and Lake Naivsha*, 2010.

[37] R. Guerrero-Lemus and L. E. Shephard, “Geothermal energy,” *Lecture Notes in Energy*. 2017.

[38] T. Dhansay, C. Musekiwa, T. Ntholi, L. Chevallier, D. Cole, and M. J. De Wit, “South Africa’s geothermal energy hotspots inferred from subsurface temperature and geology,” *S. Afr. J. Sci.*, 2017.

[39] T. Dhansay, “Geothermal technology is expensive, but it should still be part of South Africa’s energy mix,” 2015. [Online]. Available: https://theconversation.com/geothermal-technology-is-expensive-but-it-should-still-be-part-of-south-africas-energy-mix-47304.

[40] Z. Wang, “Modeling Study of a Single-Well Enhanced Geothermal System (Egs),” *Thesis*, 2009.

[41] P. Olasolo, M. C. Juárez, M. P. Morales, S. Damico, and I. A. Liarte, “Enhanced geothermal systems (EGS): A review,” *Renew. Sustain. Energy Rev.*, vol. 56, no. April, pp. 133–144, 2016.

[42] DOE, “An Evaluation of Enhanced Geothermal Systems Technology,” *U.S Dep. Energy*, pp. 1–37, 2008.

[43] E. Soldo and C. Alimonti, “From an Oilfield to a Geothermal One : Use of a Selection Matrix to Choose Between Two Extraction Technologies,” *World Geotherm. Congr. 2015*, 2015.

[44] M. Cinar, “CREATING ENHANCED GEOTHERMAL SYSTEMS IN DEPLETED OIL RESERVOIRS VIA IN SITU COMBUSTION,” in *Thirty-Eighth Workshop on Geothermal Reservoir Engineering*, 2013.

[45] M. Godec, V. Kuuskraa, T. Van Leeuwen, L. S. Melzer, and N. Wildgust, “CO2 storage in depleted oil fields: The worldwide potential for carbon dioxide enhanced oil recovery,” in *Energy Procedia*, 2011.

[46] B. M. Adams, T. H. Kuehn, J. M. Bielicki, J. B. Randolph, and M. O. Saar, “On the importance of the thermosiphon effect in CPG (CO2 plume geothermal) power systems,” *Energy*, 2014.

[47] N. Gupta and M. Vashistha, “Carbon Dioxide Plume Geothermal (CPG) System-A New Approach for Enhancing Geothermal Energy Production and Deployment of CCUS on Large Scale in India,” in *Energy Procedia*, 2015.

[48] K. Manjunath and S. C. Kaushik, “Second law thermodynamic study of heat exchangers: A review,” *Renewable and Sustainable Energy Reviews*. 2014.

[49] J. Mitrovic, *HEAT EXCHANGERS – BASICS DESIGN APPLICATIONS Edited by*

Jovan Mitrovic. .

[50] R. K. Shah and D. P. Sekulic, *FUNDAMENTALS OF HEAT*. John Wiley & Sons, 2003.

[51] S. Kakac, *Heat Exchangers: Selection,Rating and Thermal Design*. 2012.

[52] "Heat Exchanger General," pp. 1–44.

[53] S. Kakaç, H. Liu, and A. Pramuanjaroenkij, "Shell-and-Tube Heat Exchangers," *HEAT Exch. Sel. Rating, Therm. Des.*, 2012.

[54] Y. A. C. & A. J. Ghajar, *Heat and Mass Transfer: Fundamentals & Applications*. 1986.

[55] Z. M. Xu, S. R. Yang, and Z. Q. Chen, "A modified entropy generation number for heat exchangers," *J. Therm. Sci.*, 1996.

[56] V. Singh, V. Aute, and R. Radermacher, "Usefulness of Entropy Generation Minimization Through a Heat Exchanger Modeling Tool," *Int. Refrig. Air Cond. Conf.*, 2008.

[57] P. J. Yekoladio, T. Bello-Ochende, and J. P. Meyer, "Design and optimization of a downhole coaxial heat exchanger for an enhanced geothermal system (EGS)," *Renew. Energy*, 2013.

[58] J. W. Lund, "The use of downhole heat exchangers," *Geothermics*, 2003.

[59] Z. Wang, M. W. Mcclure, and R. N. Horne, "A single-well EGS configuration using a thermosiphon," *Thirty-Fourth Work. Geotherm. Reserv. Eng.*, 2009.

[60] Y. A. Cengel and M. A. Boles, "Thermodynamics An Engineering Approach," *Renewable and Sustainable Energy Reviews*. 2013.

[61] G. J. Kolb, "Economic evaluation of solar-only and hybrid power towers using molten-salt technology," *Sol. Energy*, 1998.

[62] J. Qin and E. Hu, "Technical assessment of a renewable aided power plant for different operational load," in *Energy Procedia*, 2014.

[63] C. Zhou, E. Doroodchi, and B. Moghtaderi, "Assessment of geothermal assisted coal-fired power generation using an Australian case study," *Energy Convers. Manag.*, 2014.

[64] M. M. A. Bejan, G. Tsatsaronis, *Thermal design and optimization*. 1996.

[65] I. H. Aljundi, “Energy and exergy analysis of a steam power plant in Jordan,” *Appl. Therm. Eng.*, 2009.

[66] M. M. Rashidi, A. Aghagoli, and M. Ali, “Thermodynamic analysis of a steam power plant with double reheat and feed water heaters,” *Adv. Mech. Eng.*, 2014.

[67] V. Agatonovic, “Geothermal Energy Sources , Applications and Benefits.”

[68] T. S. Lovering and H. D. Goode, “Measuring Geothermal Gradients in Drill Holes Less Than 60 Feet Deep East Tintic District, Utah,” Washington, 1963.

[69] T. J. Kotas, “Exergy concepts for thermal plant: First of two papers on exergy techniques in thermal plant analysis,” *Top. Catal.*, 1980.

[70] T. J. Kotas, “EXERGY CONCEPTS FOR THERMAL PLANTS.,” *Int. J. Heat Fluid Flow*, 1980.

[71] I. Dincer, M. M. Hussain, and I. Al-Zaharnah, “Energy and exergy use in public and private sector of Saudi Arabia,” *Energy Policy*, 2004.

[72] I. Dincer and Y. A. Cengel, *Energy, entropy and exergy concepts and their roles in thermal engineering*, vol. 3, no. 3. 2001.

[73] A. Bejan, “Second-Law Analysis in Heat Transfer and Thermal Design,” *Adv. Heat Transf.*, 1982.

[74] R. DiPippo, *Geothermal Power Plants: Principles, Applications, Case Studies and Environmental Impact: Fourth Edition*. 2015.

[75] R. K. Shah and D. P. Sekulić, “Heat Exchanger Pressure Drop Analysis,” *Fundam. Heat Exch. Des.*, 2003.

[76] U. C. Kapale and S. Chand, “Modeling for shell-side pressure drop for liquid flow in shell-and-tube heat exchanger,” *Int. J. Heat Mass Transf.*, 2006.

[77] M. Peters, K. Timmerhaus, and R. West, “Optimization Application : Pinch Technology Analysis,” in *Plant Design and Economics for Chemical Engineers*, 2003.

[78] S. Lorente and A. Bejan, “Svelteness, freedom to morph, and constructal multi-scale flow structures,” *Int. J. Therm. Sci.*, 2005.

[79] A. Bejan, “Fundamentals of exergy analysis, entropy generation minimization, and the generation of flow architecture,” *Int. J. Energy Res.*, vol. 26, no. 7, pp. 0–43, 2002.

[80] A. Bejan, “A Study of Entropy Generation in Fundamental Convective Heat Transfer,” *J. Heat Transfer*, 1979.

[81] V. Mrzljak, I. Poljak, and V. Medica-Viola, “THERMODYNAMICAL ANALYSIS OF HIGH-PRESSURE FEED WATER HEATER IN STEAM PROPULSION SYSTEM DURING EXPLOITATION,” *Brodogradnja*, vol. 68, no. 2, pp. 45–61, 2017.

[82] M. Yilmaz, O. . Sara, and S. Karsli, “Performance evaluation criteria for heat exchangers based on second law analysis,” *Exergy, An Int. J.*, 2001.

[83] A. Bejan, “The Concept of Irreversibility in Heat Exchanger Design: Counterflow Heat Exchangers for Gas-to-Gas Applications,” *J. Heat Transfer*, 1977.

[84] W. M. Kays and A. L. London, *Compact Heat Exchangers*. 1984.

[85] G. O. Brown, “The History of the Darcy-Weisbach Equation for Pipe Flow Resistance,” in *Environmental and Water Resources History*, 2002.

[86] A. BEJAN, “Forced convection: Internal flows,” *Heat Transf. Handb.*, 2003.

[87] Alle, “New equations for heat and mass transfer in turbulent pipe and channel flow,” *Int. Chem. Eng.*, 1976.

[88] V. Gnielinski, “On heat transfer in tubes,” *Int. J. Heat Mass Transf.*, 2013.

[89] A. Kraus, A. Aziz, J. Welty, and D. Sekulic, “Extended Surface Heat Transfer,” *Appl. Mech. Rev.*, 2001.

[90] D. Butterworth, “Process heat transfer 2010,” in *Applied Thermal Engineering*, 2004.

[91] B. S. Petukhov, “Heat Transfer and Friction in Turbulent Pipe Flow with Variable Physical Properties,” *Adv. Heat Transf.*, 1970.

[92] A. Bejan, *Convection Heat Transfer*. 2013.

[93] B. S. Petukhov and L. I. Roizen, “Generalized Relationships for Heat Transfer in Turbulent Flow of Gas in Tubes of Annular Section,” *High Temp.*, vol. 2, pp. 65–68, 1964.

[94] J. L. Breese, “SHELL AND TUBE HEAT EXCHANGERS.,” *ASHRAE J.*, 1984.

[95] J. E. Edwards, “Design and Rating Shell and Tube Heat Exchangers,” *Chem. Eng.*, 2008.

[96] P. Of, P. To, T. H. E. Optimal, D. Of, H. Exchangers, and G. P. Systems, “PENI Junior YEKOLADIO Submitted in partial fulfillment of the requirements for the degree MASTER OF ENGINEERING (Mechanical Engineering) in the Faculty of Engineering , the Built Environment and Information Technology,” 2013.

[97] K. C. Kushwaha and B. Koshti, “Performance Analysis and Off Design Behaviour of Feed Water Heater,” vol. 3, no. 10, pp. 9–15, 2015.

[98] T. K. Ray, A. Datta, A. Gupta, and R. Ganguly, “Exergy-based performance analysis for proper O&M decisions in a steam power plant,” *Energy Convers. Manag.*, 2010.

[99] J. S. Lim, A. Bejan, and J. H. Kim, “Thermodynamics of energy extraction from fractured hot dry rock,” *Int. J. Heat Fluid Flow*, 1992.

[100] P. P. P. M. Lerou, T. T. Veenstra, J. F. Burger, H. J. M. Ter Brake, and H. Rogalla, “Optimization of counterflow heat exchanger geometry through minimization of entropy generation,” *Cryogenics (Guildf).*, 2005.

7 APPENDICES

7.1 Appendix A-Matlab Code for Shell and Tube Counter-Flow Heat Exchanger with Area Constraint

```
clear all
clc
% T_shell = T2;
% T_tube = T1;
T2 = 491.9+273.15;%450+273.15
T1 = 238.1+273.15;
Tm = (T2+T1)/2;  %Kelvins
P = 10000; %kPa
g_opt=zeros(1,50); D_opt=zeros(1,50); Nu=zeros(1,50); St=zeros(1,50);...
N_S_min=zeros(1,50); A_opt=zeros(1,50); f=zeros(1,50);
n=1;
for A = linspace(0.01,0.02,5)
    if n==1; Spec1='-^m'; Spec2='MarkerFaceColor'; Spec3='m';end
    if n==2; Spec1='-pb'; Spec2='MarkerFaceColor'; Spec3='b';end
    if n==3; Spec1='-dg'; Spec2='MarkerFaceColor'; Spec3='g';end
    if n==4; Spec1='-vk'; Spec2='MarkerFaceColor'; Spec3='k';end
    if n==5; Spec1='-or'; Spec2='MarkerFaceColor'; Spec3='r';end
% Pn = P/(1000)/22.064; %Pn --> Normalised pressure
% m_dot = 1;
% A = 50;
% a = A*(2*rho*P)/m_dot;
Re = linspace(0,2e6,50);
col = length(Re);

for i=1:col
%D_opt=zeros(1,50); Nu=zeros(1,50); St=zeros(1,50); Ns_min=zeros(1,50);
A_opt=zeros(1,50); f=zeros(1,50);
%%
%superheated steam properties
%      tau = (Tm+273.15)/674.14;
%      %%
%      Z = 1+Pn*((0.4409392/tau)-(1.386598/tau^2)+(1.380501/tau^3)-...
%     (0.7644377/tau^4))+(Pn^2)*((56.40548/tau)-(297.0161/tau^2)+...
%     (617.8258/tau^3)-(634.747/tau^4)+(322.8009/tau^5)-
(65.45004/tau^6))+...
%     (Pn^3)*((149.3651/tau)-(895.0375/tau^2)+(2123.035/tau^3)-...
%     (2488.625/tau^4)+(1439.213/tau^5)-(327.7709/tau^6))+...
%     (Pn^4)*(151.1386-(967.3387/tau)+(2478.739/tau^2)-(3178.106/tau^3)+...
%     (2038.512/tau^4)-(523.2041/tau^5));
%     %%
%      rho = (73.874969*Pn)/(tau*Z);
%      mu = 0.1*((-22.391*tau^2)+(326.46*tau)-78.034+(6.6119/tau^2)+...
%      Pn*((65.605/tau^2)-(74.535/tau^3))+...
%     (Pn^2)*(-19.052+(124.47/tau^2)-(97.428/tau^3))+...
%     (Pn^3)*(-1281.1+(4910.2/tau)-(6293.7/tau^2)+(2699.2/tau^3)));
%     %%
%      Cp = 5.058; %2.1*2;
%      k = 0.5879; %0.5;
%      Pr = mu*Cp/k;
%Thermophysical Properties obtained from EES
     Cp = 4.673;
```

```
      k = 0.6295;
      mu = 0.0001136;
      Pr = 0.8436;
      rho = 823;
      m_dot = 92;
      a = A*(2*rho*P)/m_dot;

%%
if  Re(i) > 3000
    f(i) = (1.58*log(Re(i))-3.28)^(-2);%0.046/(Re(i)^0.2);
    %0.079/(Re(i)^0.25);
    Nu(i) = 0.012*(((Re(i))^0.87)-280)*(Pr^0.4);
    %0.023*(Re(i)^0.75)*(Pr^0.4);
elseif Re(i) < 3000 %%Re(i) < 2e6 &&
    f(i) = 16/Re(i);
    Nu(i) = 3.66;
end
    St(i) = Nu(i)/(Re(i)*Pr);
    G = m_dot/A;
    g = G/sqrt(2*rho*P); %G -> mass velocity = V*rho
    t = (sqrt(T2/T1)-sqrt(T1/T2)); %t=tau
    R = 0.4614;
    B = (R/Cp); %R=IdealGasConstant

    %%Optimisation
    g_opt(i) = ((t^2)/(3*B*(a^2)*f(i)*St(i)))^0.25;
    N_S_min(i) = (t^2)/(a*g_opt(i)*St(i)) + B*a*f(i)*(g_opt(i)^3);%+

end

%%Plots
figure(1)
grid on
hold on
plot ((g_opt(2:50)),(N_S_min(2:50)),Spec1,Spec2,Spec3)
xlabel('g_o_p_t(-)')
ylabel('N_S_m_i_n(-)')
legend('A = 0.01m^2','A = 0.0125m^2','A = 0.015m^2','A = 0.0175m^2',...
    'A = 0.02m^2')
grid on
hold off

figure(2)
hold on
plot (Re(2:50),N_S_min(2:50),Spec1,Spec2,Spec3)
xlabel('Re (-)')
ylabel('N_S_m_i_n (-)')
legend('A = 0.01m^2','A = 0.0125m^2','A = 0.015m^2','A = 0.0175m^2',...
    'A = 0.02m^2')
grid on
hold off

figure(3)
hold on
plot (Re(2:50),g_opt(2:50),Spec1,Spec2,Spec3)
xlabel('Re(-)')
ylabel('g_o_p_t(-)')
legend('A = 0.01m^2','A = 0.0125m^2','A = 0.015m^2','A = 0.0175m^2',...
```

```
    'A = 0.02m^2')
grid on
hold off
%
n=n+1;
end
**************************************************************************
```

7.2 Appendix B- Matlab Code for Shell and Tube Counter-Flow Heat Exchanger with L/r_h Constraint

```
clear all
clc
%%
T2 = 491.9+273.15; % T_shell
T1 = 238.1+273.15; % T_tube
Tm = (T2+T1)/2;  %Kelvins
P = 10000; %MPa
geometry_opt=zeros(1,50);D_opt=zeros(1,50);Nu=zeros(1,50);St=zeros(1,50);
N_S_min=zeros(1,50);A_opt=zeros(1,50);f=zeros(1,50);
n=1;
%%
for G = linspace (4600,9200,5)%(9.2/0.05,9.2/0.01,5)
    if n==1; Spec1='-^m'; Spec2='MarkerFaceColor'; Spec3='m';end
    if n==2; Spec1='-pb'; Spec2='MarkerFaceColor'; Spec3='b';end
    if n==3; Spec1='-dg'; Spec2='MarkerFaceColor'; Spec3='g';end
    if n==4; Spec1='-vk'; Spec2='MarkerFaceColor'; Spec3='k';end
    if n==5; Spec1='-or'; Spec2='MarkerFaceColor'; Spec3='r';end

Re = linspace(0,2e6,50);
col = length(Re);

for i=1:col
%% superheated steam properties
Cp = 4.673;
k = 0.6295;
mu = 0.0001136;
%mu_wall = 0.00002834;
Pr = 0.8436;
rho = 823;

%%
if  Re(i) > 2100
    %Friction factor in turbulent flow
    f(i) = (1.58*log(Re(i))-3.28)^(-2);
%     f(i) = 0.046/(Re(i)^0.2);
%    Nu(i) = 0.027*(Re(i)^0.8)*(Pr^(1/3))*(mu/mu_wall)^0.14;
    Nu(i) = 0.012*(((Re(i))^0.87)-280)*(Pr^0.4);
%    Nu(i) = 0.02155*(Re(i)^0.8018)*(Pr^0.7095);
elseif Re(i) < 2100
    f(i) = 16/Re(i);
    Nu(i) = 3.66;
end

    St(i) = Nu(i)/(Re(i)*Pr);
    t = (sqrt(T2/T1)-sqrt(T1/T2));
```

```
    R = 0.4614;
    B = (R/Cp); %R=IdealGasConstant
    g = G/sqrt(2*rho*P); %G -> mass velocity = V*rho

    geometry_opt(i) = (t)/(g*sqrt(B*f(i)*St(i)));
    N_S_min(i) =  (t^2)/(St(i)*geometry_opt(i))+...
        B*(g^2)*f(i)*geometry_opt(i);

end
%% Plots
figure(1)
grid on
hold on
plot(geometry_opt(2:50),N_S_min(2:50),Spec1,Spec2,Spec3)
xlabel('L/r_h_o_p_t(-)')
ylabel('N_S_m_i_n(-)')
legend('G = 4600 kg/s.m^2','G = 5750 kg/s.m^2','G = 6900 kg/s.m^2',...
    'G = 8050 kg/s.m^2','G = 9200 kg/s.m^2')
grid on
hold off

figure(2)
hold on
plot(Re(2:50),N_S_min(2:50),Spec1,Spec2,Spec3)
xlabel('Re (-)')
ylabel('N_S_m_i_n (-)')
legend('G = 4600 kg/s.m^2','G = 5750 kg/s.m^2','G = 6900 kg/s.m^2',...
    'G = 8050 kg/s.m^2','G = 9200 kg/s.m^2')
grid on
grid on
hold off

figure(3)
hold on
plot (Re(2:50),geometry_opt(2:50),Spec1,Spec2,Spec3)
xlabel('Re(-)')
ylabel('L/r_h_o_p_t(-)')
legend('G = 4600 kg/s.m^2','G = 5750 kg/s.m^2','G = 6900 kg/s.m^2',...
    'G = 8050 kg/s.m^2','G = 9200 kg/s.m^2')
grid on
grid on
hold off
%
n=n+1;
end
**************************************************************
```

7.3 Appendix C- Matlab Code for Downhole Coaxial Heat Exchanger with variation in Temperature Gradient

```
close all
clc
%-----------Input values----------------
n=1;
To=25+273.15; %oC
Trej=50+273.15; %oC
Tgeo=160+273.15; %oC
```

```
Tm=(Trej+Tgeo)/2; %K
L=100; %m
for Tb=300.55:1.2:302.95  %oC
%Tb=270+273.15; %oC
%for Tm=80+273.15:5:105+273.15 %oC %
if n==1; Spec1='-ok'; Spec2='MarkerFaceColor'; Spec3='k';end
if n==2; Spec1='-sr'; Spec2='MarkerFaceColor'; Spec3='r';end
if n==3; Spec1='-^g'; Spec2='MarkerFaceColor'; Spec3='g';end
% if n==4; Spec1='-hm'; Spec2='MarkerFaceColor'; Spec3='m';end
% if n==5; Spec1='-dk'; Spec2='MarkerFaceColor'; Spec3='k';end
% if n==6; Spec1='-vc'; Spec2='MarkerFaceColor'; Spec3='c';end
grad=(Tb-To)/L;
Re=linspace(0,2e6,51);
col=length(Re);
%%
%-----------Water properties-------------
co_r=999.79684; co_c=4.2174356000; co_k=0.5650285;
co_m=557.82468; co_p=0.074763403;
c1_r=0.068317355; c1_c=-0.0056181625; c1_k=0.00263638950;
c1_m=19.408782; c1_p=0.002902098;
c2_r=-0.010740248; c2_c=0.001299253; c2_k=-0.00012516934;
c2_m=0.1360459; c2_p=2.8606181e-5;
c3_r=0.000821409; c3_c=-0.000115354; c3_k=-1.5154915e-6;...
c3_m=-3.1160832e-4; c3_p=-8.1395537e-8;
c4_r=-2.30310e-5; c4_c=4.15e-6; c4_k=-0.0009412945;
%
rho=co_r+c1_r*(Tm-273.15)+c2_r*(Tm-273.15)^2+c3_r*(Tm-273.15)^2.5+...
    c4_r*(Tm-273.15)^3;
Cp=1000*(co_c+c1_c*(Tm-273.15)+c2_c*(Tm-273.15)^1.5+c3_c*(Tm-273.15)^2+...
    c4_c*(Tm-273.15)^2.5);
k=co_k+c1_k*(Tm-273.15)+c2_k*(Tm-273.15)^1.5+c3_k*(Tm-273.15)^2+...
    c4_k*(Tm-273.15)^0.5;
mu=1/(co_m+c1_m*(Tm-273.15)+c2_m*(Tm-273.15)^2+c3_m*(Tm-273.15)^3);
Pr=1/(co_p+c1_p*(Tm-273.15)+c2_p*(Tm-273.15)^2+c3_p*(Tm-273.15)^3);
%%
%------------Optimization-----------------------------------------------
Do_opt=zeros;Sgen_min=zeros;Bo=zeros;m_opt=zeros;
Ex_dest=zeros;Ex=zeros;Exo=zeros;ratio1=zeros;ratio2=zeros;Wnet=zeros;...
    En_eff=zeros;Ex_eff=zeros;
for i=1:col
if Re(i)>2300
r=0.653;
Bo(i)=(mu^6*Tm/(rho^2*Cp*Pr^0.6*grad^2))*(1-r)^4.6*(1/r^0.8-0.14/r^0.2)*...
    (1/((1-r)^2.8*(1+r)^2)+1/r^4.8);
m_opt(i)=0.238*Re(i)^1.4*Bo(i)^0.25;
Sgen_min(i)=(13.84*m_opt(i)^2*Cp*Pr^0.6*(1-r)^0.2*grad^2)/...
    (mu*(1/r^0.8-0.14/r^0.2)*Tm^2*Re(i)^0.8)+(0.0446*Re(i)^4.8*mu^5*...
    (1-r)^4.8)/(rho^2*Tm*m_opt(i)^2)*(1/((1-r)^2.8*(1+r)^2)+1/r^4.8);
Do_opt(i)=(4*m_opt(i))/(pi*mu*(1-r)*Re(i));
elseif Re(i)<2300
r=0.683;
Bo(i)=(mu^6*Tm/(rho^2*Cp*Pr*grad^2))*(1-r)^3*(3.66+1.2*r^0.5)*...
    (((1-r)/(1+r))/(1-r^4-(1+r^2)^2/log(1/r)+1/r^4));
m_opt(i)=2.642*Re(i)*Bo(i)^0.25;
Sgen_min(i)=(m_opt(i)^2*Cp*Pr*(1-r)*grad^2)/(pi*mu*(3.66+1.2*r^0.5)*...
    Tm^2)+(15.50*Re(i)^4*mu^5*(1-r)^4)/(rho^2*Tm*m_opt(i)^2)*...
    (((1-r)/(1+r))/(1-r^4-(1+r^2)^2/log(1/r)+1/r^4));
Do_opt(i)=(4*m_opt(i))/(pi*mu*(1-r)*Re(i));
end
Ex_dest(i)=To*Sgen_min(i)*L;
```

```
Ex(i)=Tgeo-Trej-To*log(Tgeo/Trej);
Exo(i)=Tgeo-To-To*log(Tgeo/To);
ratio1(i)=Ex(i)/(Tgeo-To);
ratio2(i)=Ex(i)/Exo(i);
Wnet(i)=Ex(i)-Ex_dest(i)/(m_opt(i)*Cp);
En_eff(i)=Wnet(i)/(Tgeo-To);
Ex_eff(i)=Wnet(i)/(Tgeo-To-To*log(Tgeo/To));
end
figure (1)
grid on
hold on
plot (Re,m_opt,Spec1,Spec2,Spec3)
xlabel('Re (-)')
ylabel('m_o_p_t (kg/s)')
legend('dT/dx=2.4^oC/100m','dT/dx=3.6^oC/100m','dT/dx=4.8^oC/100m')%,5)
grid on
hold off

figure (2)
hold on
plot (m_opt,Do_opt,Spec1,Spec2,Spec3)
xlabel('m_d_o_t (kg/s)')
ylabel('Do_o_p_t (m)')
legend('dT/dx=2.4^oC/100m','dT/dx=3.6^oC/100m','dT/dx=4.8^oC/100m')%,5);
grid on
hold off

figure (3)
hold on
plot (Re,Do_opt,Spec1,Spec2,Spec3)
xlabel('Re (-)')
ylabel('Do_o_p_t (m)')
legend('dT/dx=2.4^oC/100m','dT/dx=3.6^oC/100m','dT/dx=4.8^oC/100m')%,5);
grid on
hold off

figure (4)
hold on
plot (Re,Sgen_min,Spec1,Spec2,Spec3)
xlabel('Re (-)')
ylabel('Sgen, min (J/K.s.m)')
legend('dT/dx=2.4^oC/100m','dT/dx=3.6^oC/100m','dT/dx=4.8^oC/100m')%,5);
grid on
hold off
n=n+1;
end
```

7.4 Appendix D- Matlab Code for Downhole Coaxial Heat Exchanger with variation in Resource Temperature

```
close all
clc
%-----------Input values-----------------
n=1;
To=25+273.15; %oC
Trej=50+273.15; %oC
% Tgeo=160+273.15; %oC
% Tm=(Trej+Tgeo)/2; %K
L=100; %m
% for Tb=300.55:0.6:303.55 %302.95 %oC
Tb=265+273.15; %oC
for Tm=80+273.15:12.5:105+273.15 %oC
% if n==1; Spec1='-ok'; Spec2='MarkerFaceColor'; Spec3='k';end
% if n==2; Spec1='-sr'; Spec2='MarkerFaceColor'; Spec3='r';end
% if n==3; Spec1='-^g'; Spec2='MarkerFaceColor'; Spec3='g';end
if n==1; Spec1='-hm'; Spec2='MarkerFaceColor'; Spec3='m';end
if n==2; Spec1='-dk'; Spec2='MarkerFaceColor'; Spec3='k';end
if n==3; Spec1='-vc'; Spec2='MarkerFaceColor'; Spec3='c';end
grad=(Tb-To)/L;
Tgeo=2*Tm-Trej;
Re=linspace(0,2e6,51);
col=length(Re);
%%
%-----------Water properties-------------
co_r=999.79684; co_c=4.2174356000; co_k=0.5650285;
co_m=557.82468; co_p=0.074763403;
c1_r=0.068317355; c1_c=-0.0056181625; c1_k=0.00263638950;
c1_m=19.408782; c1_p=0.002902098;
c2_r=-0.010740248; c2_c=0.001299253; c2_k=-0.00012516934;
c2_m=0.1360459; c2_p=2.8606181e-5;
c3_r=0.000821409; c3_c=-0.000115354; c3_k=-1.5154915e-6;...
    c3_m=-3.1160832e-4; c3_p=-8.1395537e-8;
c4_r=-2.30310e-5; c4_c=4.15e-6; c4_k=-0.0009412945;
%
rho=co_r+c1_r*(Tm-273.15)+c2_r*(Tm-273.15)^2+c3_r*(Tm-273.15)^2.5+...
    c4_r*(Tm-273.15)^3;
Cp=1000*(co_c+c1_c*(Tm-273.15)+c2_c*(Tm-273.15)^1.5+c3_c*...
    (Tm-273.15)^2+c4_c*(Tm-273.15)^2.5);
k=co_k+c1_k*(Tm-273.15)+c2_k*(Tm-273.15)^1.5+c3_k*(Tm-273.15)^2+...
    c4_k*(Tm-273.15)^0.5;
mu=1/(co_m+c1_m*(Tm-273.15)+c2_m*(Tm-273.15)^2+c3_m*(Tm-273.15)^3);
Pr=1/(co_p+c1_p*(Tm-273.15)+c2_p*(Tm-273.15)^2+c3_p*(Tm-273.15)^3);
%%
%-----------Optimization-------------------------------------------------
Do_opt=zeros;Sgen_min=zeros;Bo=zeros;m_opt=zeros;
Ex_dest=zeros;Ex=zeros;Exo=zeros;ratio1=zeros;ratio2=zeros;Wnet=zeros;...
    En_eff=zeros;Ex_eff=zeros;
for i=1:col
if Re(i)>2300
r=0.653;
Bo(i)=(mu^6*Tm/(rho^2*Cp*Pr^0.6*grad^2))*(1-r)^4.6*(1/r^0.8-0.14/r^0.2)*...
    (1/((1-r)^2.8*(1+r)^2)+1/r^4.8);
m_opt(i)=0.238*Re(i)^1.4*Bo(i)^0.25;
Sgen_min(i)=(13.84*m_opt(i)^2*Cp*Pr^0.6*(1-r)^0.2*grad^2)/...
    (mu*(1/r^0.8-0.14/r^0.2)*Tm^2*Re(i)^0.8)+(0.0446*Re(i)^4.8*mu^5*...
```

```
    (1-r)^4.8)/(rho^2*Tm*m_opt(i)^2)*(1/((1-r)^2.8*(1+r)^2)+1/r^4.8);
Do_opt(i)=(4*m_opt(i))/(pi*mu*(1-r)*Re(i));
elseif Re(i)<2300
r=0.683;
Bo(i)=(mu^6*Tm/(rho^2*Cp*Pr*grad^2))*(1-r)^3*(3.66+1.2*r^0.5)*...
    (((1-r)/(1+r))/(1-r^4-(1+r^2)^2/log(1/r)+1/r^4));
m_opt(i)=2.642*Re(i)*Bo(i)^0.25;
Sgen_min(i)=(m_opt(i)^2*Cp*Pr*(1-r)*grad^2)/(pi*mu*(3.66+1.2*r^0.5)*...
    Tm^2)+(15.50*Re(i)^4*mu^5*(1-r)^4)/(rho^2*Tm*m_opt(i)^2)*(((1-r)/...
    (1+r))/(1-r^4-(1+r^2)^2/log(1/r)+1/r^4));
Do_opt(i)=(4*m_opt(i))/(pi*mu*(1-r)*Re(i));
end

Ex_dest(i)=To*Sgen_min(i)*L;
Ex(i)=Tgeo-Trej-To*log(Tgeo/Trej);
Exo(i)=Tgeo-To-To*log(Tgeo/To);
ratio1(i)=Ex(i)/(Tgeo-To);
ratio2(i)=Ex(i)/Exo(i);
Wnet(i)=Ex(i)-Ex_dest(i)/(m_opt(i)*Cp);
En_eff(i)=Wnet(i)/(Tgeo-To);
Ex_eff(i)=Wnet(i)/(Tgeo-To-To*log(Tgeo/To));
end

figure (1)
grid on
hold on
plot (Re,m_opt,Spec1,Spec2,Spec3)
xlabel('Re (-)')
ylabel('m_o_p_t (kg/s)')
legend('T_g_e_o=110^oC','T_g_e_o=135^oC','T_g_e_o=160^oC')%,6);
grid on
hold off

figure (2)
hold on
plot (m_opt,Do_opt,Spec1,Spec2,Spec3)
xlabel('m_d_o_t (kg/s)')
ylabel('Do_o_p_t (m)')
legend('T_g_e_o=110^oC','T_g_e_o=135^oC','T_g_e_o=160^oC')%,6);
grid on
hold off

figure (3)
hold on
plot (Re,Do_opt,Spec1,Spec2,Spec3)
xlabel('Re (-)')
ylabel('Do (m)')
legend('T_g_e_o=110^oC','T_g_e_o=135^oC','T_g_e_o=160^oC')%,6);
grid on
hold off

figure (4)
hold on
plot (Re,Sgen_min,Spec1,Spec2,Spec3)
xlabel('Re (-)')
ylabel('Sgen, min (J/K.s.m)')
legend('T_g_e_o=110^oC','T_g_e_o=135^oC','T_g_e_o=160^oC')%,6);
grid on
hold off
```

```
n=n+1;
end

**************************************************************************
```

7.5 Appendix E-First and Second Law Efficiency of Organic Rankine Cycle

```
% clear all
close all
clc
%----------Input values----------------
n=1;
To=25+273.15; %oC
Trej=50+273.15; %oC
Tgeo=160+273.15; %oC
L=100; %m
%for Tb=300.55:0.6:302.95 %oC
Tb=265+273.15; %oC
%grad=(Tb-To)/L;
Trej=linspace(50+273.15,110+273.15,51); %K
%for Tb=300.55:0.6:302.95 %oC
grad=(Tb-To)/L;
for Tgeo=110+273.15:25:160+273.15 %K
Do_opt=zeros;Sgen_min=zeros;Bo=zeros;m_opt=zeros;
Ex_dest=zeros;Ex=zeros;Exo=zeros;ratio1=zeros;ratio2=zeros;Wnet=zeros;...
    En_eff=zeros;Ex_eff=zeros;
Re=1e6;%linspace(0,2e6,51);
col=length(Trej);
for i=1:col
Tm=(Trej(i)+Tgeo)/2; %K
if n==1; Spec1='-ok'; Spec2='MarkerFaceColor'; Spec3='k';end
if n==2; Spec1='-sr'; Spec2='MarkerFaceColor'; Spec3='r';end
if n==3; Spec1='-^g'; Spec2='MarkerFaceColor'; Spec3='g';end
%%
%----------Water properties------------
co_r=999.79684; co_c=4.2174356000; co_k=0.5650285;
co_m=557.82468; co_p=0.074763403;
c1_r=0.068317355; c1_c=-0.0056181625; c1_k=0.00263638950;
c1_m=19.408782; c1_p=0.002902098;
c2_r=-0.010740248; c2_c=0.001299253; c2_k=-0.00012516934;
c2_m=0.1360459; c2_p=2.8606181e-5;
c3_r=0.000821409; c3_c=-0.000115354; c3_k=-1.5154915e-6;...
    c3_m=-3.1160832e-4; c3_p=-8.1395537e-8;
c4_r=-2.30310e-5; c4_c=4.15e-6; c4_k=-0.0009412945;
%
rho=co_r+c1_r*(Tm-273.15)+c2_r*(Tm-273.15)^2+c3_r*(Tm-273.15)^2.5+...
    c4_r*(Tm-273.15)^3;
Cp=1000*(co_c+c1_c*(Tm-273.15)+c2_c*(Tm-273.15)^1.5+c3_c*...
    (Tm-273.15)^2+c4_c*(Tm-273.15)^2.5);
k=co_k+c1_k*(Tm-273.15)+c2_k*(Tm-273.15)^1.5+c3_k*(Tm-273.15)^2+c4_k*...
    (Tm-273.15)^0.5;
mu=1/(co_m+c1_m*(Tm-273.15)+c2_m*(Tm-273.15)^2+c3_m*(Tm-273.15)^3);
Pr=1/(co_p+c1_p*(Tm-273.15)+c2_p*(Tm-273.15)^2+c3_p*(Tm-273.15)^3);
%%
%-----------Optimization-----------------------------------------------
if Re>2300
```

```
r=0.653;
Bo(i)=(mu^6*Tm/(rho^2*Cp*Pr^0.6*grad^2))*(1-r)^4.6*(1/r^0.8-0.14/r^0.2)*...
    (1/((1-r)^2.8*(1+r)^2)+1/r^4.8);
m_opt(i)=0.238*Re^1.4*Bo(i)^0.25;
Sgen_min(i)=(13.84*m_opt(i)^2*Cp*Pr^0.6*(1-r)^0.2*grad^2)/...
    (mu*(1/r^0.8-0.14/r^0.2)*Tm^2*Re^0.8)+(0.0446*Re^4.8*mu^5*(1-
r)^4.8)/...
    (rho^2*Tm*m_opt(i)^2)*(1/((1-r)^2.8*(1+r)^2)+1/r^4.8);
Do_opt(i)=(4*m_opt(i))/(pi*mu*(1-r)*Re);
elseif Re<2300
r=0.683;
Bo(i)=(mu^6*Tm/(rho^2*Cp*Pr*grad^2))*(1-r)^3*(3.66+1.2*r^0.5)*...
    (((1-r)/(1+r))/(1-r^4-(1+r^2)^2/log(1/r)+1/r^4));
m_opt(i)=2.642*Re*Bo(i)^0.25;
Sgen_min(i)=(m_opt(i)^2*Cp*Pr*(1-r)*grad^2)/(pi*mu*(3.66+1.2*r^0.5)*...
    Tm^2)+(15.50*Re^4*mu^5*(1-r)^4)/(rho^2*Tm*m_opt(i)^2)*(((1-
r)/(1+r))/...
    (1-r^4-(1+r^2)^2/log(1/r)+1/r^4));
Do_opt(i)=(4*m_opt(i))/(pi*mu*(1-r)*Re);
end
%-----------------Performance evaluation-----------------------------------
Ex_dest(i)=To*Sgen_min(i)*L;
Ex(i)=Tgeo-Trej(i)-To*log(Tgeo/Trej(i));
Exo(i)=Tgeo-To-To*log(Tgeo/To);
ratio1(i)=Ex(i)/(Tgeo-To);
ratio2(i)=Ex(i)/Exo(i);
Wnet(i)=Ex(i)-Ex_dest(i)/(m_opt(i)*Cp);
En_eff(i)=Wnet(i)/(Tgeo-To);
Ex_eff(i)=Wnet(i)/(Tgeo-To-To*log(Tgeo/To));
end

figure (1)
hold on
plot((Trej-273.15),En_eff*100,Spec1,Spec2,Spec3)
xlabel('T_r_e_j (^oC)')
ylabel('Energy efficiency (%)')
legend('T_g_e_o=110^oC','T_g_e_o=135^oC','T_g_e_o=160^oC');
axis([50 110 0 20])
grid on
hold off

figure (2)
hold on
plot((Trej-273.15),Ex_eff*100,Spec1,Spec2,Spec3)
xlabel('T_r_e_j (^oC)')
ylabel('Exergy efficiency (%)')
legend('T_g_e_o=110^oC','T_g_e_o=135^oC','T_g_e_o=160^oC')
axis([50 110 0 100])
grid on
hold off
n=n+1;
end

**************************************************************************
```

7.6 Appendix F-EES Code for Thermodynamic Cycles

```
Fluid$ = 'steam'

{Condenser Outlet and CP Inlet –> 1}
P[1]=10
X[1]=0
h[1]=enthalpy(Fluid$; P=P[1]; X= X[1])
T[1]=temperature(Fluid$; P=P[1]; h=h[1])
s[1]=entropy(Fluid$; P=P[1]; h=h[1])
v[1]=volume(Fluid$; P=P[1]; h=h[1])
eta_CP=0,85

{CP Outlet & FWH3 Inlet –> 2}
P[2]=1000
s_s[2]=s[1]
s[2]=s_s[2]*(1/eta_CP)
h[2]=enthalpy(Fluid$; P=P[2]; s=s[2])
v[2]=volume(Fluid$; T=T[2]; s=s[2])
X[2]=quality(Fluid$; T=T[2]; s=s[2])
T[2]=temperature(Fluid$; P=P[2]; h=h[2])

{Deaerator Inlet & LPT Outlet –>13}
P[13]=1000
T[13]=450 {From T-s diagram}
h[13]=enthalpy(Fluid$; P=P[13]; T=T[13])
s[13]=entropy(Fluid$; P=P[13]; h=h[13])
v[13]=volume(Fluid$; T=T[13]; s=s[13])
X[13]=quality(Fluid$; T=T[13]; s=s[13])

{HPT Inlet & Boiler Outlet 1 –>8}
P[8]=10000
T[8]=600
h[8]=enthalpy(Fluid$; P=P[8]; T=T[8])
s[8]=entropy(Fluid$; P=P[8]; h=h[8])
v[8]=volume(Fluid$; T=T[8]; s=s[8])

{FWH2 Inlet & HPT Outlet 1–>9}
P[9]=5000
T[9]=482,6
s[9]=entropy(Fluid$; P=P[9]; T=T[9])
h[9]=enthalpy(Fluid$; T=T[9]; s=s[9])
v[9]=volume(Fluid$; P=P[9]; h=h[9])
```

{FWH1 Inlet, Boiler Inlet & HPT Outlet 2->10}
P[10]=2500
T[10]=430,2
s[10]=entropy(Fluid$; P=P[10]; T=T[10])
h[10]=enthalpy(Fluid$; T=T[10]; s=s[10])
v[10]=volume(Fluid$; P=P[10]; h=h[10])

{LPT Inlet & Boiler outlet 2->12}
T[12]=600
P[12]=2500
h[12]=enthalpy(Fluid$; P=P[12]; T=T[12])
s[12]=entropy(Fluid$; P=P[12]; h=h[12])
v[12]=volume(Fluid$; T=T[12]; s=s[12])

{Condenser Inlet & LPT Outlet 2->14}
P[14]=10
X[14]=0,91
s[14]=entropy(Fluid$; P=P[14]; X=X[14])
h[14]=enthalpy(Fluid$; P=P[14]; s=s[14])
T[14]=temperature(Fluid$; P=P[14]; h=h[14])
v[14]=volume(Fluid$; P=P[14]; h=h[14])

7.7 Appendix G-Thermodynamic Cycle with two LPFWH

	h (kJ/kg)	P (kPa)	s (kJ/kg/K)	T (ºC)	$\dot{m}\left(\frac{kg}{s}\right)$	$\psi\left(\frac{kJ}{kg}\right)$	$\dot{X}\left(\frac{kJ}{s}\right)$
1	191,7	10	0,6489	45,79	0,685	2,8217	1,932864
2	193,6	1500	0,6501	45,93	0,685	4,3639	2,989285
3	323,6	1500	1,039	77,02	0,685	18,4134	12,61317
4	432,8	1500	1,34	93,7	0,685	37,87	25,94111
5	844,8	1500	2,315	198,3	1	159,17	159,174
6	857,2	10000	2,32	200,3	1	170,08	170,0832
7	1058,5	10000	2,727	244,3	1	250,04	250,0362
8	1406,35	10000	3,358	310,9	1	409,75	409,7535
9	3625	10000	6,902	600	1	1571,8	1571,76
10	3415	5000	6,951	491,9	0,15	1347,2	202,0726
11	3234	2500	7,007	397,7	0,0725	1149,5	83,33543
12	3234	2500	7,007	397,7	0,7775	1149,5	893,7006
13	3686	2500	7,596	600	0,7775	1425,8	1108,594
14	3522	1500	7,632	522,3	0,0925	1251,1	115,7277
15	2987,3	160	7,842	257,7	0,0266	653,8	17,39105
16	2870,9	80	7,928	197,5	0,0302	511,8	15,45509
17	2599	10	8,195	53,72	0,6282	160,3	100,6703
18	1096	5000	2,811	252,3	0,15	262,5	39,37374
19	890,2	2500	2,408	208,3	0,2225	176,8	39,34824

20	357,1	160	1,134	85,02	0,0266	23,6	0,627471
21	225,8	80	0,7543	53,93	0,0568	5,5	0,312212
Cold water	104,8	101	0,3669	25	30	0	0
Hot water	154,8	101	0,5312	37	30	1	30

7.8 Appendix H-Assessment of Ethics in Research Projects form

APPLICATION FORM

Please Note:
Any person planning to undertake research in the Faculty of Engineering and the Built Environment (EBE) at the University of Cape Town is required to complete this form **before** collecting or analysing data.The objective of submitting this application *prior* to embarking on research is to ensure that the highest ethical standards in research, conducted under the auspices of the EBE Faculty, are met. Please ensure that you have read, and understood the **EBE Ethics in Research Handbook**(available from the UCT EBE, Research Ethics website) prior to completing this application form: http://www.ebe.uct.ac.za/usr/ebe/research/ethics.pdf

APPLICANT'S DETAILS		
Name of principal researcher, student or external applicant		Christa Nsanzinteko Nsanzubuhoro
Department		Mechanical Engineering
Preferred email address of applicant:		nsnchr001@myuct.ac.za
If a Student	Your Degree: e.g., MSc, PhD, etc.,	MSc. Mechanical Engineeering
	Name of Supervisor (if supervised):	Prof. Tunde Bello-Ochende
If this is a researchcontract, indicate the source of funding/sponsorship		Thermodynamic Optimisation and Second Law Analysis of Complex Geothermal Energy System
Project Title		

I hereby undertake to carry out my research in such a way that:

- there is no apparent legal objection to the nature or the method of research; and
- the research will not compromise staff or students or the other responsibilities of the University;
- the stated objective will be achieved, and the findings will have a high degree of validity;
- limitations and alternative interpretations will be considered;
- the findings could be subject to peer review and publicly available; and
- I will comply with the conventions of copyright and avoid any practice that would constitute plagiarism.

SIGNED BY	Full name	Signature	Date
Principal Researcher/ Student/External applicant	Christa Nsanzinteko Nsanzubuhoro		**17 Feb 2017**

APPLICATION APPROVED BY	Full name	Signature	Date
Supervisor (where applicable)	Prof. Tunde Bello-Ochende		**17 Feb 2017**
HOD (or delegated nominee) Final authority for all applicants who have answered NO to all questions in Section1; and for all Undergraduateresearch (Including Honours).	Prof. Tunde Bello-Ochende		**17 Feb 2017**
Chair : Faculty EIR Committee For applicants other than undergraduate students who have	Click here to enter text		Click here to enter a date.